EXPERIMENTAL EFFECTS OF HIGH SHOCK PRESSURE ON MATERIALS OF GEOLOGICAL AND GEOPHYSICAL INTEREST

Thesis by

Rex Vincent Gibbons

In Partial Fulfillment of the Requirements

for the Degree of

Doctor of Philosophy

California Institute of Technology

Pasadena, California

1974

(Submitted April 19, 1974)

Acknowledgments

I appreciate the hospitality and assistance of Dr. E. C. T. Chao while doing the interference microscopy at his laboratory at the United States Geological Survey, Washington, D.C. I similarly appreciate the assistance of Dr. J. M. Christie in doing transmission electron microscopy at the University of California, Los Angeles.

Technical assistance during operation of the shock-loading facility at California Institute of Technology was ably provided by John Lower and Dave Johnson. Larry Burdick helped in the shock-loading of some of the samples. Expert assistance at sample machining and manufacture of the sample assemblies and gun accessories was provided by Elmer Steffensen, Charles Hudson, and Richard Wickes. Bill Barbour, Laszlo Lenches, and Joe Galvan helped with the drafting. Thanks for everything, b'ys.

I thank Dr. G. R. Rossman for his assistance and the use of his laboratory at Caltech in the spectrographic studies and Dr. A. L. Albee and A. Chodos for their assistance with the Caltech electron microprobe. For the opportunity to use the shock-loading facility and the x-ray and microscopic equipment at the Seismological laboratory, I thank Dr. T. J. Ahrens.

My research at California Institute of Technology

was sponsored under grants NGL-05-002-105 (National Aeronautics and Space Administration), GA 21396 (National Science Foundation), and DA-ARO-D-31-124-72-G64 (Army Research Office). I acknowledge this support and all other monetary support received at Caltech.

I thank Dr. T. J. Ahrens for his assistance and support as my academic and research advisor during my tenure at Caltech. (I also thank him for the sailing, despite the mal de mer.)

For other assistance and helpful discussions at Caltech, scientific and otherwise, I especially thank Dr. D. L. Anderson, Dr. R. P. Sharp, Dr. C. R. Archambeau and Dr. D. Harkrider. Discussions of the project with Drs. A. L. Albee, E. S. Gaffney, B. Kamb, J. Kleeman, P. Lagus, G. R. Rossman, E. M. Shoemaker, L. T. Silver, and H. P. Taylor were also helpful.

I appreciate the hospitality and assistance of the staff at the Seismo Lab. Thank you all for everything you did for me. It was a pleasure to work with you during those last five years of the Donnelley Lab. And super-thanks to the great 1973 Seismo SuperShocks softball family; you kept me going when I needed it most.

Lastly, thanks to my wife, Marge, and our daughter, Kim. It's been a long five years but you two make it worth it. Thanks, Marge, for the typing.

Abstract

Shock recovery studies have been performed on a number of materials of geological and geophysical significance using a shock-loading propellant gun. These materials, including silicate glasses, feldspar, orthopyroxene, and pyroxenoid, have been shock-loaded to pressures up to approximately 550 kilobars. Optical and electron microscopic, optical spectral, and x-ray diffraction studies have been carried out on the recovered samples to determine the permanent effects of the shock-loading and the applicability of such information to research on naturally shocked lunar and terrestrial rocks and meteorites. The data on the pyroxene and feldspar are discussed in terms of their usefulness in interpreting, understanding, and calibrating the pressure and temperature conditions of shock metamorphism. The most significant observations include (1) the behavior of the silicate glasses, especially the occurrence of permanent densification until high post-shock temperatures cause reversion to low density glass, (2) the permanent reduction of Mn(III) to Mn(II) by shock-loading to 496 kilobars, (3) the shock vitrification of calcic plagioclase to diaplectic and shock-fused glasses at pressures above 300 kilobars, (4) the shock-production of deformation lamellae in bronzite, and

(5) the formation of shock glass in bronzite at 226 kilobars.

Table of Contents

List of Figures

LIST OF TABLES

Chapter I. INTRODUCTION

Only during the last two decades have geologists really become aware of 'shock metamorphism' as a significant geological phenomenon. Prior to this, very little attention was given to either the possible effects of high shock pressures on geological materials or the possible sources of such pressures. However, with the discovery of a high pressure phase of silica (coesite) at Meteor Crater, Arizona by Chao et al. (1960), a great deal of interest developed and now it is generally accepted that shock compression can produce spectacular and characteristic metamorphic effects in rocks and minerals.

The initial interest was in the moon and the question which has been raised since craters were first observed on the moon, of whether those craters were of volcanic or impact origin. On the earth this interest was directed to apparent terrestrial meteorite impact craters like Meteor Crater, Arizona (for example, Shoemaker, 1963). Many such craters were geologically mapped and petrographically studied to determine possible effects of shock-loading. By 1965 there were some sixty terrestrial localities (O'Connell, 1965) on the list of prime hypervelocity impact sites, as determined on the basis of overall structure and probable shock metamorphic features. These include the Ries crater, Germany (for example, Stöffler, 1966), probably the most extensively

studied single terrestrial crater, and several Canadian craters (for example, Dence, 1968). More recently, with the great interest in the Apollo lunar program, the emphasis has shifted somewhat to the effects of meteorite impacts on the moon; those scientists who previously had studied terrestrial impact craters directed their attention to shock metamorphism in the returned lunar rocks (for example, Chao et al., 1970; Engelhardt et al., 1970; and Short, 1970).

Right now, a major reason for experimental studies on shock metamorphism is the study of lunar rocks. We need a detailed knowledge of the behavior of common rocks and rock-forming minerals under well-controlled experimental shock-loading conditions of pressure and temperature in order to fully characterize the shock metamorphic histories of lunar rocks. It was partly for this reason that I carried out the shock wave experiments described in this work. For the same reason, other workers have recently done similar-type shock recovery experiments on a number of geological materials (for example, Stöffler and Hornemann, 1972; Short, 1968a; Kleeman and Ahrens, 1973; Hörz and Quaide, 1973).

The need to fully characterize the P,T effects of shock metamorphism in various rock-types has also led to experimental studies of a different nature. Those

are the studies of craters produced by nuclear and chemical explosions. Contrasted to laboratory-scale experiments, those are more like the meteorite impact in scale and produce similar effects (for example, Short, 1968b, 1969 and James, 1969a). They have one big drawback in that conditions of shock-loading cannot be as closely controlled as in laboratory experiments.

However, in the final characterization of shock metamorphism, permanent shock effects caused by artifical explosions, laboratory shock recovery experiments, and natural meteorite impacts must all be considered. It was to bring together workers in all these different areas that two recent conferences were held on shock metamorphism (French and Short, 1968; Hörz, 1971). These were attempts to summarize the status of all investigations of shock metamorphism and to characterize the diagnostic shock effects that could be used immediately in studies of lunar samples and terrestrial impact craters. They were attempts to look at the available data and determine the path to follow in further studies of shock metamorphism, in order to get a fuller understanding of the physical processes and conditions of shock-loading. They primarily resulted in additional data on natural and experimental impact phenomena. A number of review papers (for example, Chao, 1968; Engelhardt and Stöffler,

1968; and Stöffler, 1971) presented schemes of progressive shock metamorphism based essentially on observations of natural impact phenomena. Unfortunately, the available experimental data were insufficient for an adequate characterization of the temperature and pressure conditions of the various observed shock metamorphic facies. A more recent review by Stöffler (1972) suffers from this same malady and helps to emphasize the point that there is a need for a systematic experimental study of shock metamorphism of the common rocks and minerals. The present work is part of such a systematic study.

Chapter II.

DESCRIPTION OF THE 20-mm RECOVERY GUN FACILITY AND EXPERIMENTAL RECOVERY PROCEDURES; BRIEF OUTLINE OF SHOCK WAVE THEORY PERTINENT TO SHOCK RECOVERY EXPERIMENTS

Introduction

In the last few years, experimental techniques have been developed to measure the thermodynamic properties of shock compression of geological and geophysical materials, in particular those which can be determined using the Hugoniot equation of state. Since such techniques are destructive of the samples studied, shock recovery techniques had to be developed to study the irreversible effects of shock compression in materials of interest. Various techniques have been used to recover shocked samples. Techniques commonly used are (1) explosive systems, called plane-wave generators (for example, Duvall and Fowles, 1963), and (2) gas or powder driven ballistic systems (for example, Hörz and Ahrens, 1969). The gun facility described herein is a powder-driven ballistic system which has been developed during the past seven years at California Institute of Technology by Ahrens and co-workers (for example, Hörz and Ahrens, 1969; Gibbons and Ahrens, 1971).

The Gun Facility

The particular shock apparatus used in this study was designed and built by Mr. Sol Giles in the autumn of 1970 and installed during the winter of 1971. In carrying out 199 shots (for sample recovery, temperature measurement, and velocity calibration) with this gun since that time, I have routinely recovered mineral samples from shock-loading to pressures as high as 550 kilobars, for projectile velocities as fast as 1.8 km/sec.

The recovery facility consists essentially of a 3-meter long gun barrel and a separate box-type recovery chamber (Figure 1). The gun barrel is constructed from a 10-ft (3-meter) long Shelby stainless steel 4130 tube with a 2-inch (51 mm) outside diameter and a 3/4-inch (19 mm) bore. The bore is honed smooth to a diameter of approximately 20 mm; this leaves 15½ mm thick walls, more than sufficient for safety on the basis of the gun's performance since January, 1971 for more than 200 shock-loading experiments. The gun barrel is attached to an I-beam by five 30 cm long case-hardened steel clamps which are adjustable for alignment purposes. The I-beam is bolted to a floating concrete pier; this is required for gun barrel stability and to reduce shot-associated vibration of the adjacent laboratory facilities. There is still substantial vibration, caused by the air shock

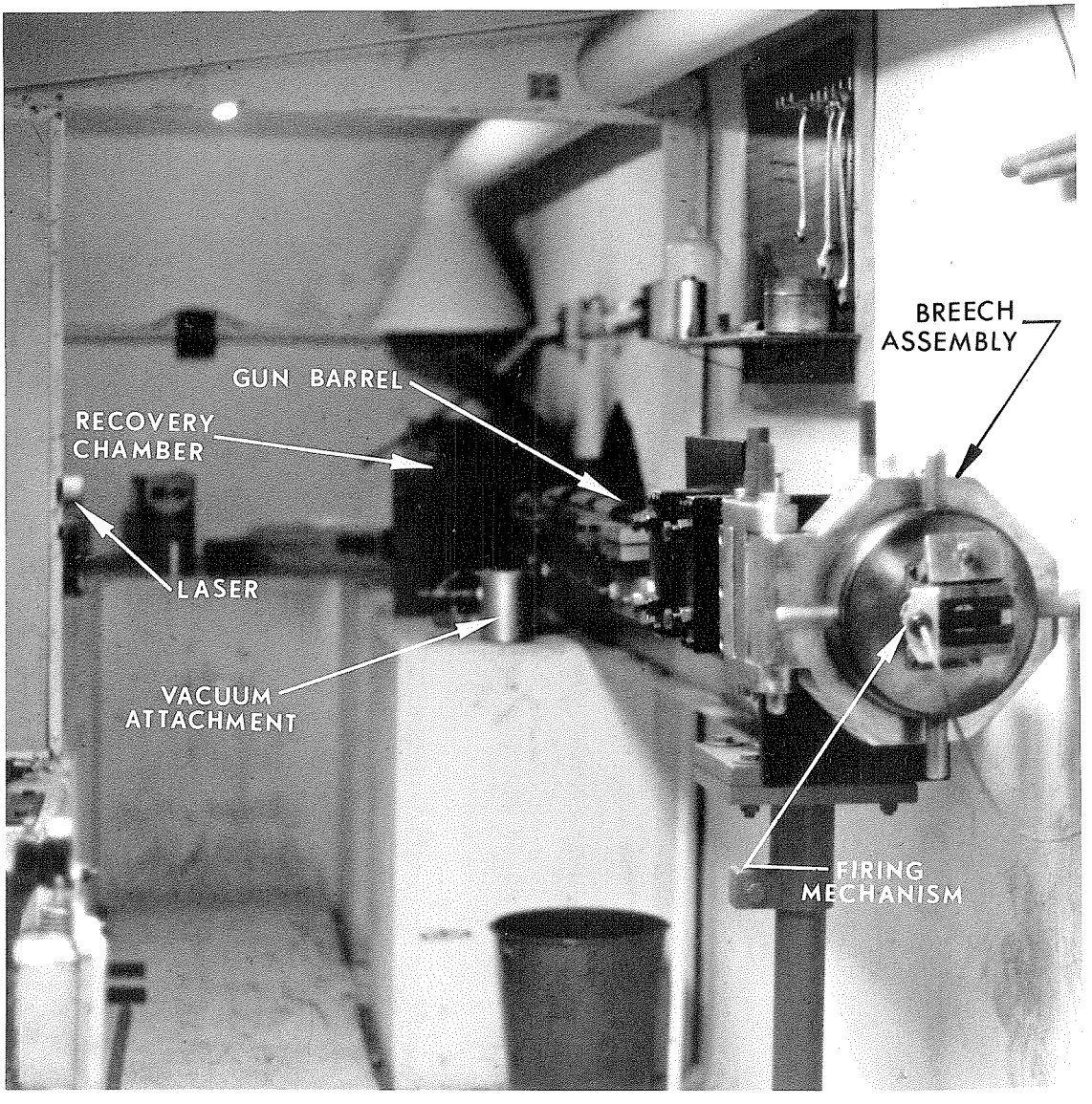

FIGURE 1. The gun.

produced by any high velocity shot; such air shock effects can only be eliminated by constructing a completely enclosed vacuum facility.

A massive breech assembly is screwed onto one end of the gun barrel (Figure 1). Breech block one is attached to the barrel with a close tolerance NF-3 thread; this block is machined to hold a case-hardened steel 4130 insert in vacuum fit against Lexan plastic projectiles (the inserts are custom designed shell casings that are made to accommodate ordinary shotgun and rifle shells). Breech block two is a massive gate-like assemblage which screws onto block one and locks the shell insert tightly against the Lexan projectile. A firing pin is inserted through the center of block two from a solenoid firing mechanism to the primer in the shotgun shell.

One other attachment for the gun barrel is an optional removable vacuum cylinder (Figure 1). This cylinder is used when it is desirable to evacuate the gun barrel before firing. It slips onto the muzzle and seals with two O-rings; a 3-mil thick mylar window covers the bore. A vacuum pump can then evacuate the barrel to approximately 10^{-2} torr. However, this vacuum is very inefficient and much needs to be done to prevent leakage around the various seals and connections. In this condition the use of the barrel evacuation technique is

very impractical. It has no effect on reducing air shock and gives an increase in projectile velocity of just 0.15 km/sec at peak velocity. Under normal circumstances it is much easier and exceedingly more practical to obtain the desired projectile velocities by changing the propellant load rather than evacuating the barrel. There are no practical reasons to evacuate the barrel for all except the peak 0.15 km/sec and everything associated with doing so is a hindrance to normal working procedures. However, if the barrel vacuum can be made more efficient, it will probably extend the peak pressure range beyond 1.8 km/sec.

Next to the gun barrel (maybe it should be more correctly named the 'projectile accelerator'), the most important component of the facility is the recovery chamber. The chamber is essentially a rectangular box (90 X 30 X 30 cm^3) with a hinged cover and with a 5 cm diameter projectile entrance in one end. It is made of 1 cm thick aluminum.

Before shock-loading, a sample assembly is mounted in the recovery chamber (Figure 5 shows the general relationships but details of the target seat and backstop are not illustrated). Using a laser - mirror system, the assembly is centered and aligned perpendicular to the

projectile path. This assures planarity of the impact within the accuracy of the flying projectile technique.

The sample assemblies consist of sample discs, sample containers, and cylindrical target blocks (Figure 2).

The sample discs used in the present experiments were 4.75 mm in diameter and up to 1 mm in thickness, depending on the character of the specimen. These dimensions were chosen to minimize edge effects and other effects of rarefaction waves generated at the flyer plate and target cylinder free surfaces. In general, the discs may be single crystal mineral, rock, or powder. In the present work solid discs of single crystals and glasses were used.

To prepare the discs from crystalline material or glass stock, there are two equally good techniques. By one method, thin wafers are sawn from a specimen; discs of 4.75 mm (0.1875-inch) diameter are cored from these wafers using either standard diamond core drills or custom-made core drills. For a variety of reasons some specimens may not be suitable for this method but may be suitable for coring into 4.75 mm diameter rods; those rods can then be sliced into thin discs. Such discs are ground and polished to a final thickness between 0.15 mm (0.006-inch) and 1.0 mm (0.040-inch). This thickness is

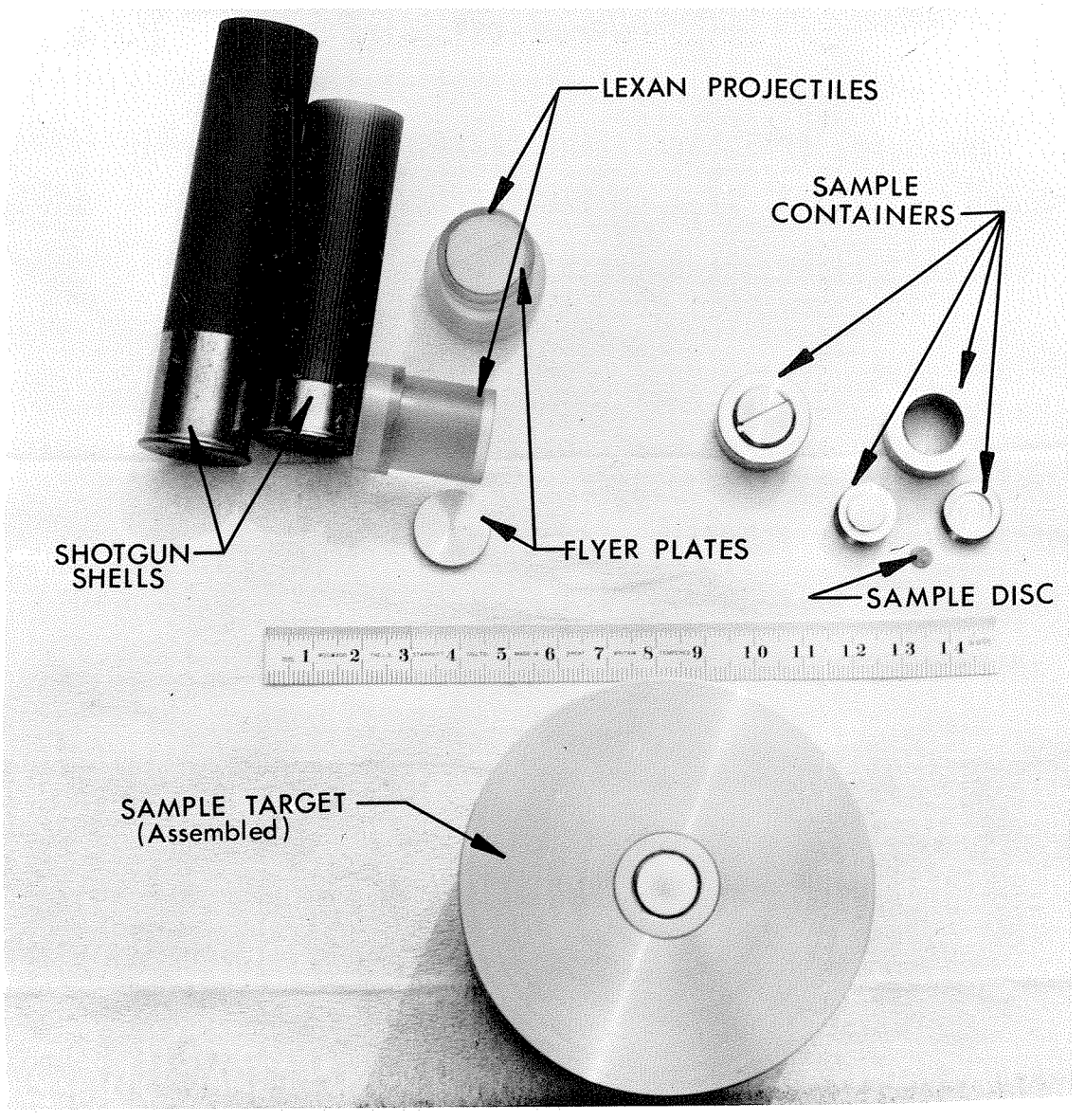

FIGURE 2. Materials used in shock-loading. Lexan projectiles (breakaway-type) with metal flyer plates, 10-gauge and 12-gauge shotgun shells, sample containers (assembled and disassembled), sample disc, and target cylinder with mounted sample container.

often determined by the character of the specimen, in particular its resistance to spalling during grinding. Glass discs can be easily ground to 0.15 mm but it is almost impossible to grind fragile mineral discs thinner than 0.5 mm.

For shock-loading the sample discs are screwed into metal sample containers which are in turn mounted into massive cylindrical target blocks. These target cylinders can be of any suitable metal; other materials, for example, plexiglas, can also be used for special shock conditions. The cylinders used most commonly have been stainless steel 304 and aluminum 2024. Stainless steel 304 was used in most of the experiments discussed. Two prime reasons for the use of those materials are (1) their Hugoniot equations of state are well-determined and (2) their availability. Another reason for using aluminum is that its shock impedance is a fair match for that of geological material. This is not so for stainless steel, which has a much higher shock impedance; however, an advantage of steel is that higher pressures can be obtained using a shock reverberation technique (described later). This reason is even more important for tungsten, in which pressures 30% higher than those for steel could be reached. However, drawbacks with tungsten are its expense, availability, machinability, and brittleness.

The dimensions of the cylinders used were 6.35 cm (2½-inches), 7.62 cm (3-inches), and 10.16 cm (4-inches) in diameter and 7.62 cm (3-inches) or more in length. The 7.62 cm (3-inch) diameter targets were found to be most suitable for machining and handling and were used whenever available. Those dimensions are more than adequate in consideration of the possible effects of rarefaction waves on the samples during shock-loading.

The sample containers should be of the same material as the target cylinders or something of similar shock impedance. In some cases sample containers were machined directly out of the target cylinders. However, since this is a very awkward machining problem, other designs, of separate sample containers, were developed. Two designs found to be most successful in shock recovery are (1) a 19 mm (3/4-inch) diameter, 12.7 mm (½-inch) long cylinder with a two-piece screw-in plug and (2) a 25.4 mm (1-inch) diameter, 12.7 mm (½-inch) long cylinder with a one-piece screw-in plug (Figures 2 and 2A).

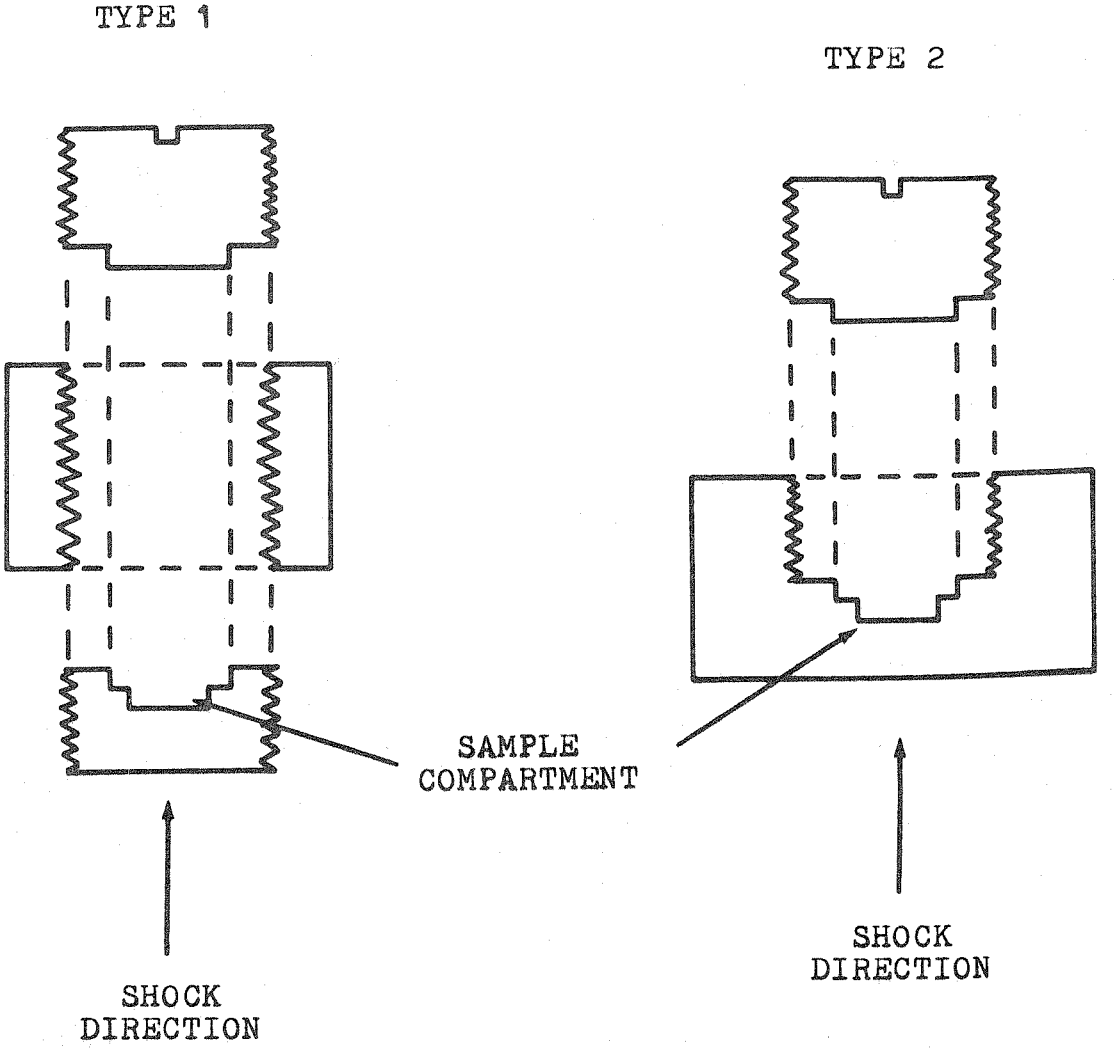

FIGURE 2A. Two sample container designs. Type 1: a 3/4-inch (19 mm) diameter, ½-inch (12.7 mm) long cylinder with a two-piece screw-in plug. Type 2: a 1-inch (25.4 mm) diameter, ½-inch (12.7 mm) long cylinder with a one-piece screw-in plug.

Shock-loading and Recovery

Shock waves were induced in the samples by impacting the target cylinders with high speed flyer plates imbedded in the front surface of Lexan plastic projectiles. The projectiles were launched at speeds up to 1.8 km/sec using the previously described propellant gun. Breakaway-type projectiles were used (see Figure 2). These projectiles are machined to tolerances of $\pm$ 0.0005 inches to provide what is essentially a vacuum-tight fit to the bore of the gun barrel, this tight fit helps to prevent blow-by of the hot gases and to assure that the pressure of the exploding propellant load will mainly be spent in accelerating the projectile down the barrel. The breakaway shoulder on the projectile is in a similarly tight fit with the breech insert to prevent loss of propellant pressure by leakage backwards through the breech.

The flyer plates are flat discs; they can be of almost any machinable material, metal, plastic, mineral or otherwise, depending on the requirements of the experiment. Besides machinability, the only essential requirement is that its Hugoniot equation of state be well-known, since this is necessary for accurate and dependable pressure determination. The plates most commonly used were of pure tungsten, brass (Cu 65%, Zn 33%, Pb 2%), tungsten alloy (90%, Ni 7%, Cu 3%), stainless steel

304, and aluminum 2024. Lexan, teflon, and plexiglas have also been used. The dimensions of the discs were 0.625-inch (15.9 mm) diameter and 0.100-inch (2.5 mm) thickness. A typical distance-time diagram in Figure 3 shows that the peak shock pressure pulse lasts one microsecond in the sample for such a flyer plate. Increasing the plate thickness to 0.200-inch (5 mm) increases the duration of the shock pulse to 2 microseconds, and so forth. However, there are limitations. As the plate thickness is increased, the plate mass is increased; accordingly the projectile velocity attained per powder load is decreased and the peak shock pressure is decreased. The trade-offs are such that it is most efficient to use 0.100-inch (2.5 mm) thick flyer plates for the sample configuration which gives the most successful recovery.

A large variety of propellants has been used in the shock-loading. Several types of rifle, pistol, and shotgun powders have been used in searching for the most practical and most efficient. I have found that two types, one pistol and the other shotgun powder, are sufficient. For low velocity shots Bullseye Red Dot shotgun powder was found to be quite satisfactory; for high velocities H110 pistol powder proved most efficient (Figure 4). These powders were used in ordinary plastic shotgun shells of 10, 12, and 20 gauges and in 0.300

FIGURE 3

x-t diagram of the impact of a 2.5 mm thick tungsten alloy flyer plate(1) against a stainless steel 304 target(2) containing a fused silica sample disc(3). OE is the trajectory of shock wave in the flyer plate, A is the pole of centered rarefaction wave, ABE and AD are rarefaction waves, and OBC is the trajectory of the advance of the flyer plate-target interface. Attenuation of the shock pulse in the sample starts at 1 microsecond after the initial shock and 0.7 microseconds after the sample has reached peak pressure.

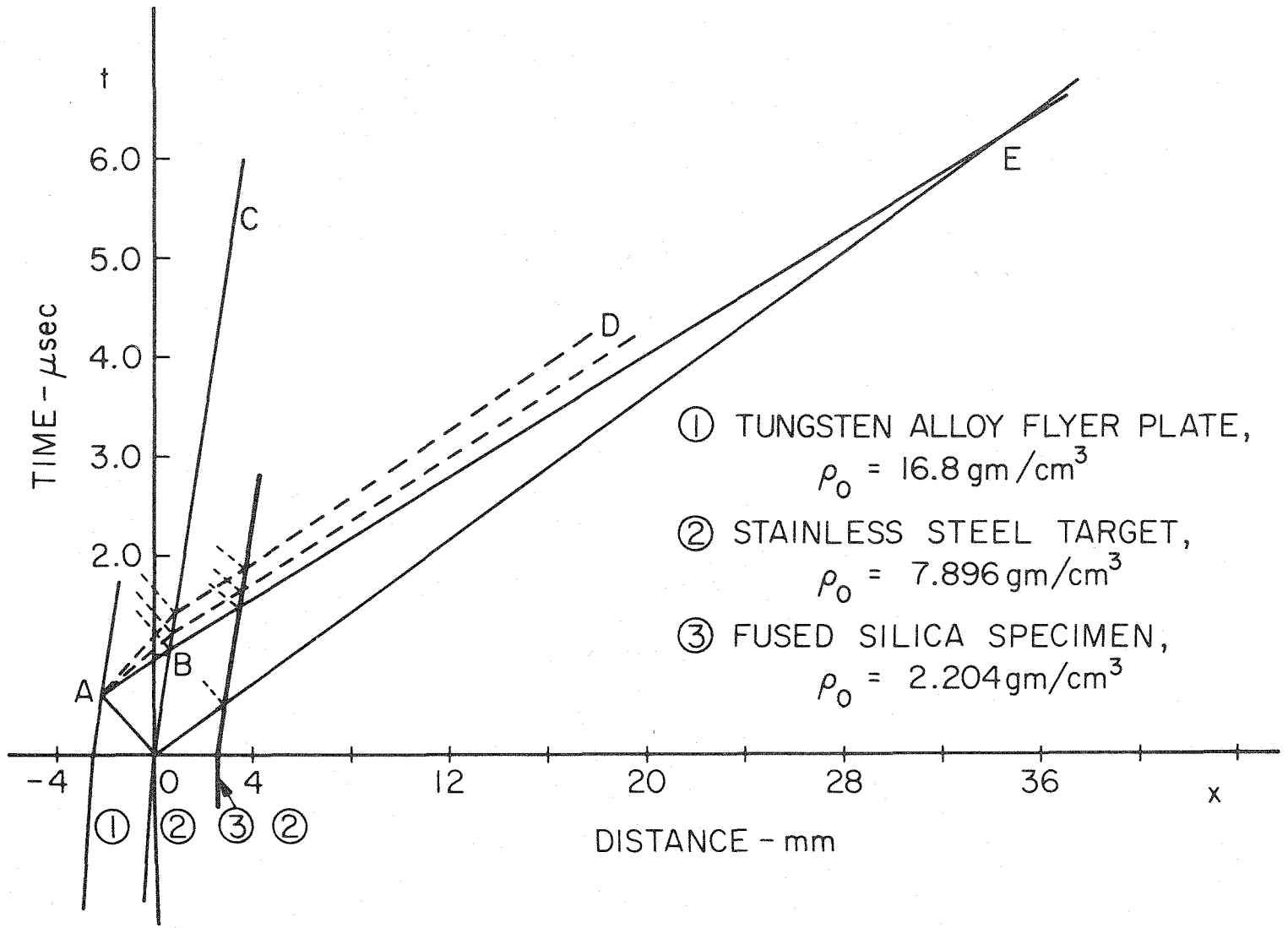
t
6.0
5.0
4.0
3.0
2.0
TIME - μsec
A
B
C
D
E
-4
0
4
12
20
28
36
x
① ② ③ ②
DISTANCE - mm
① TUNGSTEN ALLOY FLYER PLATE,
ρ_0 = 16.8 gm/cm^3
② STAINLESS STEEL TARGET,
ρ_0 = 7.896 gm/cm^3
③ FUSED SILICA SPECIMEN,
ρ_0 = 2.204 gm/cm^3

FIGURE 4

Projectile velocity-powder load curves for Bullseye Red Dot shotgun powder and H110 pistol powder. These data are for 0.100" (2.5 mm) pure tungsten flyer plates on breakaway-type Lexan projectiles (gun barrel not evacuated). The Bullseye powder was used in 12-gauge and the H110 in 10-gauge shotgun shells.

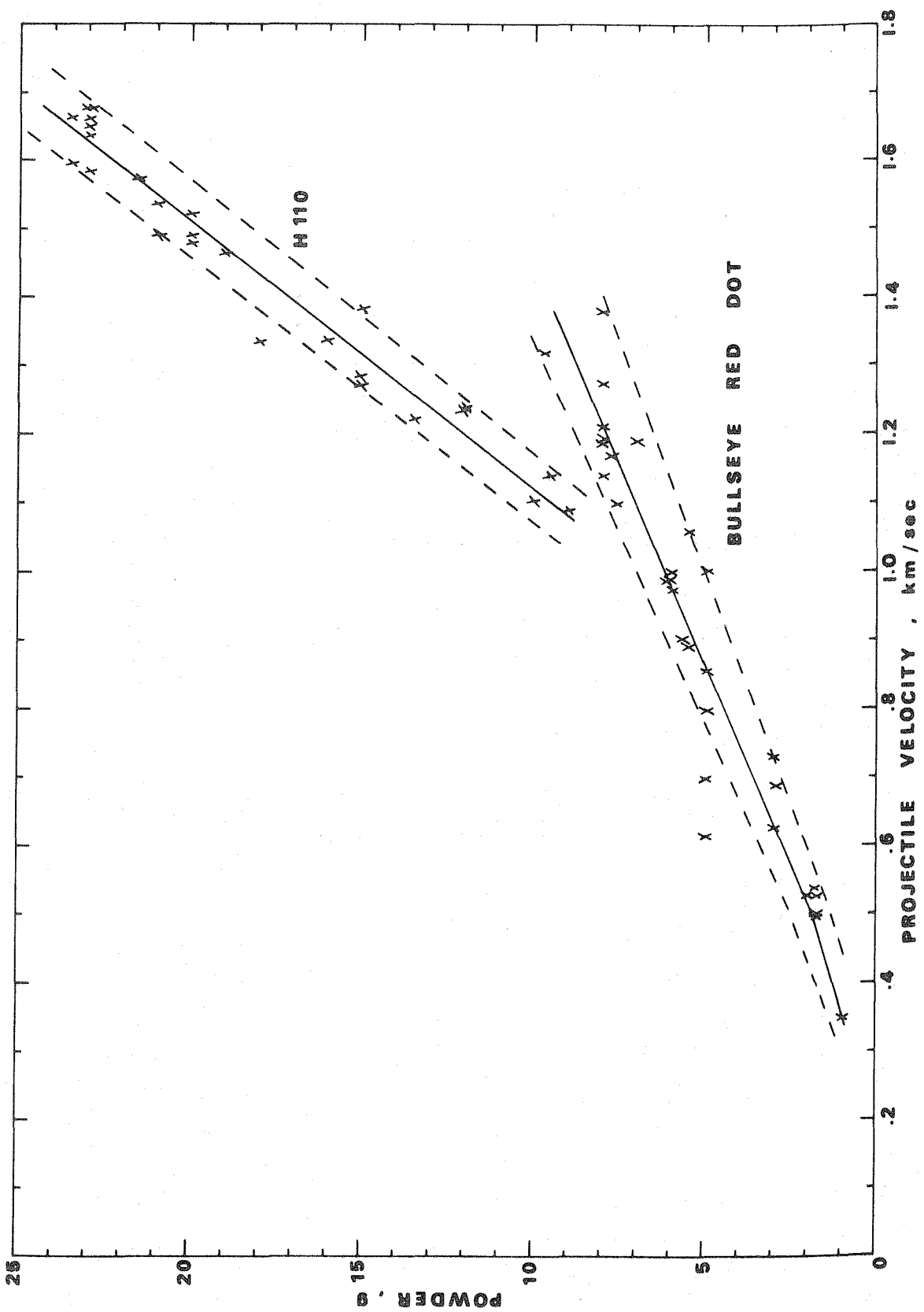
H 110
BULLSEYE RED DOT
POWDER , g
PROJECTILE VELOCITY , km/sec
0
5
10
15
20
25
.2
.4
.6
.8
1.0
1.2
1.4
1.6
1.8

and 0.460 magnum caliber brass rifle shells. Powder loads up to approximately twenty-five grams could be used. Custom-built shell inserts were manufactured for each shell size for insertion in the gun breech. The disposable shotgun shells are both least expensive and most convenient. Custom-built brass shells of variable capacity were found to be quite inefficient (they tended to jam irretrievably in the breech after high pressure shots) in spite of their great expense compared to the five-cent shotgun shells. Standard 20 mm machine gun shells were never used; they will probably make an efficient shell for larger capacity loads.

After shock-loading, the sample container is recovered from the recovery chamber either (1) still in the target cylinder or (2) separate from the cylinder, having been popped out by the rarefaction wave. In either case, to remove the sample from the container, the metal enclosing it must be carefully machined away on a lathe or a mill. After a successful shot, this machining is the most critical part of any recovery experiment. Unless great care is taken (even after much practice and experience), it is quite possible to lose the sample at this stage. Successful removal requires a very delicate, almost surgical, touch; 100% recovery is the result. Now the specimen is available for what-

ever mineralogical, petrographic, or geochemical studies anyone should desire to do on it.

Velocity Measurement and Pressure Determination

Shock pressures in the samples are determined graphically using an 'impedance matching' technique which will be described later. The only raw datum required to determine a pressure is the projectile velocity, which is measured just before impact of the flyer plate onto the target at a few millimeters in front of the target. An earlier version of this technique has been described by Hörz and Ahrens (1969).

A light detector system consisting of a helium-neon laser, a photodiode, two mirrors, and a dual beam oscilloscope is used (Figure 5). The laser is set up perpendicular to the projectile path; the primary laser beam intersects the path and is reflected between two mirrors and back across the path to the photodiode, whose output is being monitored by the oscilloscope. Upon firing, as the projectile breaks the laser beam at its two intersections, the photodiode output is written on the oscilloscope at rates of 20, 50, or 100 microseconds per centimeter, depending on the requirements of the particular shot, as dictated by the particle velocity.

A typical oscilloscope trace is shown in Figure 6. The two peaks represent the two projectile-laser beam intersections; the distance between those peaks is a

FIGURE 5

Impact geometry for projectile velocity measurement. Just before impact the projectile intersects two laser beams (A,B) of known separation (AB). The breaks are recorded on an oscilloscope as peaks in a time trace of the photodiode output (see Figure 6). The distance AB, approximately 200 mm, is measured to $\pm$ 0.5 mm each time the laser beam is realigned.

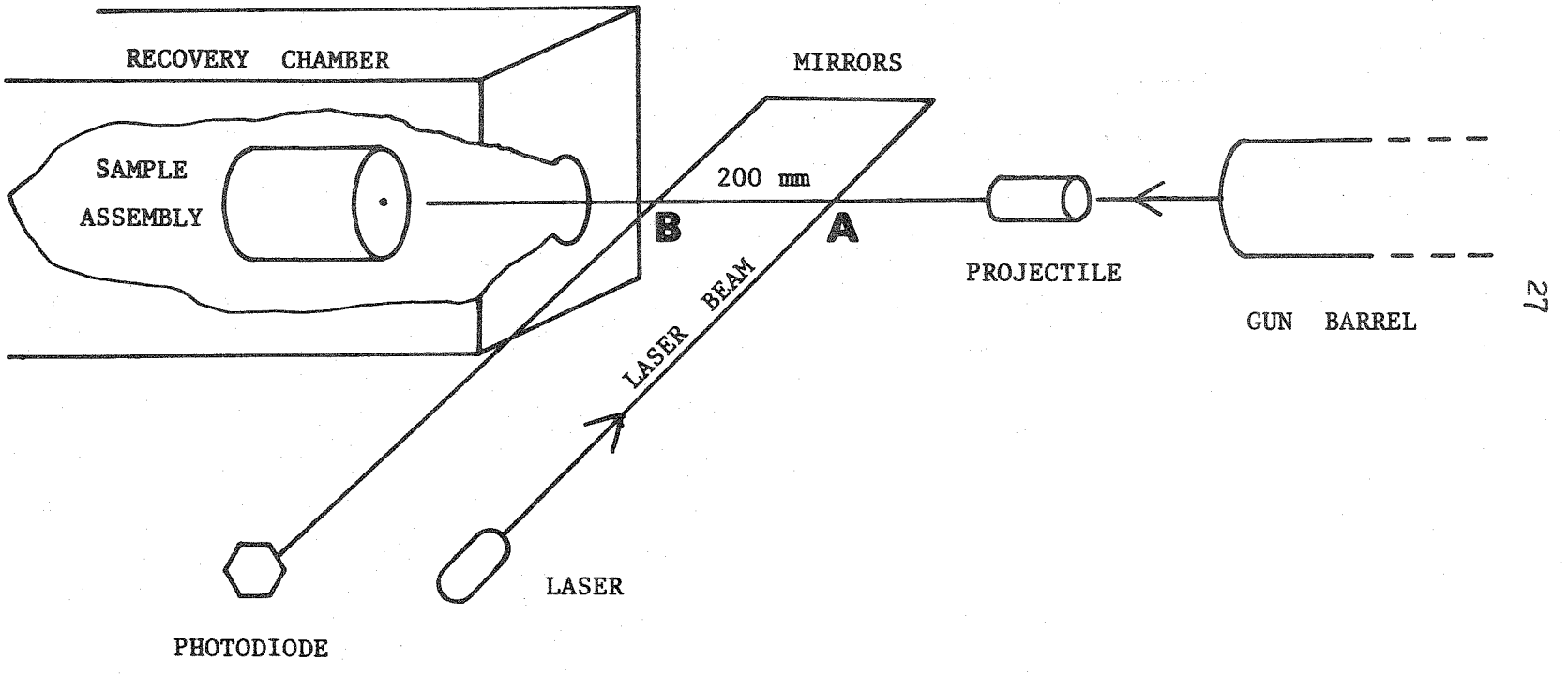
RECOVERY CHAMBER
MIRRORS
SAMPLE
ASSEMBLY
200 mm
B
A
PROJECTILE
GUN BARREL
LASER BEAM
LASER
PHOTODIODE

FIGURE 6

A typical oscilloscope trace for projectile velocity measurement. Note the two peaks representing the projectile laser beam intersections. The lower trace is a time calibration for a writing rate of 20-microseconds per centimeter. The distance between the two peaks is measured to $\pm$ 0.5 microseconds. This record is for shot 114 of rhodonite, projectile velocity = 1.572 km/sec and pressure = 496 kb.

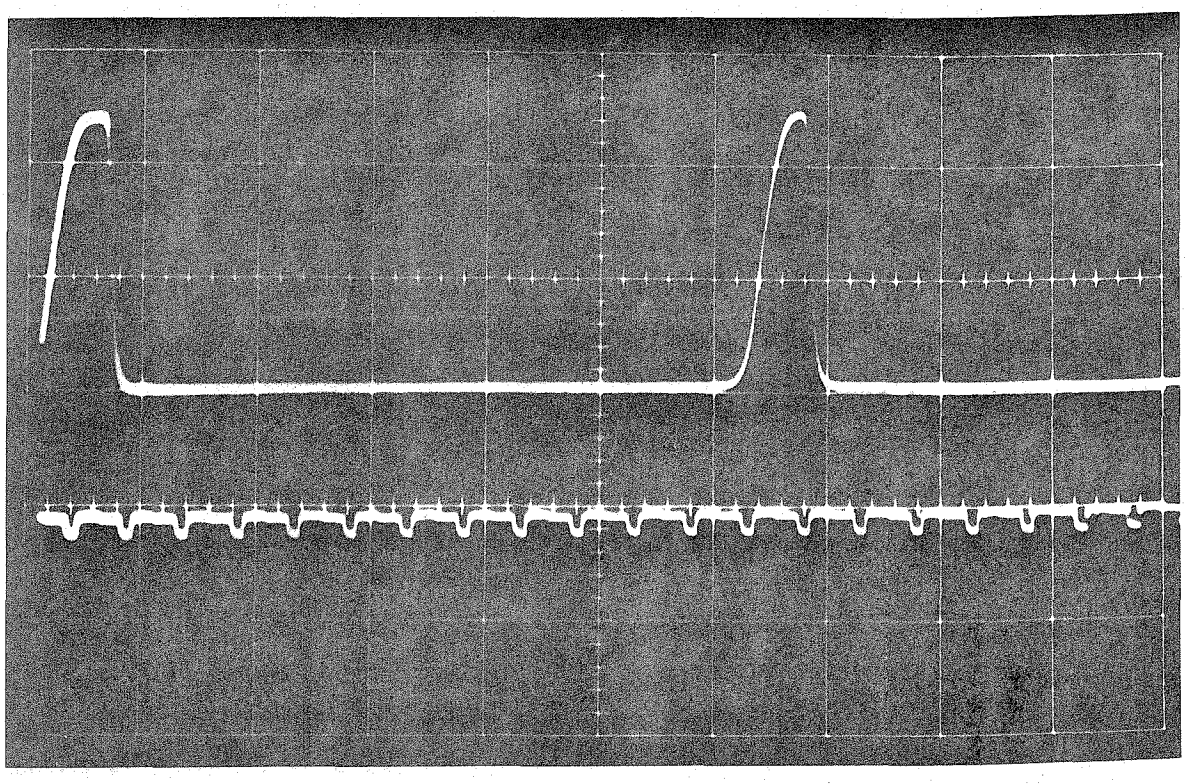

measure of the time required for the projectile to traverse the distance between the two intersections. This latter distance is fixed at approximately 200 mm (it is measured to $\pm$ 0.5 mm each time the laser is realigned). The time trace distance between the two peaks is measured to $\pm$ 0.5 μsec for times between 100 and 400 μsec. Combining the two measurements, it is possible to calculate the projectile velocity within $\pm$ 1%.

The peak shock pressure reached in the sample can now be determined using the graphical 'impedance matching' method (Duvall and Fowles, 1963 and Figures 7 and 8). The calculated projectile velocity, the Hugoniot of the target material, and the Hugoniot of the flyer plate are the essential data (see McQueen et al., 1970 for Hugoniot data). Only flyer plate and target cylinder materials with known Hugoniots are used so that only projectile velocity must be measured in each experiment. In the example shown in Figure 7, the Hugoniot of the sample material is also used. This is to show how, in our sample configuration, shock wave reverberations bring the sample pressure from its initial shock pressure up to the peak pressure of the target cylinder. Accordingly, the sample's Hugoniot is not really required since its final peak pressure will be the same as that of the target in this multiple-shock reflection-type design. Thus

FIGURE 7

Graphical representation of the 'impedance matching' method of determining shock pressures using as an example an impact of a tungsten flyer plate into a stainless steel target containing a specimen of fused silica at a free-flight velocity of 1 km/sec. B is the peak pressure attained in the target; C is the initial pressure in the fused silica. CD, DE represent shock reverberations in the fused silica that progressively increase its shock pressure until the peak pressure B of the target is reached. The time required to reach peak pressure is approximately 0.3 microseconds.

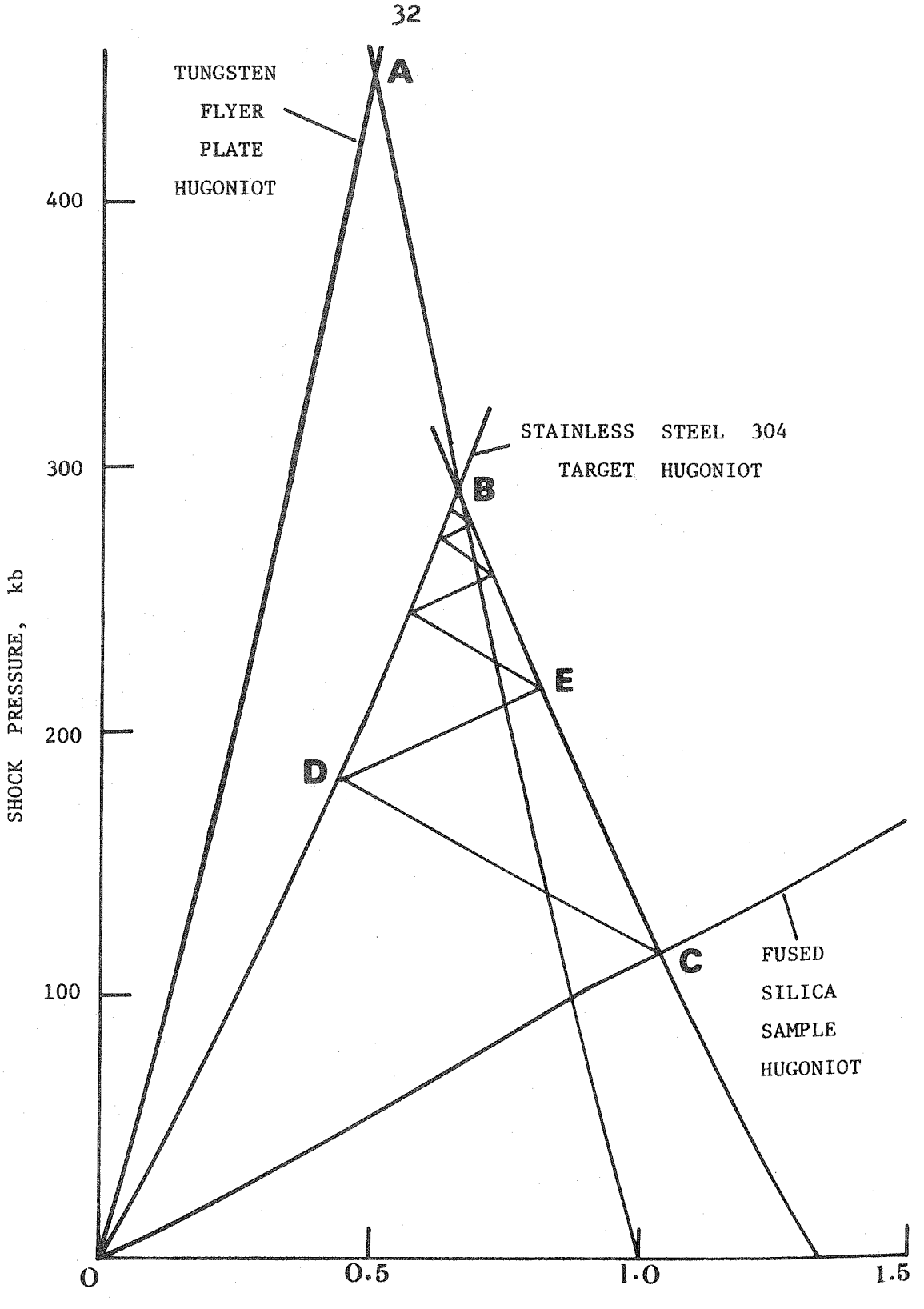
TUNGSTEN
FLYER
PLATE
HUGONIOT
A
STAINLESS STEEL 304
TARGET HUGONIOT
B
E
D
C
FUSED
SILICA
SAMPLE
HUGONIOT
400
300
200
100
SHOCK PRESSURE, kb
0
0.5
1.0
1.5
PROJECTILE VELOCITY, km/sec

FIGURE 8

Shock pressure-projectile velocity curves determined by 'impedance matching' for a number of flyer plate materials and stainless steel 304 target cylinders (see McQueen et al., 1970 for the Hugoniot data). One example of tungsten flyer plate onto tungsten target cylinder (W/W) is included to show the increased range of pressures attainable using only tungsten sample assemblies. Extending the tungsten curves to 2.5 km/sec shows that 860 kilobars can be reached using stainless steel 304 targets and 1280 kilobars using tungsten targets. Those curves are approximately linear at high pressures. The two curves for Lexan represent the range of its available Hugoniot data.

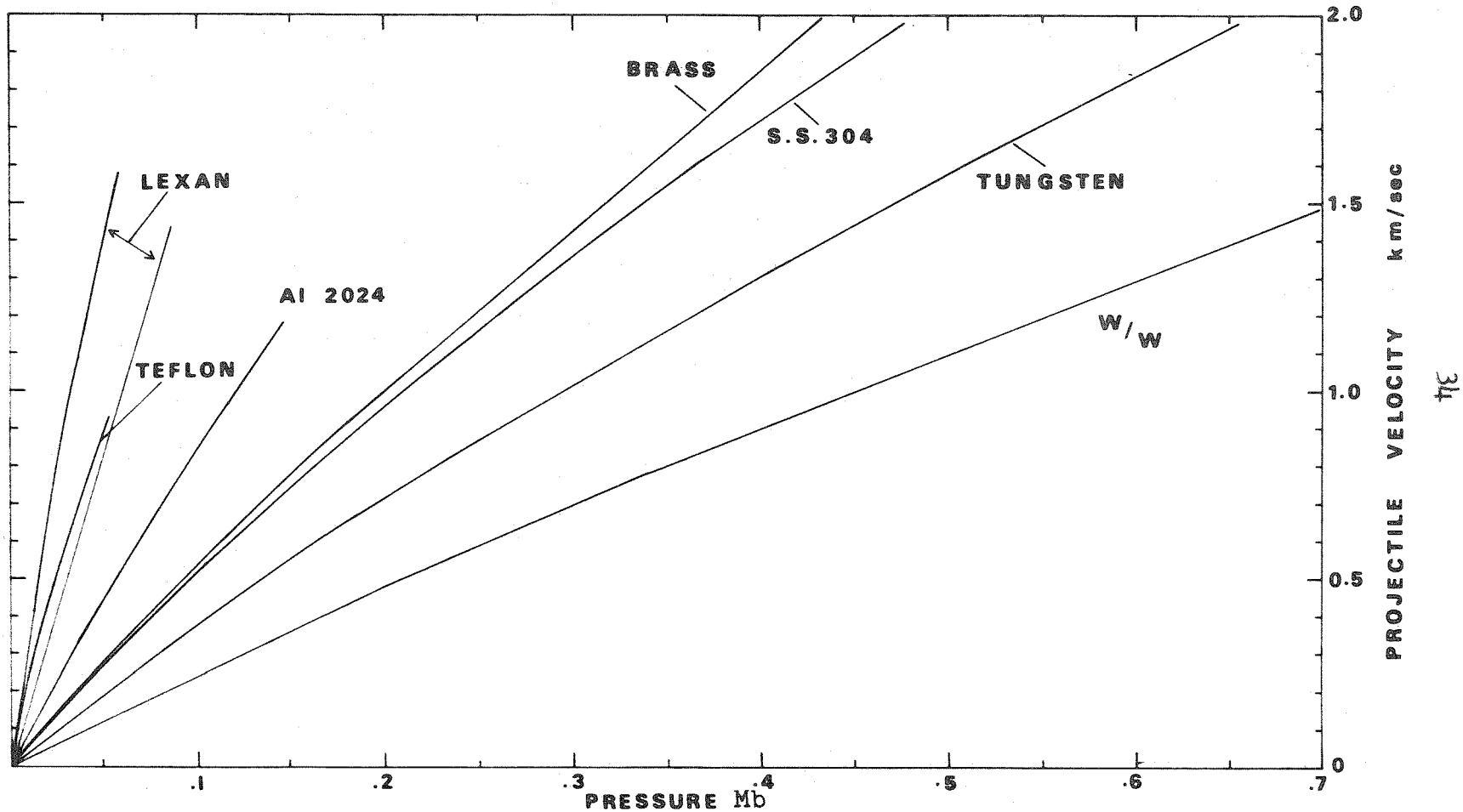
BRASS
S.S. 304
TUNGSTEN
LEXAN
Al 2024
TEFLON
W/W
2.0
1.5
1.0
0.5
0
.1
.2
.3
.4
.5
.6
.7
PRESSURE Mb
PROJECTILE VELOCITY km/sec

recovery experiments can be performed using those techniques on minerals and rocks whose Hugoniots have not yet been determined. This is an advantage of this technique over the single-shock technique.

For the example used in Figure 7, the pressure-time diagram in Figure 9 shows the relative increase in shock pressure for each shock reverberation until peak pressure is reached. The distance-time diagram given in Figure 3 for the same example shows how the shock and rarefaction waves advance through the target for this 1 km/sec shot. From a consideration of these three figures, it is clear that for our typical experiment shock-wave reverberations across the sample raised its pressure to the peak pressure of the target cylinder before a rarefaction wave originating from the back surface of the flyer plate caught up to and attenuated the peak shock pressure. The period of peak shock pressure in the samples, before rarefaction attenuation, was approximately 1 microsecond; this time corresponds to the two-way shock transit time through a 2.5 mm thick flyer plate (Gibbons and Ahrens, 1971).

We have given the error of projectile velocity measurement as within $\pm$ 1%. Combining this with errors due to inaccuracy of the Hugoniots and application of the graphical impedance match solution increases the errors

FIGURE 9

Relative time-shock stress diagram of the example shock wave experiment described in figures 3 and 7, showing variation of the pressure pulse with time. AB indicates the peak strength of the pressure pulse in the target. CDEFG represents the pressure pulse in the sample with CD, DE, etc. representing the shock wave reverberations. GHK exemplifies the attenuation of the pressure pulse by the rarefaction waves. The time from beginning to end of the shock pulse is approximately 1 microsecond for a 2.5 mm thick flyer plate.

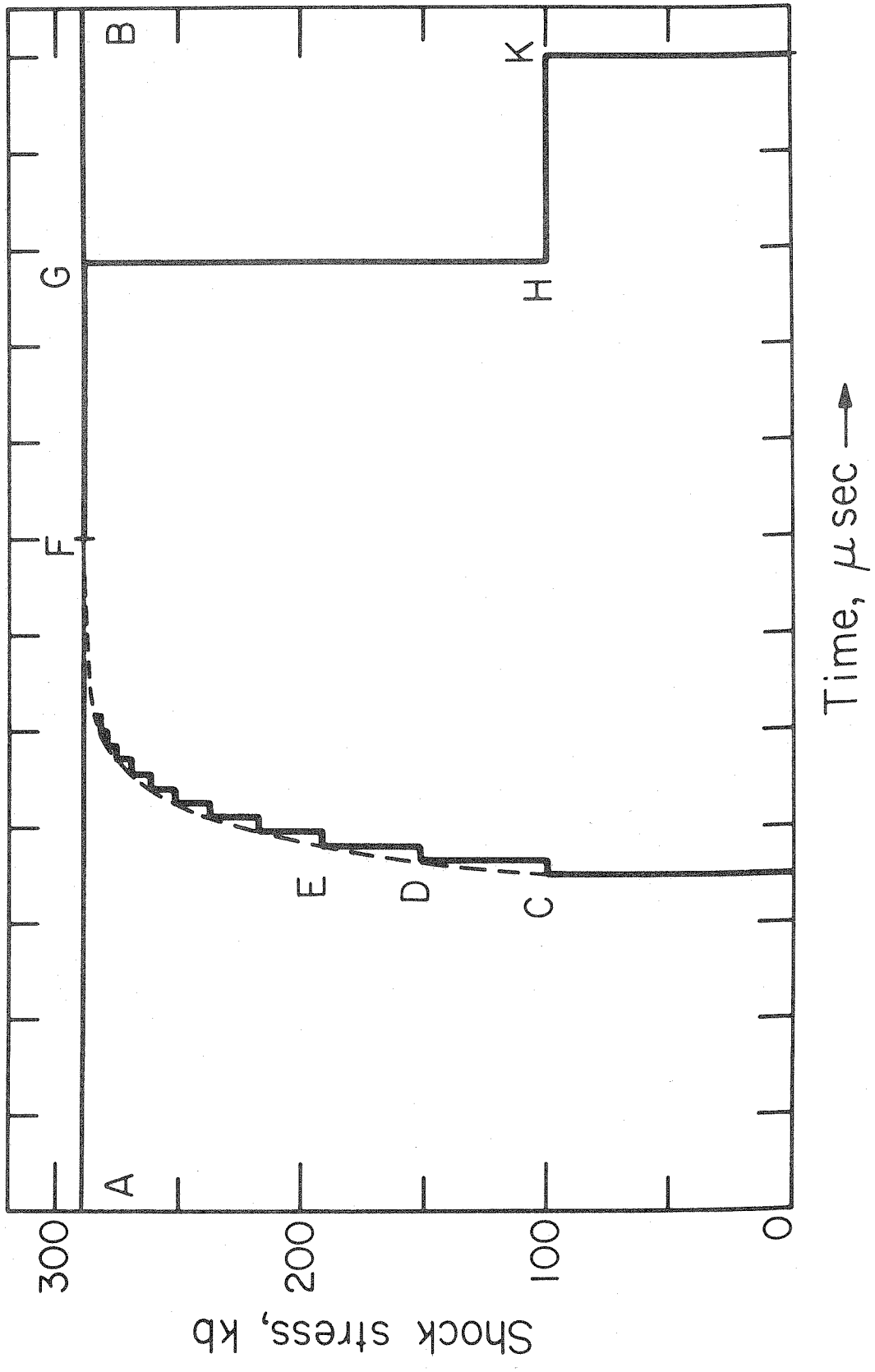
Shock stress, kb
300
200
100
0
Time, μsec
A
B
C
D
E
F
G
H
K

in the shock pressures to approximately $\pm$ 3%; these errors may vary somewhat depending on the quality of the Hugoniots of the different flyer plates and target materials used.

Shock Wave Theory Pertaining to Recovery Experiments

The Rankine-Hugoniot equations (for a derivation see Rice et al., 1958) describe the behavior of materials as a result of shock compression. In the derivation of those equations, it is assumed that:

1. the shock wave is steady-state in time, implying that a shock velocity can be defined;
2. the flow is one-dimensional planar;
3. there is continuity; and
4. short enough times are involved for the system to be post-shock adiabatic.

On this basis, the three basic Rankine-Hugoniot equations can be obtained (for example, Duvall, 1962; McQueen et al., 1967). These equations express the conservation of mass, momentum, and energy. For a coordinate system in which the material in front of the shock is at rest, they are respectively

$$\rho_o/\rho = (U_s - u_p)/U_s \qquad (1)$$

$$P - P_o = \rho_o U_s u_p \qquad (2)$$

$$\text{and } E - E_o = \tfrac{1}{2}(P + P_o)(V_o - V) \qquad (3)$$

The zero subscript refers to the initial state ahead of the shock wave; the non-subscripted quantities refer to the shock state. The equations relate the pressure

(P), internal energy (E), specific volume (V), or density (ρ) behind the shock wave to these same properties ahead of the shock wave in terms of the particle velocity (u_p) and shock velocity (U_s) of the shock wave. Equation (3) is the well-known Rankine-Hugoniot equation of state (for example, Ahrens et al., 1969a; Duvall, 1968; and Stöffler, 1972). It describes the locus of all the shock states (P, E, V) reached by shock compression of any solid from its initial state (P_o, E_o, V_o). As this locus is represented graphically in pressure-volume or pressure-particle velocity planes, it is commonly referred to as the Hugoniot curve, or more simply as the Hugoniot.

Isothermal and isentropic compressions are essentially reversible processes. Shock wave compression, on the other hand, is an irreversible process. Consideration of the Hugoniot shows that shock compression requires irreversible work, which results in the production of post-shock heat (for example, Stöffler, 1972, and Ahrens and O'Keefe, 1972). The thermodynamic path of shock compression between any two states in a shocked material is a Raleigh line between those two states (Figure 10). The thermodynamic path of decompression is the release adiabat. The compression is nonisentropic while the adiabatic release is isentropic,

FIGURE 10

Shock pressure-specific volume Hugoniot and release adiabat curves for fused silica (after Rosenberg et al., 1968). The thermodynamic path between the initial state and shock state $A(P_1, V_1)$ is the straight line AV_o, referred to as the Raleigh line. The waste energy produced by shock compression to state A along the Raleigh line followed by expansion along the release adiabat is the hatched area between the Raleigh line and the adiabat. It is this area of the PV-plane which represents the energy causing post-shock temperature increases. The zero pressure volume of the release adiabat is not necessarily, and usually not, the same as that of the initial volume. However, I have chosen an example for which it is equal to the initial volume within the errors of experimental data (see Figure 16).

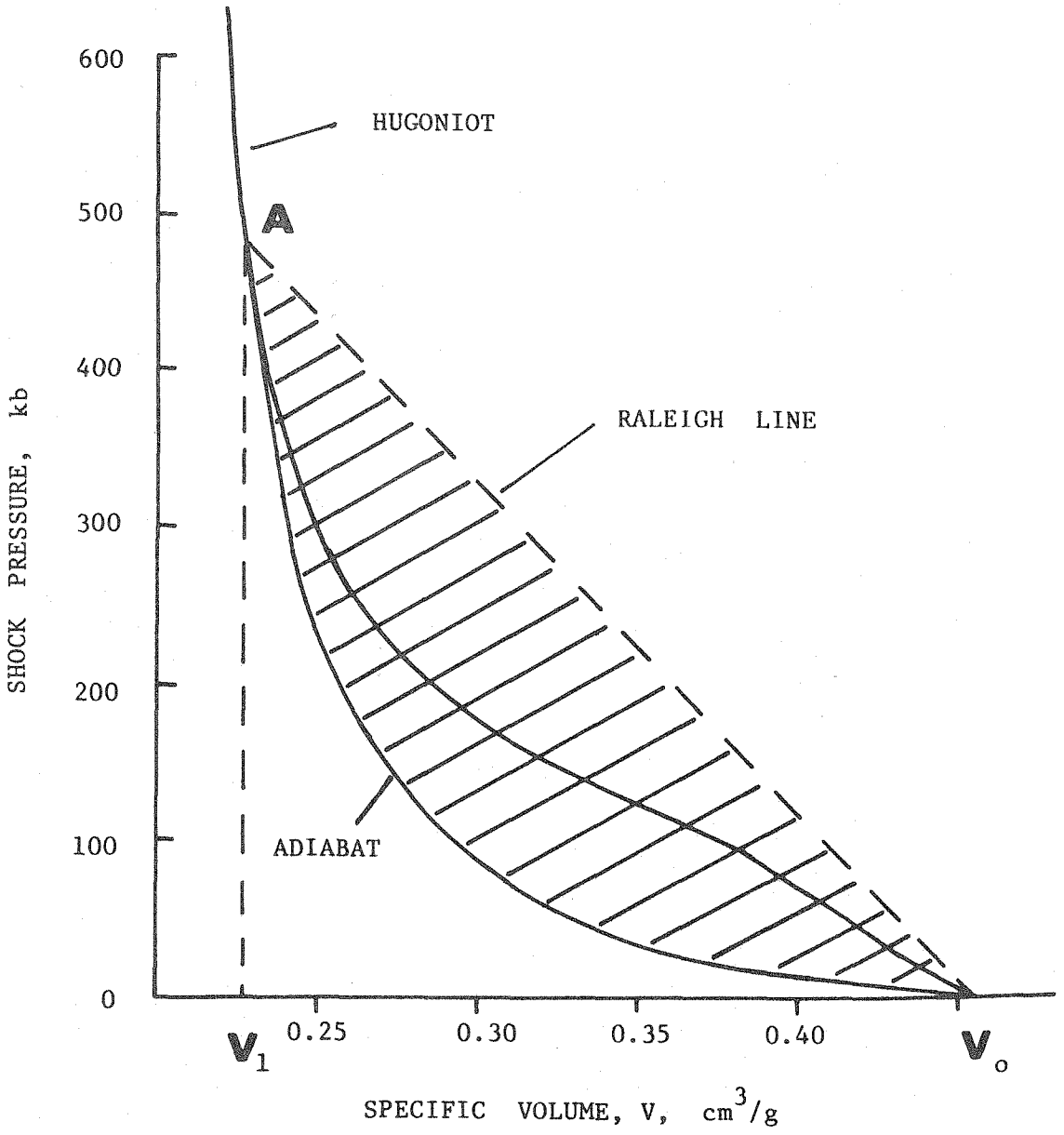
600
500
400
300
200
100
0
SHOCK PRESSURE, kb
HUGONIOT
A
RALEIGH LINE
ADIABAT
V_1
0.25
0.30
0.35
0.40
V_o
SPECIFIC VOLUME, V, cm^3/g

resulting in the increase in entropy represented by the hatched area in Figure 10. Referring again to this figure, note that the work done in the shock compression is represented by the area beneath the Raleigh line of the triangle AV_1V_o. The amount of this work that is returned by adiabatic expansion is the area AV_1V_o beneath the adiabat. The hatched area between the adiabat and Raleigh line is the waste energy which increases the post-shock temperature. It is obvious that at low pressures the amount of residual energy is minimal; at progressively higher pressures the residual energy increases more and more rapidly in amount, giving rapidly increasing post-shock temperatures (see the post-shock temperatures and energy in Table 5).

Post-shock temperature is a very desirable quantity to know in studying shock compressed rocks and minerals in view of its effects on the resultant physical properties of those materials. For example, selective melting, vaporization, solid state isotropization, and high pressure phase formation all appear to have some dependence on post-shock temperatures. To date there have been some attempts to measure post-shock temperatures in shocked materials (for example, Burdick and Gibbons, 1972), but there has been very little success on obtaining really usable data. Accordingly, Hugoniot and release adiabat data have been used to calculate the

shock and post-shock temperatures (for example, Walsh and Christian, 1955; Wackerle, 1962; Borg, 1972; Ahrens and Gregson, 1964; Ahrens et al., 1969b). A particular shortcoming of this has been the lack of experimental release adiabat data for most geological materials resulting in calculations based on various assumptions about adiabats, Hugoniots, and other thermodynamic parameters. Better temperature calculations have been made since the recent experimental determination of release adiabats for a number of geologic materials (see Ahrens and Rosenberg, 1968; Ahrens et al., 1969b ; Petersen et al., 1970; and Rosenberg et al., 1968). However, until actual measurements of shock and post-shock temperatures are obtained, there will be much skepticism of some of these calculated results.

Another feature of the Hugoniot that is very pertinent to shock recovery experiments is its shape, in particular, the relationship of its shape to the physical properties and parameters of the material (for example, the Hugoniot of fused silica in Figure 11). The Hugoniots of most geologic materials exhibit three phase regimes (for example, McQueen et al., 1963); these are the low pressure phase regime (I, lpp), the high pressure phase regime (III, hpp), and the mixed phase regime (II). Materials shocked along the Hugoniot to states within the lpp regime (I) relax to their

FIGURE 11

Fused silica Hugoniot (Rosenberg et al., 1968 and Wackerle, 1962) showing the low pressure phase regime (I, lpp), the mixed phase regime (II), and the high pressure phase regime (III, hpp).

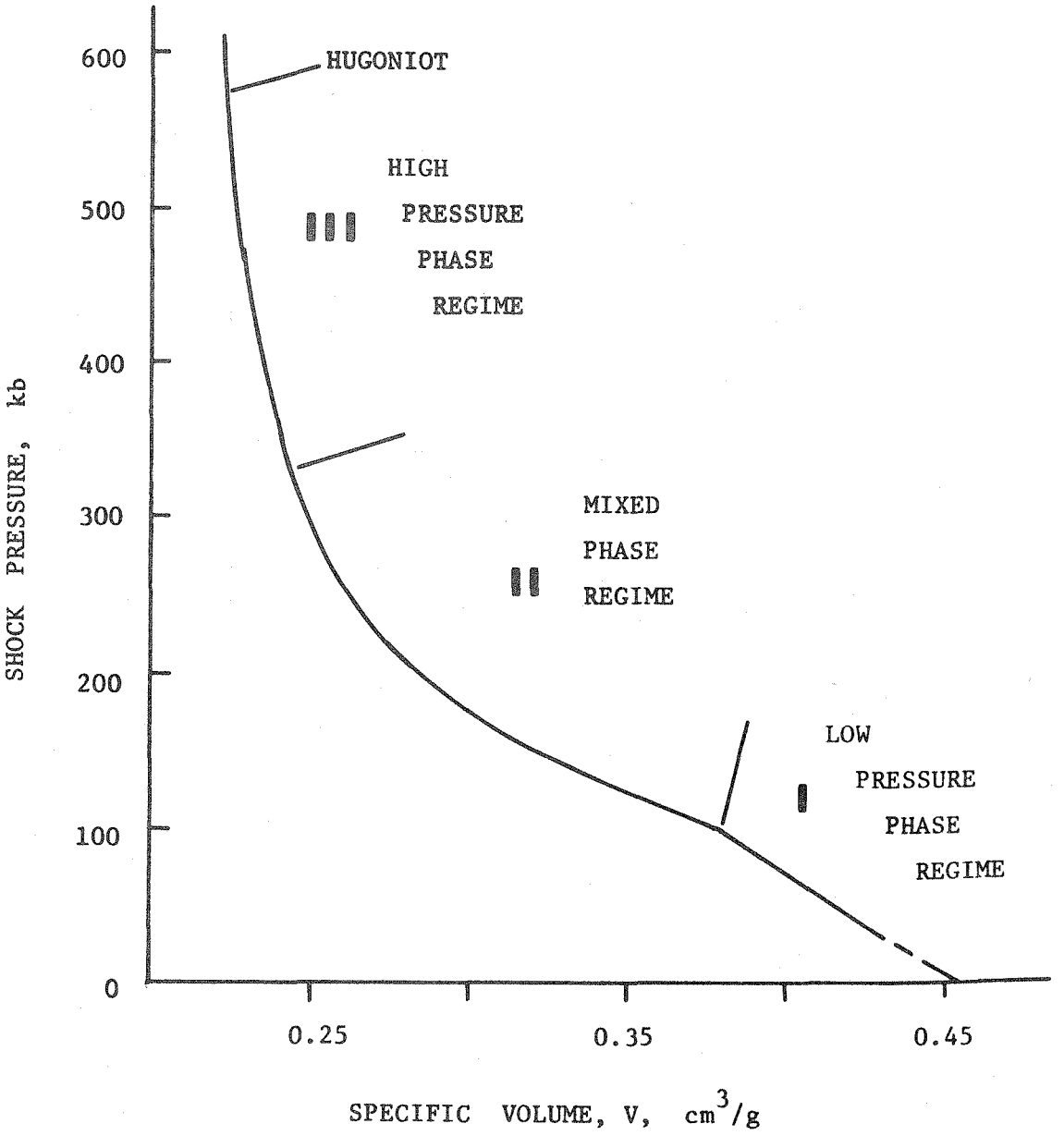
600
500
400
300
200
100
0
HUGONIOT
HIGH
PRESSURE
PHASE
REGIME
MIXED
PHASE
REGIME
LOW
PRESSURE
PHASE
REGIME
SHOCK PRESSURE, kb
0.25
0.35
0.45
SPECIFIC VOLUME, V, cm3/g

initial state upon adiabatic expansion. Materials shocked to states within the hpp regime (III) relax to the initial state, a shock-fused glass, a high pressure phase, or a mixture of all these, depending on post-shock temperatures and other factors. Materials shock-loaded to states within the mixed phase regime (II) behave similarly to regime (III) materials except that any shock glass is primarily solid state glass since post-shock temperatures are generally insufficient to cause melting.

Another oft-mentioned feature of Hugoniots, the Hugoniot elastic limit (HEL), is not a critical parameter in view of most observations on shocked rocks and minerals. However, in my studies on silicate glasses, the HEL is comparable to the threshold of permanent densification due to shock-loading.

Chapter III.

Abstract

The changes in refractive index caused by shock compression have been measured for tektite, soda-lime and silica glasses shocked to pressures up to 460 kb. For shock compression below 80 kb for fused silica and 40 kb for tektite and soda-lime glasses, compression is reversible as the refractive indices are within 0.0025 of the starting values. Index increases of 0.01, 0.04, and 0.06 are observed for soda-lime, tektite, and silica glasses shocked to pressures of 80, 130, and 140 kb respectively. For soda-lime glass subjected to shock pressures between 80 and 230 kb there is a decrease in the post-shock refractive index to n = 1.5211 at 230 kb. For fused silica shocked to pressures of 140 to 460 kb, refractive index drops from 1.52 to 1.47. The reasons for these decreases in index are not obvious. New values calculated for post-shock temperatures for fused silica based on recent release adiabat data, for example 1000°C for a shock state at 250 kb, suggest that the decreases in refractive index are caused by a combination of adiabatic relaxation during decompression and reconstructive transformation from a shock-induced stishovite-like high pressure phase to a low density glass, at post-shock temperatures high enough to cause annealing. Post-shock densities calculated from the refractive index

data agree closely with those calculated from the release adiabat data.

Introduction

Shock recovery experiments to peak pressures of 460 kb have been carried out on three series of silicate glasses, namely tektite, soda-lime, and silica. The purpose of these experiments has been to determine the changes in refractive index produced by shock densification in order to use these data to help deduce the pressure and temperature histories of naturally shocked lunar and terrestrial glasses. The fused silica has been of special significance because of its simple composition and because other investigators have studied its shock densification and equation of state (for example, Arndt et al., 1971, and Wackerle, 1962). Permanent increases in density of silica glass were first observed by Bridgman and Simon (1953) in static isothermal compression studies; they observed a threshold of densification of approximately 100 kb. Subsequent static high pressure studies of fused silica by Roy and Cohen (1961), Kennedy et al. (1962), Craig (1969) and others have yielded similar results but with thresholds of densification of less than 60 kb. Recently, Bless (1970) observed comparable irreversible densification of fused silica in isentropic magnetic pinch experiments to more than 100 kb.

SiO_4-tetrahedra, which comprise fused silica, are

the major network-forming polyhedra in all silicate glasses; the other glasses differ from fused silica by the presence of such network-modifying cations as Mg^{++}, Fe^{++}, Ca^{++}, Na^{+}, and K^{+}, which occupy possible 6-, 8-, and 12-fold sites in the irregular network. As those larger cations are added to the silica glass, the threshold pressure for irreversible densification progressively decreases. Therefore, it was suspected that shock compression of fused silica might provide a pattern for the behavior of the tektite and soda-lime glasses and maybe for other silicate glasses as well (Gibbons and Kleeman, 1970).

Experimental Procedures

The glasses studied were tektite (indochinite IC298 from American Meteorite Laboratory), soda-lime (cover glass 19130 from Kimble (Exax)), and fused silica (General Electric schlieren grade type 151). Chemical compositions of the first two glasses were quoted in Ahrens et al. (1970). Initial zero pressure densities were 2.44 $\pm$ 0.02 $g.cm^{-3}$, 2.43 $\pm$ 0.02 $g.cm^{-3}$ (R. L. Fleischer, private communication to Dr. T. J. Ahrens, 1970), and 2.204 $\pm$ 0.003 $g.cm^{-3}$ respectively.

The samples were machined into thin wafers from which discs 4.75 mm in diameter were cored; the discs were ground and polished to a final thickness of 0.15 mm. The finished specimens were loaded into aluminum 2024 or stainless steel 304 sample containers for shock-loading. After shock-loading the sample containers were machined open to recover the shocked specimens. The character of the specimens varied from solid discs to coarsely fractured and finely crushed and powdered. Refractive indices were measured by standard immersion techniques and by interference microscopy. X-ray diffraction was done by standard Debye-Scherrer techniques, using 114.6 mm diameter cameras.

Experimental Results

The data on shock pressure and refractive index are given in Tables 1, 2, and 3 for tektite glass, soda-lime glass, and fused silica, respectively. Graphical plots of these data (Figures 12, 13, and 14) correlate a range of refractive index within a specimen with the peak shock pressure to which the specimen was shock-loaded.

For shock compression below 80 kb for fused silica and 40 kb for the tektite and soda-lime glasses, shock densification appears reversible, since the changes in refractive index are within 0.0025 of the starting values. Index increases of 0.01, 0.04, and 0.06 are observed for soda-lime, tektite, and silica glasses shocked to pressures of 80, 130, and 140 kb, respectively. For soda-lime glass in the pressure range 80 to 230 kb, there is an equivalent decrease in index to the sub-initial value n = 1.5211. Similar behavior is exhibited by fused silica shocked to pressures between 140 and 460 kb; however, for fused silica there is a refractive index plateau for material shocked to pressures between 140 and 300 kb, an index decrease of 0.025 for material shocked to pressures between 300 and 310 kb, and a low-density glass for material shocked to pressures up to 460 kb. The tektite glass was not shocked to pressures greater than 130 kb; however, on the basis of the behavior

of the fused silica and soda-lime glass it is expected that similar behavior would result.

FIGURE 12

Refractive index-shock pressure graph of tektite glass data. The sizes of the open data-point circles indicate the precision of the data.

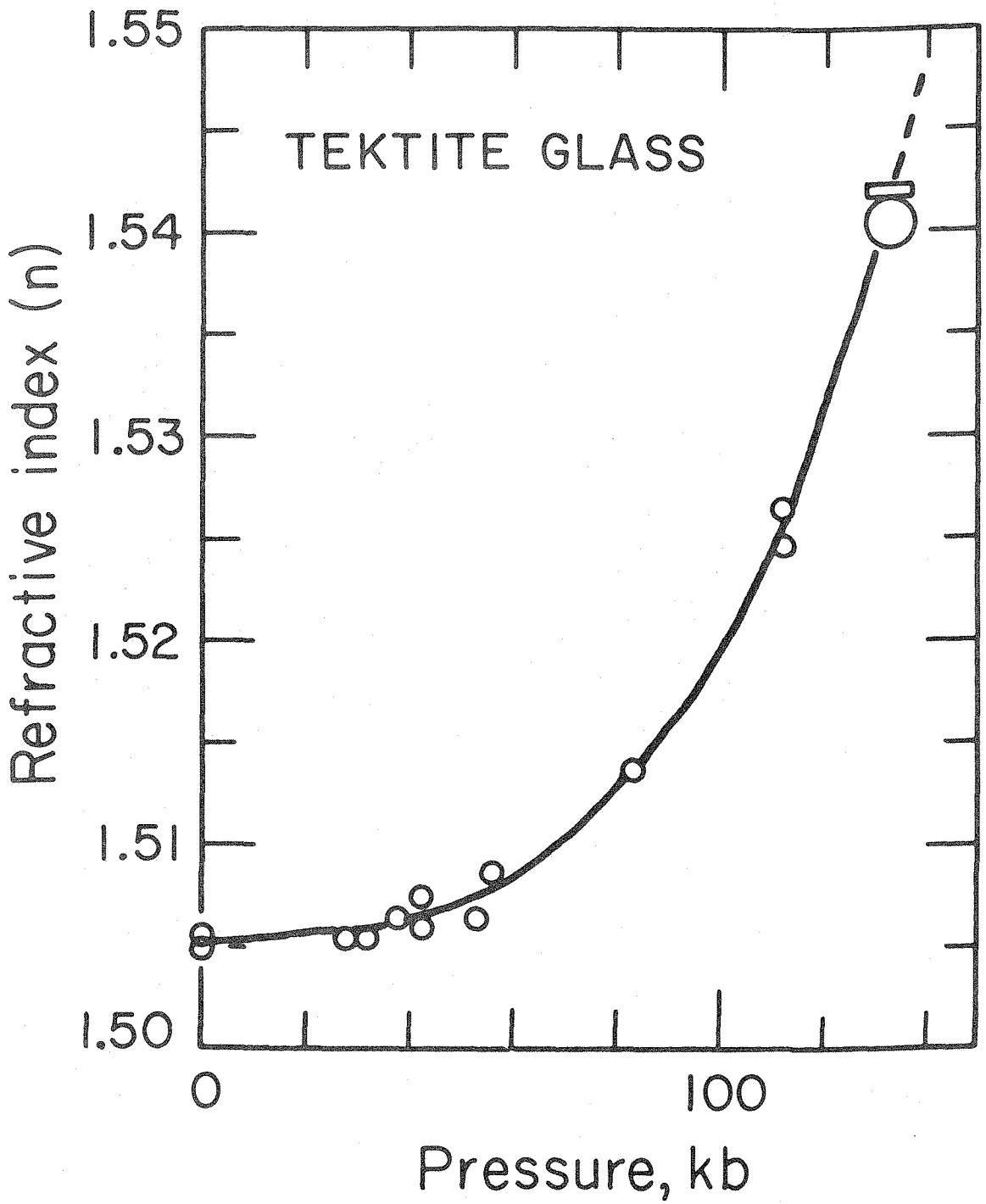
TEKTITE GLASS
Refractive index (n)
1.55
1.54
1.53
1.52
1.51
1.50
0
100
Pressure, kb

FIGURE 13

Refractive index-shock pressure graph of soda-lime glass data. The sizes of the open data-point circles indicate the precision of the data.

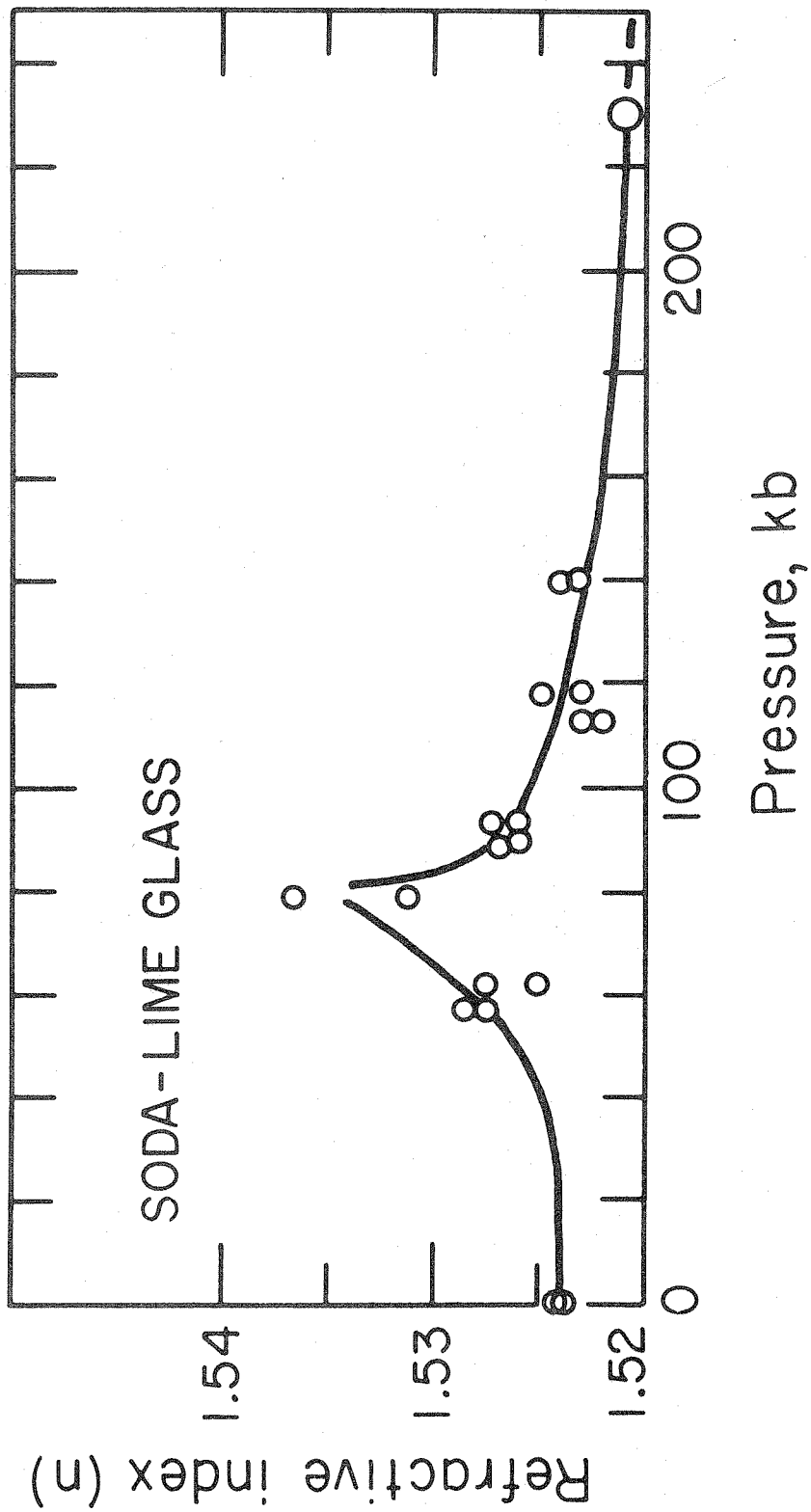
SODA-LIME GLASS
Refractive index (n)
1.54
1.53
1.52
0
100
200
Pressure, kb

FIGURE 14

Refractive index-shock pressure graph of fused silica data. The sizes of the open data-point circles indicate the precision of the data; lines joining circles indicate the range of refractive index observed in some specimens. The filled circles are the data of Arndt et al. (1971), which have been reproduced for comparison.

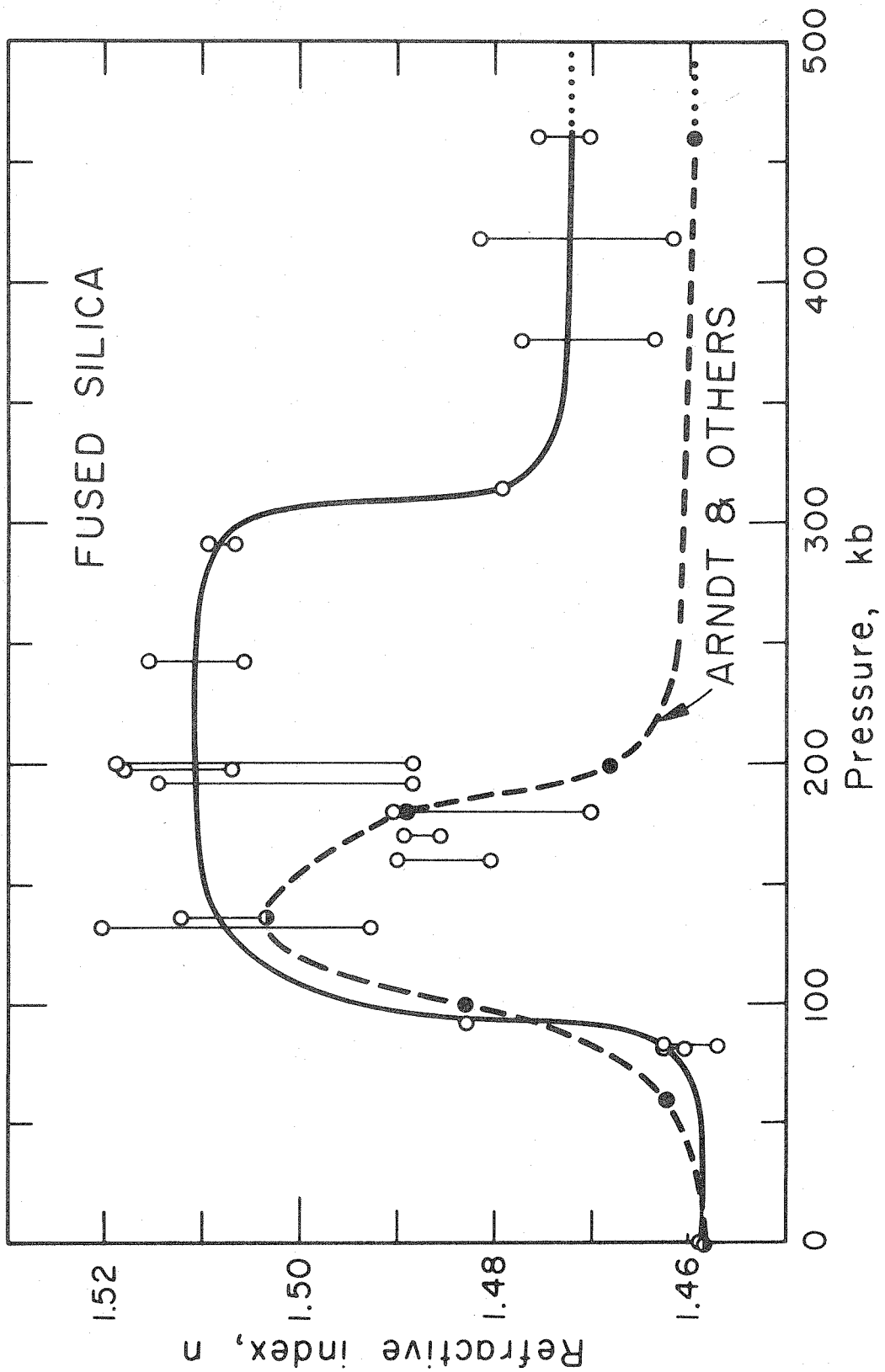
FUSED SILICA
ARNDT & OTHERS
Refractive index, n
1.52
1.50
1.48
1.46
0
100
200
300
400
500
Pressure, kb

TABLE 1

Refractive Index Measurements of
Shock-Loaded Tektite Glass

Shot Number	Shock Pressure, kb	Refractive Index (n)
...	0	1.5051 ± 0.0002[a]
		1.5055 ± 0.0005
119	43 ± 2	1.5060 ± 0.0005
120	56 ± 3	1.5087 ± 0.0005
122	53 ± 2	1.5065 ± 0.0005
123	32 ± 2	1.5055 ± 0.0005
124	28 ± 2	1.5055 ± 0.0005
142	133 ± 10	1.5419 ± 0.0002[a]
		1.5404 ± 0.0005
143	38 ± 2	1.5065 ± 0.0005
144	42 ± 3	1.5075 ± 0.0005
152	112 ± 2	1.5247 ± 0.0002[a]
		1.5265 ± 0.0005
145	83 ± 4	1.5137 ± 0.0007

[a] Measurements by interference microscopy; all others by standard immersion methods.

TABLE 2

Refractive Index Measurements of
Shock-Loaded Soda-Lime Glass

Shot Number	Shock Pressure, kb	Refractive Index (n)	
		Interference Method[a]	Immersion Method
...	0	1.5239	1.5242 ± 0.0005
IV	57	1.5275	1.5285 ± 0.0005
150	62 ± 2	1.5249	1.5275 ± 0.0009
151	79 ± 2	1.5367	1.5312 ± 0.0010
148	113 ± 2	1.5220	1.5230 ± 0.0010
147	118 ± 2	1.5229	1.5249 ± 0.0010
164	134 ± 3	1.5239	1.5233 ± 0.0009
167	230	1.5211	1.5211 ± 0.0011
179	93 ± 2	1.5261	1.5272 ± 0.0010
180	89 ± 2	1.5262	1.5266 ± 0.0010

[a] Error, ± 0.0002.

TABLE 3

Refractive Index Measurements of Shock-Loaded Fused Silica

Shot Number	Shock Pressure, kb	Refractive Index (n)		
		Interference[a] Method	Immersion[b] Method	Average
...	0	1.4579	1.4588	1.4584
R1	170	1.4894	1.4855	1.4875
R2	198	1.5180 1.5116	1.5070	1.5122
R5	140	1.4902 1.4805		1.4851
156	92 ± 2		1.4828	1.4828
157	132 ± 5	1.5109 1.5203	1.4930	1.5081
158	82 ± 2	1.4570 1.4590	1.4626	1.4595
159	81 ± 2	1.4606	1.4628	1.4617

R7	192	1.4908 1.4885 1.5147	1.4980
R8	136	1.5036 1.5122	1.5079
R9	314	1.4794	1.4794
R10	290	1.5068 1.5096	1.5082
R11	242	1.5057 1.5155	1.5106
R12	200	1.4884 1.5191	1.5038
R13	180	1.4902 1.4702	1.4802
R14	376	1.4774 1.4638	1.4706
R15	418	1.4617 1.4818	1.4718
R16	460	1.4756 1.4703	1.4730

[a] Error, ± 0.0002

[b] Error, ± 0.0010

Discussion

Figures 15 and 16 show the Hugoniot and release adiabat data for fused silica (Rosenberg et al., 1968 and Wackerle, 1962). The Hugoniot data reflect the low-pressure, mixed phase, and high-pressure regimes that McQueen et al. (1963) recognized as representing respectively, fused silica, a mixture of fused silica and a high-density phase, and the high-density phase, presumably stishovite (for example, DeCarli and Milton, 1965). Wackerle (1962) recognized the Hugoniot elastic limit (HEL) of fused silica as 98 kb; the discontinuity that he observed at 262 kb represents complete transformation to some form of the high-density phase.

Post-shock densities were calculated from the measured refractive indices of fused silica using a modified Gladstone-Dale law:

$$(n - 1)/\rho = (n_o - 1)/\rho_o \qquad (4)$$

where n, n_o, ρ, and ρ_o are the initial and final refractive indices and densities, respectively. Anderson and Schreiber (1965) have found that refractive index-density relationships of silica polymorphs are quite close ($\pm$1.5%) to the Gladstone-Dale law at low density. Specific volumes calculated from the post-shock densities range from 0.406 to 0.453 $\pm$ 0.004 cm^3/g; this range is comparable

FIGURE 15

Shock pressure-particle velocity Hugoniot and release adiabat data for fused silica (reproduced from Rosenberg et al., 1968).

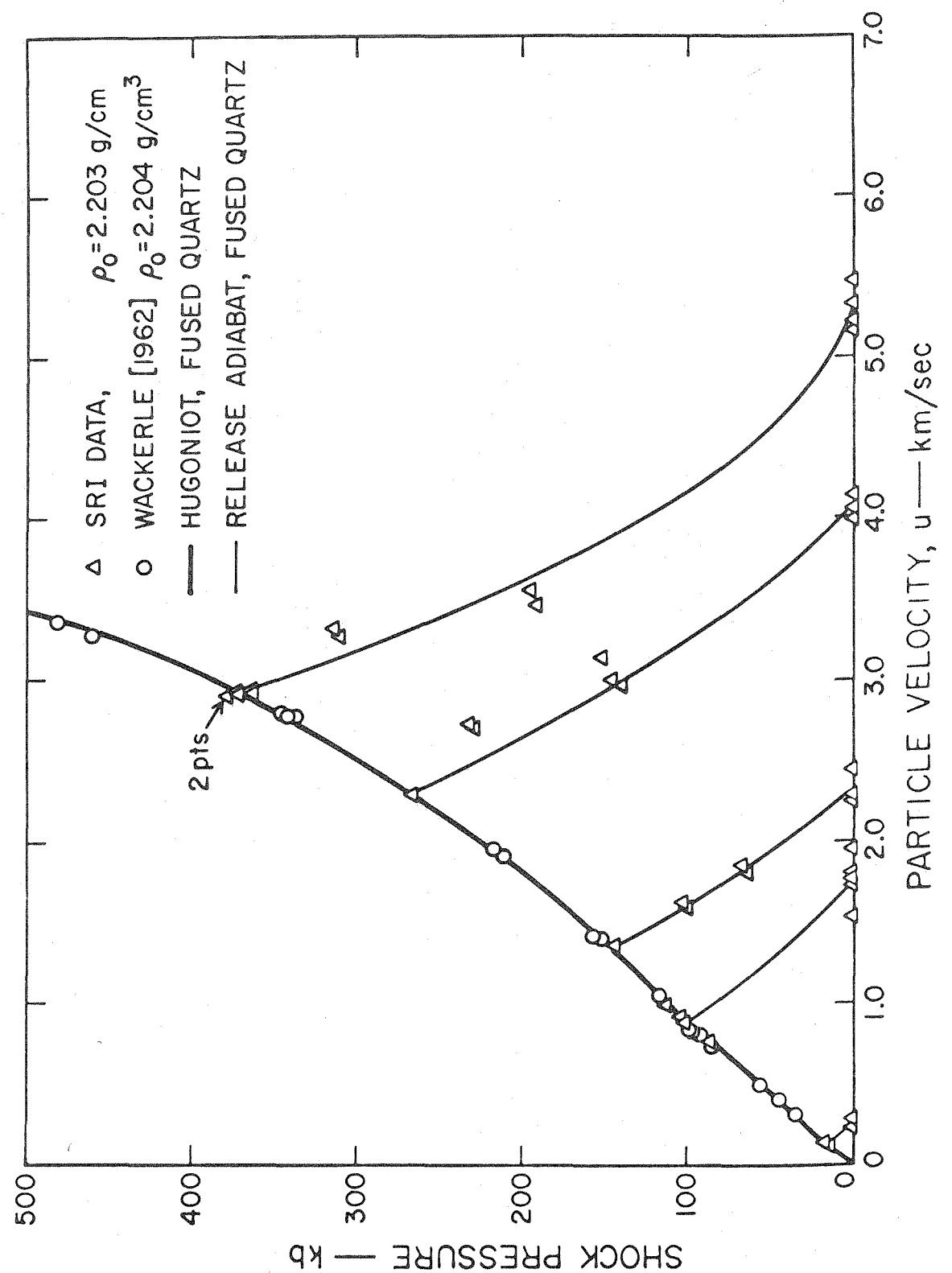
SHOCK PRESSURE — kb
PARTICLE VELOCITY, u — km/sec
0
100
200
300
400
500
1.0
2.0
3.0
4.0
5.0
6.0
7.0
Δ SRI DATA, ρ_0=2.203 g/cm
o WACKERLE [1962] ρ_0=2.204 g/cm^3
HUGONIOT, FUSED QUARTZ
RELEASE ADIABAT, FUSED QUARTZ
2 pts

FIGURE 16

Shock pressure-specific volume Hugoniot and release adiabat data for fused silica (reproduced from Rosenberg et al.,1968). Specific volumes calculated from our fused silica refractive index data for material shocked to pressures up to 460 kb according to the Gladstone-Dale law fall within the range 0.4 to 0.45 cm^3/g.

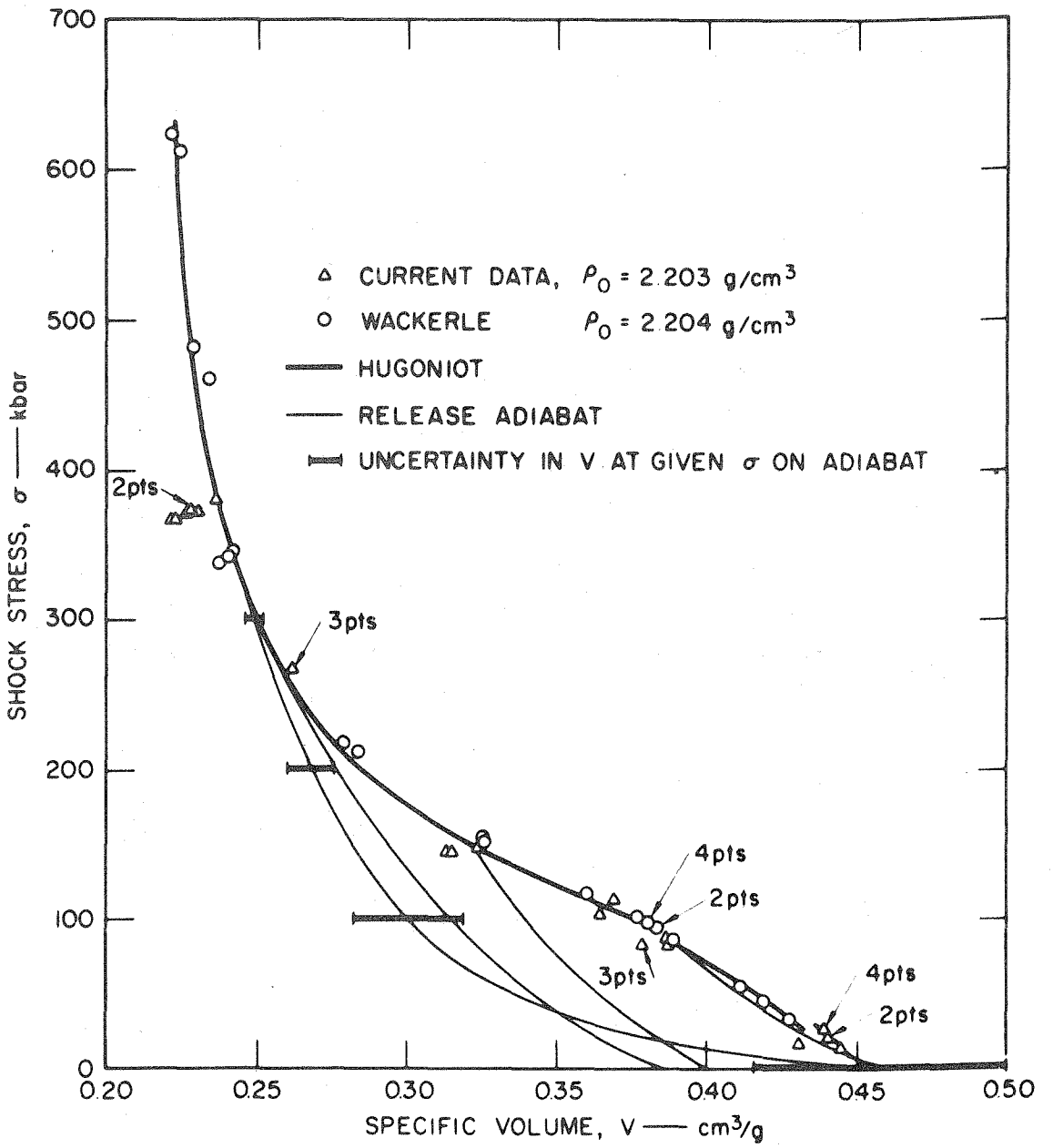
700
600
500
400
300
200
100
0
0.20
0.25
0.30
0.35
0.40
0.45
0.50
SHOCK STRESS, σ —— kbar
SPECIFIC VOLUME, V —— cm³/g
△ CURRENT DATA, ρ_0 = 2.203 g/cm³
○ WACKERLE ρ_0 = 2.204 g/cm³
HUGONIOT
RELEASE ADIABAT
UNCERTAINTY IN V AT GIVEN σ ON ADIABAT
2pts
3pts
4pts
2pts
3pts
4pts
2pts

to that of the release-adiabat specific volumes illustrated in Figure 16 (these data are tabulated in Table 4). These results indicate that there is some relationship between post-shock density and range of stability of the different phases along the Hugoniot. At peak pressure, the recovered fused silica is not irreversibly compressed to a maximum density; the final state appears to be quite dependent on the release adiabat path from the peak pressure. It is interesting that adiabatic release from the highest shock pressure, 460 kb, results in a glass of lower post-shock density, 2.27 g/cm^3, than release from 290 kb, 2.44 g/cm^3. This may arise by reconstructive transformation of a stishovite-like material to a high-density glass and subsequent annealing as a result of the higher post-shock temperature after shock-loading to 460 kb.

Besides annealing effects, the release adiabat specific volumes that correspond to the ambient pressure, post-shock temperature states will be slightly higher (by the thermal expansion) than those inferred from the room temperature refractive index data. This difference is negligible ($\approx$0.2%) on the accuracy level of the present study.

TABLE 4

Post-shock Specific Volumes of Fused Silica
(Calculated by the Gladstone-Dale Law)

Shot Number	Shock Pressure, kb	Post-shock Volume, cm^3/g	Release Adiabat[a] Volume, cm^3/g
...	0	0.454	
159	81	0.450 ± 0.001	0.454 ± 0.03
158	82	0.453	
156	92	0.431	
157	132	0.409	
R8	136	0.410 ± 0.003	0.40 ± 0.03
R5	160	0.429	
R1	170	0.427	
R13	180	0.433	
R7	192	0.418	
R2	198	0.406	
R12	200	0.413	
R11	242	0.407 ± 0.004	0.385 ± 0.03
R10	290	0.409	
R9	314	0.434 ± 0.004	0.45 ± 0.04
R1	376	0.442	
R15	418	0.441	
R16	460	0.440 ± 0.003	0.45 ± 0.04

[a] See Figure 16.

We have observed reversible compression of the silica glass to 80 ± 3 kb; this result is compatible with the dynamic HEL value observed by Wackerle (1962). A somewhat lower pressure threshold for permanent densification of less than 60 kb has been obtained by Bless (1970) in magnetic pinch experiments under rapid isentropic conditions. Arndt et al. (1971) have studied samples recovered from single shock experiments and obtained an apparent elastic limit of 55 ± 5 kb; they also observed a decrease in refractive index for fused silica shocked to pressures of 140 to 200 kb (Figure 12). In our experiments, sample shock pressures were attained through multiple shock reflection rather than single shock (the 460 kb shock of Arndt et al. (1971) was also produced by multiple shock reflection). Differences between post-shock temperatures calculated for the two techniques are illustrated in Table 5, compared with those calculated by Wackerle (1962) for single shock experiments on the basis of different assumptions about release adiabats.

As stated above, the tektite and soda-lime glasses are modifications of fused silica caused by the addition of larger network-modifying cations to the silica tetrahedra; the elastic limits and permanent compressibilities of the glasses should be lower than those of fused silica

because of the effects of such cations on the stability of the glass structural network of silica (plus alumina for the tektite and soda-lime) polyhedra. Our results do show the elastic limit (here taken to mean the peak pressure of no irreversible compaction) to be 40 $\pm$ 5 kb for each of these glasses. Dremin and Adadurov (1964) observed a dynamic elastic limit (HEL) ranging from 36 to 73 kb, depending on sample thickness, for a soda-lime glass of only slightly different composition from ours; the data are obviously compatible.

The permanent densification observed for those glasses above their elastic limits may represent compaction like that observed under isothermal static compression by Bridgman and Simon (1953) and others. It is probably equivalent to the proportion of the shock compression that has become locked in upon adiabatic release of the shock-loaded glass to zero pressure. Right here it is legitimate to ask if some of this shock-produced irreversible densification is due to the formation of a high density crystalline phase, since the peak pressures are within the mixed-phase regimes of the respective Hugoniot equations of state. No such phase has been detected either optically or with standard Debye-Scherrer x-ray diffraction. However, a very small amount of stishovite has been detected in the fused silica

using x-ray powder-diffraction on chemically treated recovered glass (Kleeman and Ahrens, 1973). Such a small amount is not sufficient to be detected in refractive index measurements or to affect the refractive indices within the errors of the measurements. The behaviors of the fused silica and soda-lime glass at pressures above 140 and 80 kb, respectively, are similar. Although the post-shock specific volumes calculated for fused silica are compatible with release-adiabat data (Figure 16 and Rosenberg et al., 1968), the double-valued nature of the refractive index-pressure graphs of those two glasses does warrant discussion.

For the soda-lime glass one explanation is that the refractive index decrease above 80 kb is an annealing effect of high shock and post-shock temperatures. Ahrens et al. (1970) calculated these temperatures for this particular soda-lime glass to pressures of 100 kb; the maximum calculated temperature increase was only 55°C at 80 kb. However, the release adiabat data for fused quartz suggest that those calculated temperatures may be an extreme lower bound to the actual post-shock temperatures reached as a result of the shock-loading. Chao and Bell (1968) and Bell and Chao (1969) have carried out experiments on the annealing effects of high temperatures on shock and statically densified silicate glasses and found

that temperatures on the order of 500°C and more are required to anneal feldspar glasses in times of a few seconds. Therefore, it can be concluded that: (1) annealing is not a principal mechanism causing the refractive index decrease or (2) the high shock pressure has a large undetermined effect on the temperature required to anneal the glass or (3) the temperatures calculated by Ahrens et al. (1970) do not adequately represent the achieved temperatures, and the actual post-shock temperatures are sufficient to anneal the glass. A combination of (2) and (3) may be the most reasonable answer.

For fused silica, more consideration of the behavior of refractive index at high pressure must be given to the pressure range of 140 to 300 kb, which is represented by almost a plateau in refractive index. This pressure range is essentially within the mixed-phase regime of the silica Hugoniot; if a mixture of the low pressure fused silica phase and the high pressure stishovite-like phase persisted after pressure release, we should expect a continuous increase in refractive index for pressures to 300 kb. However, if the high pressure phase relaxed to a low density glass by adiabatic release and post-shock annealing, we should expect an averaging of the refractive indices of a severely compacted low pressure phase material and a low density glass; the result could

be the index plateau we observe. Since no stishovite was observed in optical microscopic studies and in standard x-ray powder diffraction using 114.6 mm Debye-Scherrer techniques and only an insignificant fraction of a percent was detected using x-ray diffraction on chemically concentrated samples (Kleeman and Ahrens, 1973), it may be assumed that adiabatic release of the shock-loaded silica resulted in almost complete relaxation of the transformed material to a low density glass, thus giving the described averaging effect. The sharp drop in refractive index of fused silica shocked to pressures between 300 and 310 kb, as well as the low refractive indices measured on fused silica shocked to higher pressures, may be caused by post-shock temperatures reaching annealing temperatures of silica glass at those pressures. Thus, shock-loading to 300 kb or greater transforms the low pressure phase tetrahedrally coordinated silica network to a high pressure phase 6-fold coordinated network which decompresses after pressure release to a low density glass of 4-fold coordinated silica containing a fraction of a percent of crystalline high pressure phase stishovite.

Post-shock Temperatures

The Hugoniot and release adiabat data in Figures 15 and 16 have been used to calculate post-shock temperatures for fused silica shocked to states in the 100 to 500 kb pressure range. Temperatures have been calculated for both multiple-shock reflection-type experiments (case 1 of Table 5 and Figure 17) and single shock experiments (case 2 of Table 5 and Figure 17).

For case 2 we assume the net thermal energy resulting from shock compression followed by adiabatic release is given by

$$E_2 = \int_{298^\circ K}^{T^\circ K} C_p dT \qquad (5)$$

which equals the difference between the shock energy given by the Rankine-Hugoniot equation

$$E_S = (\tfrac{1}{2})(P + P_o)(V_o - V) \qquad (6)$$

and the adiabatic release energy

$$E_R = - \int_{V_o'}^{V} PdV \qquad (7)$$

In those equations, P_o and V_o represent initial pressure and specific volume respectively, V is specific volume at peak pressure, P, T is post-shock temperature in

FIGURE 17

Calculated post-shock temperatures in silica. A(case 1): for multiple-shock reflection-type shock-loading. B(case 2): for single-shock type shock-loading. C: from Wackerle (1962). (This is a plot of the data in Table 5).

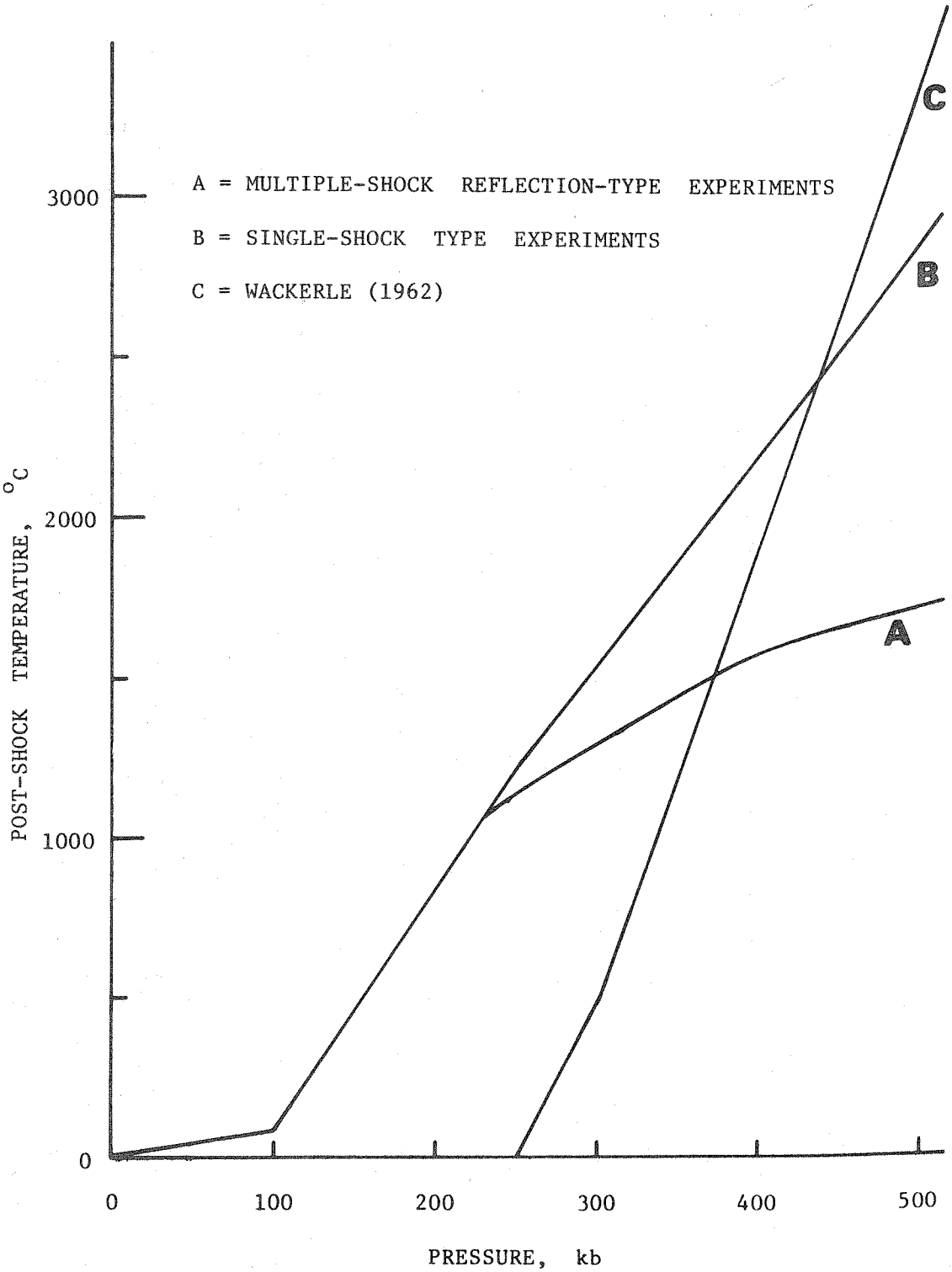
A = MULTIPLE-SHOCK REFLECTION-TYPE EXPERIMENTS
B = SINGLE-SHOCK TYPE EXPERIMENTS
C = WACKERLE (1962)
A
B
C
POST-SHOCK TEMPERATURE, °C
0
1000
2000
3000
0
100
200
300
400
500
PRESSURE, kb

TABLE 5

Post-shock Temperatures of Fused Silica
(Calculated Using the Hugoniot and Release Adiabat Data in Figure 16)

Shock Pressure, kb	Case 1[a]		Case 2[b]		
	E_1 Thermal Energy, cal/mole	T, °C	E_2 Thermal Energy cal/mole	T, °C	T, °C[c]
100	650	80	650	80	0
150	5,720	450	5,720	450	0
250	18,070	1170	19,050	1220	0
300	19,830	1260	23,920	1480	470
400	26,200	1590	38,610	2180	1860
500	28,340	1700	53,690	2820	3310

[a] For multiple-shock reflection-type experiments.

[b] For single-shock type experiments.

[c] Post-shock temperatures from Wackerle (1962).

degrees Kelvin, C_p is the specific heat of fused silica at constant pressure, and V_o' is the post-shock volume.

For case 1, numerous reverberations of the shock pulse across the sample add successively smaller increments to the initial sample pressure until peak pressure is reached (Figure 7). As a result the total shock energy is given by

$$E_S = \tfrac{1}{2} \sum_{k=0}^{\infty} (P_{k+1} + P_k)(V_k - V_{k+1}) \qquad (8)$$

The states P_k, V_k, $(k \neq 0)$ represent the series of shock pressures and specific volumes achieved along the infinite series of Hugoniots centered at states P_{k-1}, V_{k-1} that are achieved via shock wave reverberation in the sample. The total shock energy for case 1 is less than the total shock energy for case 2. Assuming that the fused quartz-stishovite phase change occurs reversibly (as is certainly closely valid in the present experiments), the net thermal post-shock energy is given by

$$E_{1 \text{ or } 2} = \int_{298^\circ K}^{T^\circ K} C_p dT = E_S - E_R \qquad (9)$$

where E_S is given by equations 8 and 6 for cases 1 and 2. The energy term corresponding to the work done against

ambient pressure on expansion from 298°K to T is negligible. Numerical integration of equation 9 for post-shock energies yields the values given in Table 5. The empirical formula for the molal heat-capacity equation of fused silica

$$C_p \text{ (cal/mole } ^\circ\text{K)} = 13.38 + 3.68 \times 10^{-3}T - 3.45 \times 10^{5}T^{-2} \qquad (10)$$

given by Kelley (1960) is used in equation 9 to yield the post-shock temperature given in Table 5. Uncertainties in E_R reflecting the uncertainties in the adiabats give rise to errors in the calculated post-shock temperatures of ≈10% at low pressures, ranging to ≈20% at 500 kb.

The post-shock temperatures calculated by Wackerle (1962) for single-shock experiments are much lower than those we have calculated for pressures up to 300 kb but are comparable to our single-shock temperatures at higher pressures. The differences in the calculated results arise to a minor degree from Wackerle's assumption of a constant specific heat C_v and constant $(\partial P/\partial E)_v$; in addition, Wackerle ignored the elastic compressions and performed numerical integration along extrapolated 'equilibrium' curves. However, the major factor producing the differences in post-shock temperature is our use

of the new release adiabat data in Figure 16. Since below 300 kb the actual release curves lie below the Hugoniot rather than above, as is implicit in Wackerle's formulation, the differences in T are great at the lower pressures. At much higher pressures the assumptions in Wackerle's calculation should, within the present state of our knowledge, be approximately valid.

On the basis of annealing studies on fused silica, Arndt et al. (1971) have found that temperatures of 300°C have a significant effect on the relaxation of densified fused silica. Therefore, in view of our calculated temperatures, annealing could play a major role in causing the drop in refractive index of fused silica shocked to 300 kb and higher pressures.

Conclusions

1. Variation in the percentage of network-forming polyhedra of silica and alumina affects the threshold of densification and the maximum permanent compression that may result from shock-loading. The Hugoniot elastic limit is compatible with the threshold of permanent densification.

2. Post-shock annealing may be a mechanism for the relaxation of high density silicate glasses to low density glasses for material shocked to below 150 kb. It is almost certainly a factor for shock pressures above this level.

3. Partial transformation of the low pressure phase of fused silica to a high pressure stishovite-like phase followed by adiabatic release and almost 100% recovery to a low density glass probably occurs for shock compressions up to ≈300 kb. Above this pressure, annealing at high post-shock temperatures of completely transformed material can account for the low density glass that is recovered.

4. Despite the double-valued nature of the soda-lime and fused silica refractive index versus shock pressure relations (Figures 13 and 14), if the pressure regime of naturally shocked glasses can be determined by other means, our data should be useful

in interpreting pressure and temperature histories of those glasses.

Chapter IV.

A SPECTROGRAPHIC INTERPRETATION OF THE SHOCK-PRODUCED COLOR CHANGE IN RHODONITE ($MnSiO_3$): THE SHOCK-INDUCED REDUCTION OF Mn(III) TO Mn(II)..... 87

Abstract

Samples of rhodonite ($MnSiO_3$-pyroxenoid from Franklin, New Jersey) have been shock-loaded to pressures up to 496 kilobars. Spectroscopic studies of five recovered samples show a decreasing Mn^{3+} content upon recovery from successively higher shock pressures; after shock-loading to 496 kb, the Mn^{3+} has essentially disappeared. No corresponding change in the optical spectrum results from heating rhodonite to 1250°C for 3.5 hours in a reducing atmosphere. Rhodonite heated to 1360° under the same conditions melts incongruently to manganese-rich glass and silica with disappearance of the 540 nm Mn^{3+} absorption band. The color change in the shocked rhodonite arises from irreversible reduction of Mn^{3+} during high shock pressures and possible high shock temperatures. It is suggested that Mn^{3+} is reduced to Mn^{2+} by water present in the sample during the shock event.

Introduction

Rhodonite ($MnSiO_3$, variety fowlerite, from Franklin, New Jersey) has a characteristic pink color. During optical microscopic and x-ray diffraction studies performed while attempting to characterize shock-induced phase changes in this rhodonite, it was observed that this color was not present in intensely shocked samples (Gibbons, 1972). Absorption spectra of several specimens, both shocked and unshocked, were measured to determine what optically apparent physical or chemical change was occurring as a result of the shock wave experiments (Gibbons et al., 1974).

The characteristic color of this variety of rhodonite is caused by a prominent absorption band in the visible region of the spectrum at 540 nm due to an electronic transition in Mn^{3+}. This absorption band decreases in intensity with increasing shock pressure and disappears by 496 kb.

A series of experiments have been performed to determine the shock pressures required to cause this phenomenon, and to obtain spectroscopic information on the effect of the high shock pressure event upon the manganese in the samples.

Experimental Procedures

A specimen of coarsely crystalline rhodonite (analysis in Table 6) was sawn into slabs, parallel to (001), from which several discs 4.75 mm in diameter were cored and prepared for shock recovery experiments. The discs were placed in stainless steel 304 sample containers for shock-loading. The experimental conditions and results of the shock-loading experiments are summarized in Table 7. The accuracy of the shock pressures is $\pm$ 3% at lower pressures and $\pm$ 6 kb at pressures above 200 kb.

Five samples were recovered, and hand ground and polished to approximately 0.15 mm thickness for spectroscopic studies. This preparation was made very difficult in the lower pressure specimens because of the pervasive shock-induced fracturing and crushing. The two higher pressure specimens were recovered as more compact discs, especially the 496 kb sample, and were much easier to grind and polish, not spalling and pulling apart so readily and much less fragile.

Optical absorption spectra were obtained on those samples between 300 and 2500 nm on a Cary 17I spectrophotometer. Infrared spectra were obtained with a Perkin-Elmer model 180 infrared spectrophotometer. For further characterization all specimens were studied by

optical microscopy; the highest pressure specimen was also x-rayed using standard Debye-Scherrer techniques to confirm the partial vitrification. The fraction x-rayed was completely x-ray amorphous.

TABLE 6

Analysis* of Rhodonite from Franklin, New Jersey

Oxide	Weight %
SiO_2	46.94
MnO[b]	37.18
CaO	6.09
ZnO	5.72
MgO	1.93
FeO[a]	1.86
Al_2O_3	0.06
K_2O	0.03
	99.81

* Average of analyses made on two fragments by A. Chodos using the California Institute of Technology electron microprobe, May 26, 1972.

[a] Total Fe as FeO.

[b] Total Mn as MnO. The concentration of Mn^{3+} calculated on the basis of sample thickness = 0.075 cm, absorbance of the 540 nm Mn^{3+} band = 0.3, and ϵ = 20 is 0.3%. The ϵ value was estimated from known values of Mn^{3+} absorbance in $Mn(H_2O)_6^{3+}$ and $Mn(oxalate)_3$ (Dingle, 1966), and tourmaline (Manning, 1973).

TABLE 7

Experimental Conditions For Rhodonite Recovery Shots

Shot Number	Flyer[a] Plate (on Lexan)	Sample Container	Sample Thickness, mm	Impact Velocity, m s^{-1}	Peak Shock Pressure, kb
114	W	S.S.304[b]	0.675	1572	496
151	W	S.S.304	0.625	1284	390
198	W	S.S.304	0.5	750	210
196	S.S.304	S.S.304	0.5	658	132
195	Al 2024	S.S.304	0.5	674	78

[a] 2.5 mm thick tungsten (W), stainless steel 304 (S.S.304), and aluminum 2024 (Al 2024) flyer plates

[b] Stainless steel 304, 3/4" diameter

Optical Spectra

The optical spectrum of an unshocked rhodonite specimen (Figure 18, spectrum A) shows, within the infrared, a weak band at about 2300 nm, a more intense band at 1530 nm, and the dominant band at 1035 nm. In the visible-ultraviolet prominent bands occur at 540 nm and 345 nm, with less intense shoulders at 360 nm and 440 nm. A second component at 411 nm appears on the 408 nm band, which in turn is a closely spaced doublet.

The optical spectrum of a rhodonite recovered from shock-loading to 496 kb (Figure 18, spectrum B) displays a relatively sharp asymmetric band at 418 nm and a very weak band at 520 nm. The 540 nm band has disappeared completely. The near-infrared region now has a much broader absorption band with a maximum in the vicinity of 1035 nm; the 1530 nm band has also disappeared. New features in the 2230-2450 nm and 1710 nm regions arise from organic materials used in preparation of the recovered sample. All features are superimposed upon a background, steadily rising towards the ultraviolet, which results from scattering from the pervasively internally-shattered specimen recovered from the shock experiment.

The 540 nm band, which is attributed to Mn^{3+} (see below), decreases in intensity at shock pressures above

210 kb. In the spectra of samples shocked to pressures from 78 to 210 kb, the area of the Mn^{3+} band remained essentially unchanged, whereas at 390 kb it was about two-thirds as great as it was at 210 kb, and by 496 kb it had disappeared completely revealing the band at 520 nm (Figure 19).

Other changes in the spectra involve the character and position of the set of sharp bands near 408 nm attributable to Mn^{2+}. In the standard sample and those shocked to pressures from 78 to 210 kb, the band system remains split indicating crystalline order in the mineral and distortion of the multiple Mn^{2+} sites away from regular octahedral geometry. This splitting, which appears as a series of well-resolved, closely-spaced bands on the low energy side of the 408 nm band in expanded scale spectra, is too small to be resolved at the scales of Figures 18 and 19. In the 390 kb and 496 kb samples, no appreciable splitting is observed, probably because of disorder and partial vitrification of those specimens produced by the shock process. The shift of the band to 420 nm in the 496 kb sample may be another indicator of its vitrification; in the other samples it stays at 408 nm. The 496 kb sample was found to be predominantly optically and x-ray amorphous.

FIGURE 18

Absorption spectra of rhodonite. A = spectrum of unshocked sample. B = spectrum of sample shocked to 496 kb. The Mn^{3+} absorption bands occur at 540 nm and 1530 nm. The intense band at 1035 nm is due to Fe^{2+}; the bands between 340 and 450 nm are due to Mn^{2+}.

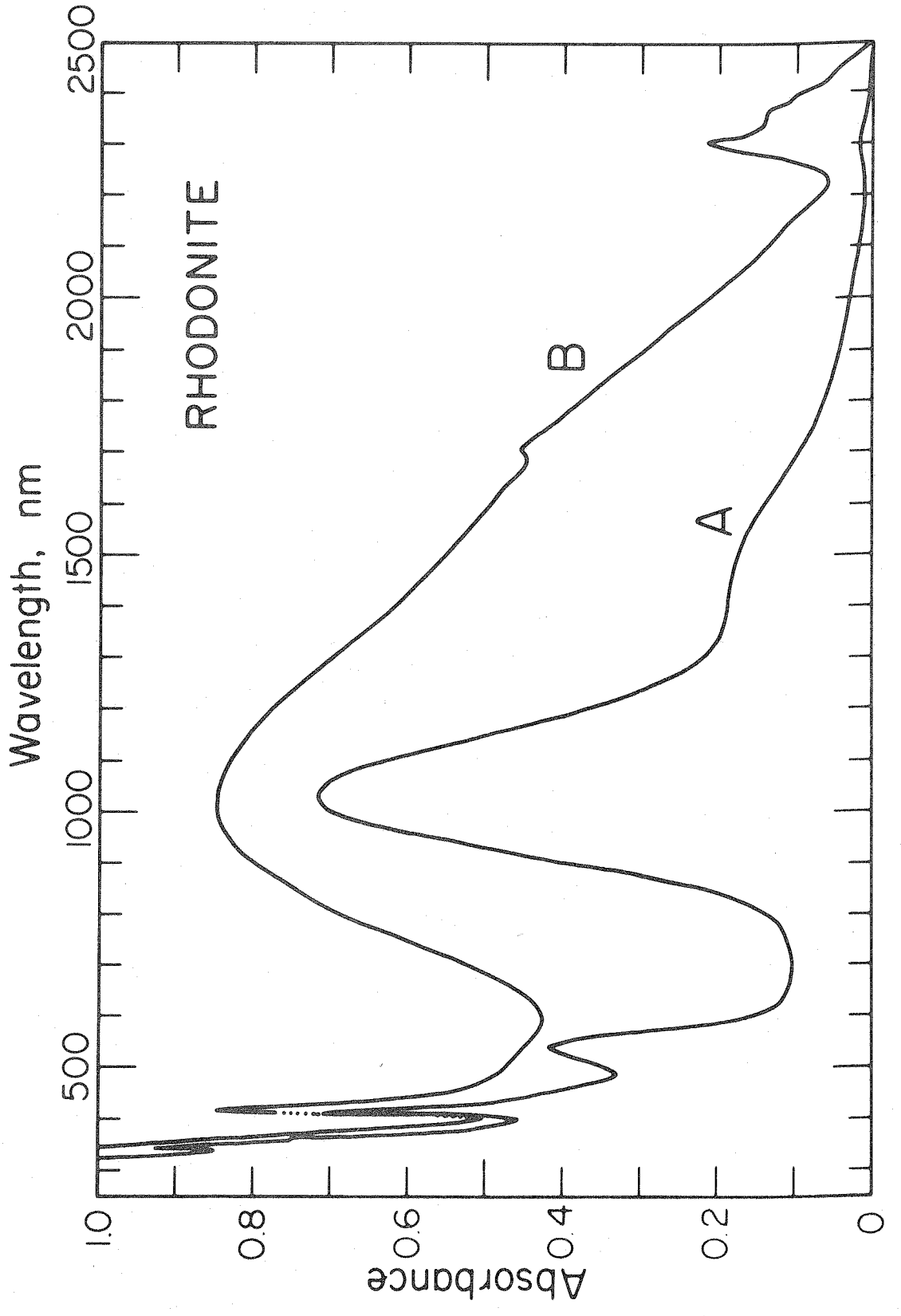
RHODONITE
B
A
Wavelength, nm
500
1000
1500
2000
2500
Absorbance
1.0
0.8
0.6
0.4
0.2
0

FIGURE 19

Rhodonite spectra. The spectra of three samples recovered after being shock-loaded to 210, 390, and 496 kilobars are compared with the spectrum of an unshocked rhodonite (A) showing the loss of the Mn^{3+} band at 540 nm in the more intensely shocked samples. These spectra have been normalized to represent the absorbance of a sample of 0.15 mm thickness but have been drawn with vertical displacement in absorbance for purposes of contrast and clarity.

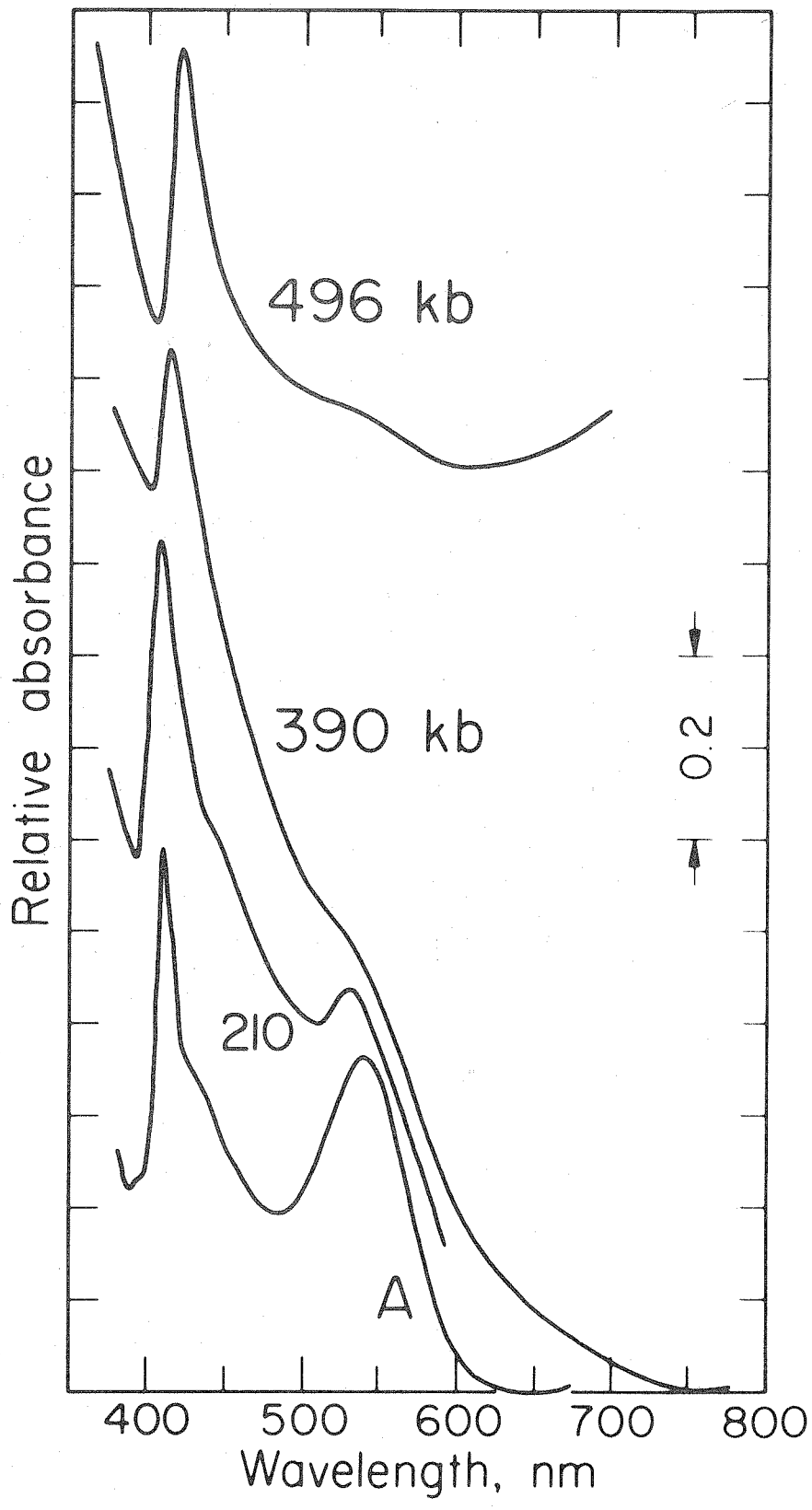
496 kb
390 kb
210
A
0.2
Relative absorbance
400
500
600
700
800
Wavelength, nm

Assignment

Peacor and Niizeki (1963) describe the crystal structure of rhodonite as planes of octahedrally coordinated cations alternating with planes of tetrahedrally coordinated Si-ions between planes of close-packed oxygens. In each unit cell there are four distorted octahedral sites available for the manganese cations, and a fifth site of irregular seven-coordination which calcium preferentially fills.

The assignment of the spectral features to Mn^{3+}, Mn^{2+}, and Fe^{2+} follows well-established assignment schemes for these ions in other systems. Divalent iron in orthopyroxenes produces two absorption features in the near-infrared, a strong band near 1000 nm in α-polarization and a weaker band near 1900 nm in β-polarization (Bancroft and Burns, 1967). Analogous ferrous iron features appear in the spectra of manganese pyroxenes and pyroxenoids. In the spectrum of pyroxmangite (Figure 1, Manning, 1968) we assign to Fe^{2+} the bands labelled 9800 and 4750 cm^{-1} (1020 and 2105 nm) and, in the case of our rhodonite, the band at 1035 nm. The low energy Fe^{2+} band is not pronounced in the rhodonite orientation shown here. However, in the spectrum of a rhodonite from Broken Hill, New South Wales, Australia, of higher relative iron concentration, low Mn^{3+} concentration, and greater thickness (not illustrated), a feature assignable to the low energy

Fe^{2+} band occurs at 2280 nm. A weak feature can be seen in the New Jersey rhodonite spectrum in the vicinity of 2300 nm. The most intense of the Fe^{2+} spin-forbidden bands occurs at about 500 nm in orthopyroxenes and can be seen at 506 nm in the Broken Hill rhodonite spectrum in both our spectrum and that reported by Keester and White (1966). Its intensity is too low to be important in the New Jersey rhodonite.

The Mn^{2+} spectrum in rhodonite has been reported previously by Keester and White (1966) and Manning (1968). We agree with their choice of an octahedral symmetry to assign the spectra and with their assignment of the 408 nm system to the $^6A_1 \rightarrow (^4A_1, {}^4E)$ transition and the 440 nm band to the $^6A_1 \rightarrow {}^4T_2$ transition of Mn^{2+}. However, we do not agree with the assignment of the 540 nm band to the $^6A_1 \rightarrow {}^4T_1$ transition, but instead will show below that the 540 nm band is properly assigned to Mn^{3+}. The remaining Mn^{2+} transition, $^6A_1 \rightarrow {}^4T_1$, which is expected to have an intensity comparable to the $^6A_1 \rightarrow {}^4T_2$ 440 nm band, is instead assigned to the band at 520 nm which appears in the shocked samples. This band is analogous to the 514 nm band in rhodonite from which Mn^{3+} has been removed thermally. The same band is observed as a shoulder on the 540 nm band in Keester and White's (1966) spectrum.

The remaining two important bands at 540 and 1530 nm are attributed to Mn^{3+}. In Jahn-Teller distorted octahedral oxygen environments, Mn^{3+} has a prominent absorption band in the 470-560 nm region (Dingle, 1966; Burns, 1970; Burns and Strens, 1967; and Davis et al., 1968), with which we associate the 540 nm rhodonite band. The low energy absorption feature arising from the transition between the components of the Jahn-Teller split ^5E_g state can appear over the range of 5000 to 20,000 cm^{-1} (Davis, et al., 1968). We assign the 1530 nm rhodonite band to this transition because (1) its intensity is not correlated with the intensity of the 1035 nm Fe^{2+} band, (2) it is qualitatively correlated with the Mn^{3+} band (in low Mn^{3+} material, the intensity of the 1530 nm band is too low to provide meaningful quantitative data) and (3) it disappears along with the 540 nm Mn^{3+} band upon shock-loading.

Discussion

Trivalent manganese is lost in rhodonite after shock-loading to high pressures.

Burns (1970), in an outline of crystal field theory, briefly describes the Jahn-Teller effect on certain transition metal ions. In summary, if the distribution of electrons in the d-orbitals of a transition metal ion is such that the ground state is degenerate, the coordination polyhedra will distort spontaneously to remove the degeneracy and make one energy level more stable (Jahn and Teller, 1937). High spin Mn^{3+} with d^4 electronic configuration is susceptible to such distortion and the Mn^{3+} ion is stabilized in distorted octahedra. Conversely, Mn^{3+} is less stable in a regular octahedral site and in this environment will have a tendency to oxidize or reduce to the more stable electronic configurations of Mn^{4+} or Mn^{2+}. From the crystal structure of rhodonite it is known that all cation sites are distorted from octahedral symmetry so that Mn^{3+} could be stabilized in all five sites. Pressures and temperatures produced by shock-loading to more than 210 kb are probably sufficient to affect the regularity of the manganese octahedra. Any destruction of crystalline order probably increases the regularity of the octahedra and decreases the stability of the Mn^{3+} ions. Hence, Mn^{3+} could be reduced to Mn^{2+}

as a result of shock-loading to very high pressures. The alternative of oxidation to Mn^{4+} is not considered further since, concurrent with the loss of the Mn^{3+} spectrum, there is not the growth of a $Mn^{4+}(d^3)$ spectrum whose (spin-allowed) intensity would be expected to be comparable to that of the Mn^{3+} being lost.

The effect of temperature alone must be considered since appreciable increases in sample temperature accompany the shock-loading. In order to determine this effect, two samples were heated to 1250°C and 1360 °C respectively; this is below and above the peritectic melting point of 1291°C. Each sample was held for 3.5 hours in a reducing atmosphere of 99% argon and 1% H_2 at atmospheric pressure. The 1250°C sample was cooled to room temperature in about 1 hour; the other was quenched more rapidly in about 15 minutes.

The spectra of the standard and the 1250°C sample are compared in Figure 20. There is only a small change in the relative intensities of the Mn^{2+} and Mn^{3+} bands and essentially no color change in the sample. Heating to 1250 °C for 3.5 hours does not appreciably affect the oxidation state of the manganese in rhodonite.

The spectra of the standard and the 1360°C sample are contrasted in Figure 21 . The 540 nm Mn^{3+} band is not present. Since the melting was done in a reducing

FIGURE 20

Rhodonite spectra. A = spectrum of unshocked sample shown in Figure 18. B = spectrum of unshocked rhodonite specimen which was held at 1250°C for 3.5 hours showing that the Mn^{2+} band at 408 nm and the Mn^{3+} band at 540 nm are present in both spectra. (The incongruent melting point of rhodonite is 1291°C).

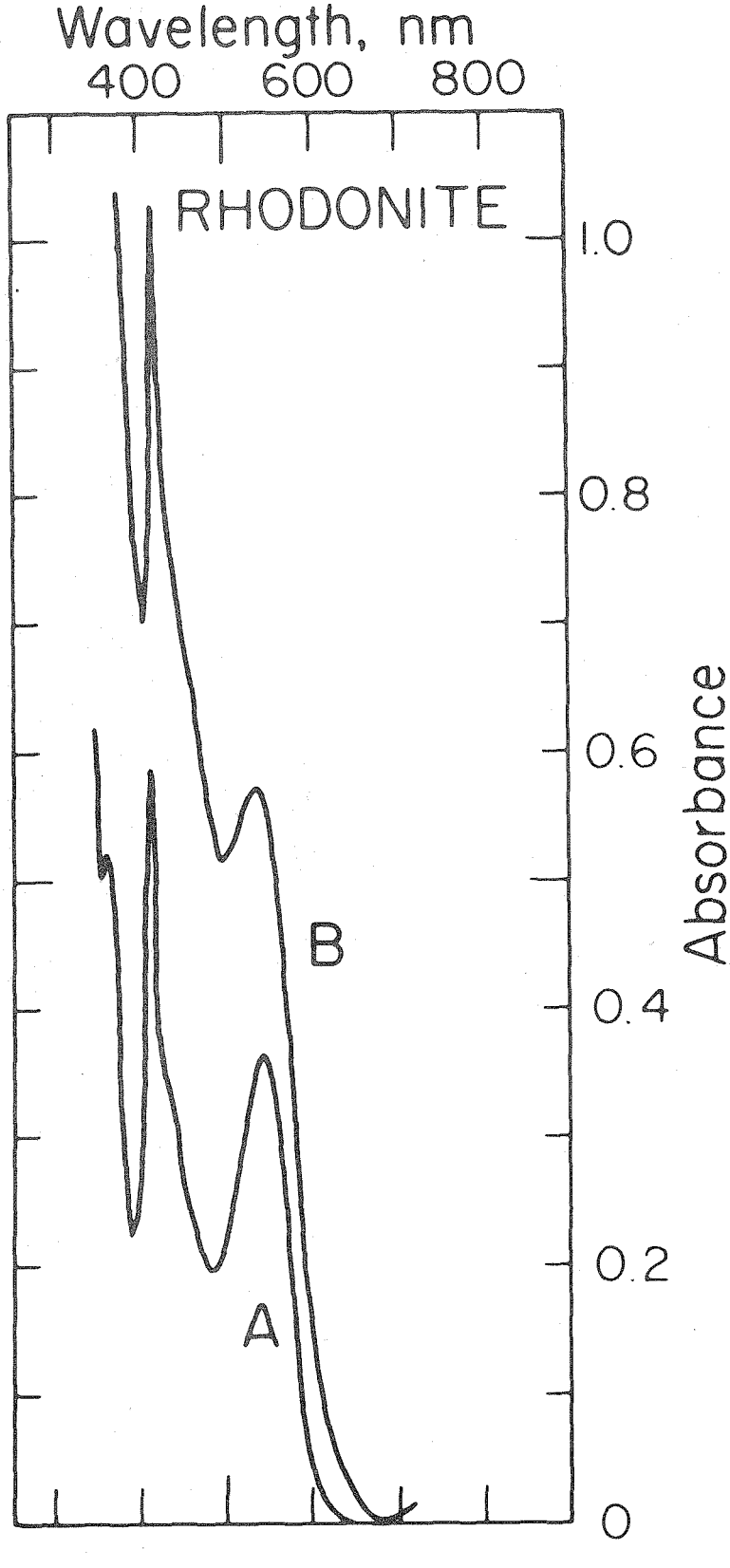
Wavelength, nm
400
600
800
RHODONITE
1.0
0.8
0.6
0.4
0.2
0
Absorbance
B
A

FIGURE 21

Rhodonite spectra. A = spectrum of the unshocked sample shown in Figure 18. B = spectrum of an unshocked rhodonite specimen which was held at 1360°C for 3.5 hours showing the disappearance of the Mn^{3+} band at 540 nm and the presence of a band at 514 nm which is assigned to the $^{6}A_{1g} \rightarrow {}^{4}T_{1g}$ electronic transmission in Mn^{2+}.

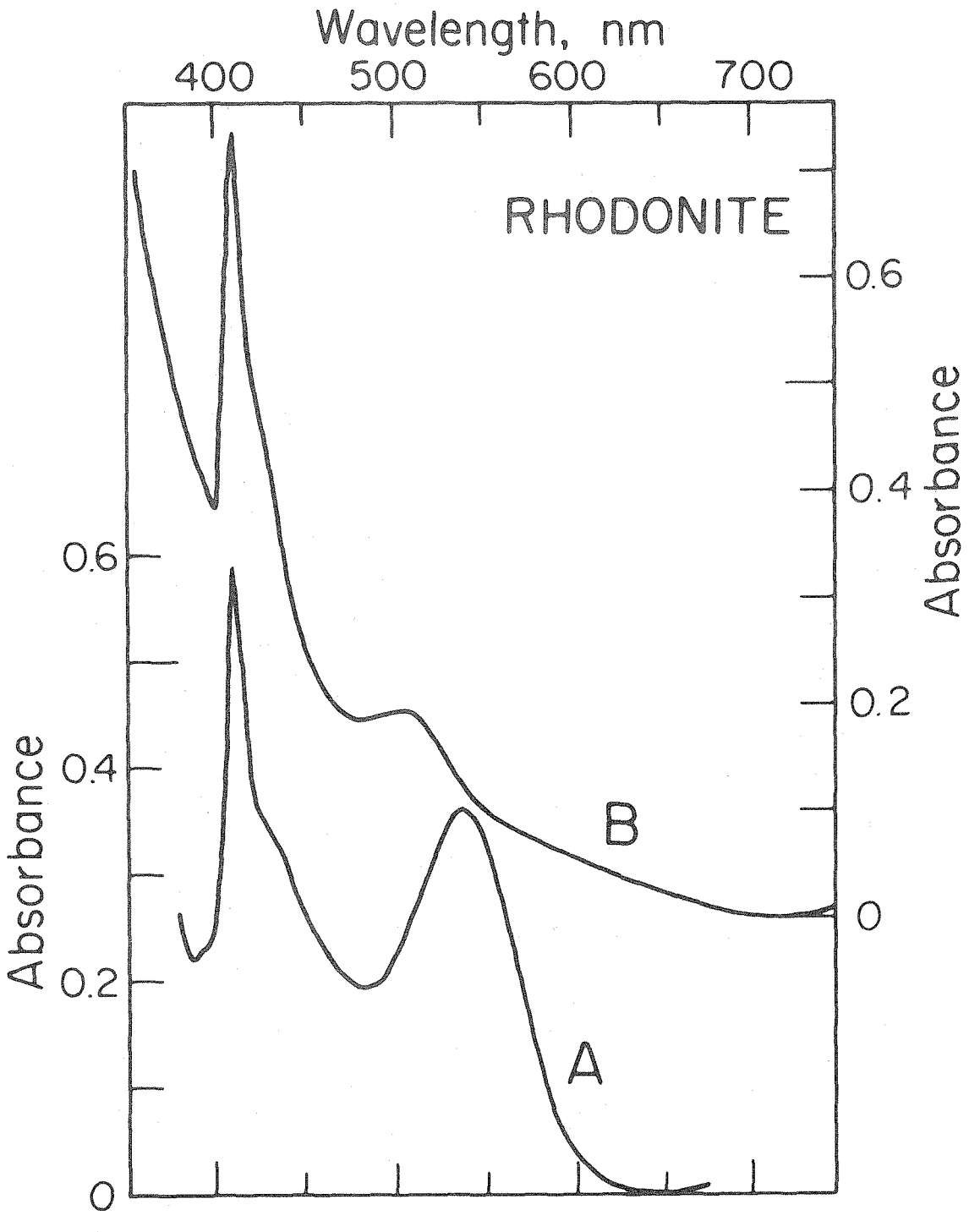
Wavelength, nm
400
500
600
700
RHODONITE
B
A
Absorbance
0
0.2
0.4
0.6
Absorbance
0
0.2
0.4
0.6

atmosphere, the Mn^{3+} was probably reduced to Mn^{2+}. The feature at 514 nm in the spectrum of the heated sample is assigned to $^6A_1 \rightarrow {}^4T_1$ transition in Mn^{2+}. Since the melted sample, which is a quenched multicrystalline assemblage, will not retain the exact same environment about the manganese ions as exists in rhodonite, the positions and intensities of the spectroscopic bands are expected to differ from those of rhodonite. The spectrum of the melted sample in the 400-470 nm region nevertheless bears considerable similarity to the rhodonite spectrum and suggests that there should be a Mn^{2+} band in the vicinity of 510-520 nm in rhodonite. In fact, a weak shoulder at 520 nm has been observed on the 540 nm Mn^{3+} band in the spectra of shocked and unshocked rhodonites.

Reduction of transition metal ions with increasing pressure has been observed in at least two other instances. Drickamer et al. (1970, 1972) have observed a reversible reduction of Fe^{3+} to Fe^{2+} in a variety of compounds and Burns et al. (1972) have reported similar $Fe^{3+} \rightarrow Fe^{2+}$ reduction in a synthetic ferric amphibole, using static compression apparatus. Production of Mn^{2+} from Mn^{3+} in $CaCO_3$ by high temperatures has been observed by Low and Zeira (1972) in ESR spectral studies by heat-treating aragonite and transforming it to calcite. Mn^{3+} is stabilized in the aragonite but unstable in the more

regular calcite structure.

Drickamer proposes that Fe^{3+} is reduced to Fe^{2+} by transfer of electrons form nonbonding ligand orbitals to metal 3d antibonding orbitals. Low and Zeira believe that the electrons required for the Mn^{3+} to Mn^{2+} reduction in $CaCO_3$ may originate from a charge compensating cation or by release from structural vacancies as a result of higher temperatures.

In analogy to Drickamer's (1970) proposal, a possible source of electrons would be the oxygen ligands of the Mn^{3+}. One is then faced with the difficulty of accounting for the fate of the electron-deficient oxide, which tends to be highly unstable. A more reasonable source of electrons would be the charge-compensating cations, in particular Fe^{2+}. The reaction $Fe^{2+} + Mn^{3+} \rightarrow Fe^{3+} + Mn^{2+}$ is feasible since divalent iron is present at greater concentrations than the trivalent manganese. We prefer another hypothesis, however, discussed below. We also rule out the possibility that electrons trapped in crystal defects could be present in anywhere near the quantity needed to reduce the estimated 0.3% Mn^{3+} (see Table 6).

Infrared spectroscopic studies (Figure 22) show that the unshocked rhodonite contain both a trace of isolated hydroxyl groups and a greater amount of molecular water.

FIGURE 22

Infrared absorption spectra of rhodonite slabs. A = after shock-loading to 496 kb, 0.315 mm thick. B = before shock-loading, 0.505 mm thick.

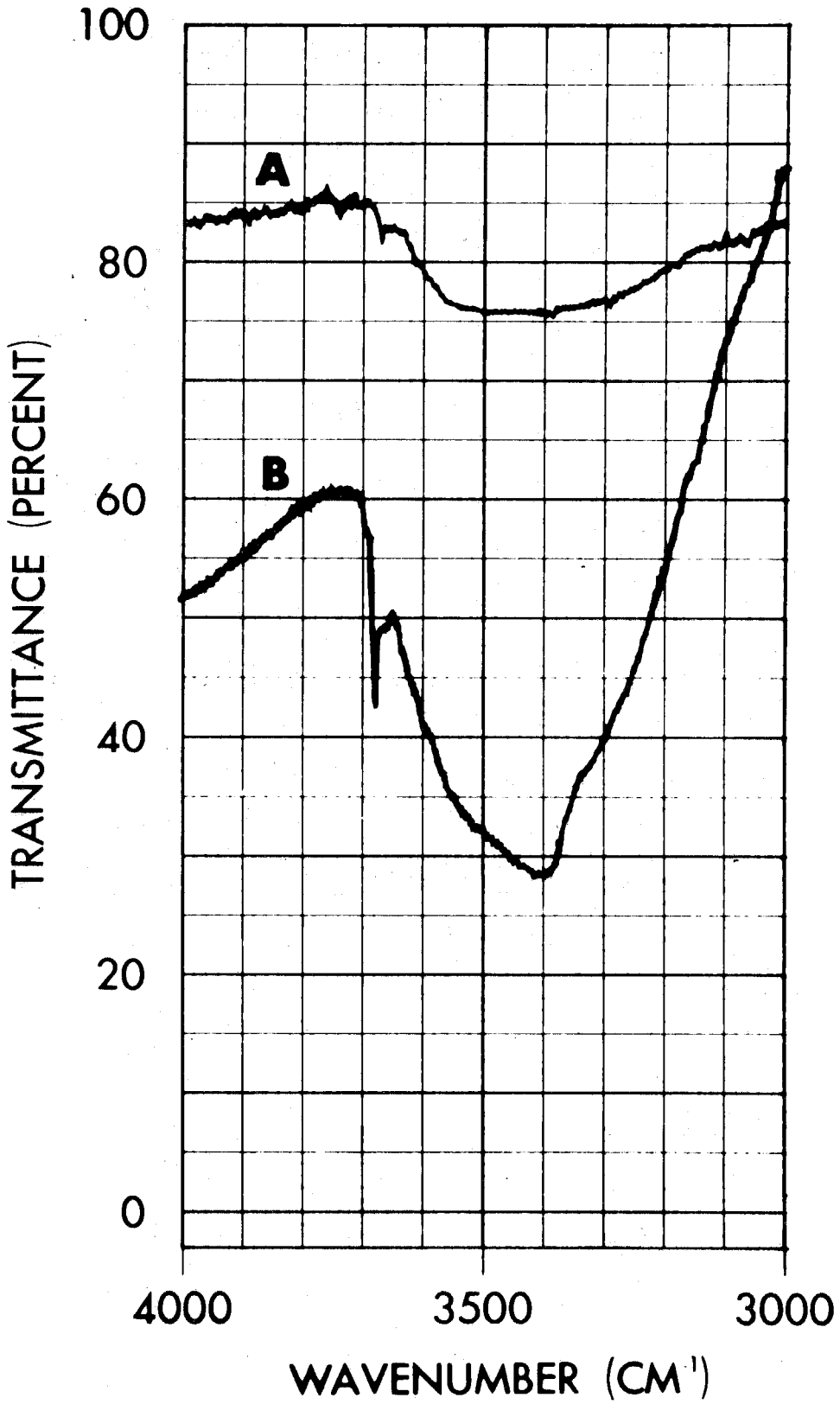
100
80
60
40
20
0
A
B
TRANSMITTANCE (PERCENT)
4000
3500
3000
WAVENUMBER (CM⁻¹)

The hydroxide stretching bands are a pair of sharp absorption features at 3680 and 3663 cm^{-1}. The more intense 3680 cm^{-1} band has an absorption coefficient of 2.7 cm^{-1}. In the specimen shocked to 496 kb, the hydroxide band occurs at 3665 cm^{-1} and has been reduced in intensity to 0.3 cm^{-1}. Water present in the unshocked specimen produces an absorption band with maximum absorption at about 3400 cm^{-1} with an absorption coefficient of 7.6 cm^{-1} whereas the 496 kb shocked specimen shows a considerably reduced absorption intensity of 1.4 cm^{-1}. Since the rhodonite used in these experiments is internally fractured, much of the water present need not be in the crystal structure but, instead, could reside within the fractures. For comparison, a gem-quality rhodonite from Franklin, New Jersey, free of fractures and low in Mn^{3+}, has only a weak water band at 3423 cm^{-1} with an absorption coefficient of 0.96 cm^{-1}, somewhat lower than the shocked sample.

The presence of water in the rhodonite samples, wherever its location, is important since it provides a species with which Mn^{3+} can react. From a comparison of the intensity of the water absorption in the unshocked specimen to that in materials of known water content, we estimate that the initial sample contains about 5.5 mg H_2O cm^{-3}, or 3.1 mmole H_2O cm^{-3}. The Mn^{3+} concentration

which was estimated to be 0.3% corresponds to 0.2 mmole Mn^{3+} cm^{-3}. Water is thus present in a large stoichiometric excess. At room temperature most manganese (III) compounds are unstable in aqueous solution with respect to disproportionation to Mn(II) and Mn(IV) compounds. It is proposed that under the conditions of the shock, the Mn^{3+} ions are reduced to divalent manganese by water or its decomposition products. Similarly, in ferric amphibole, Burns et al. (1972) postulate that Fe^{3+} to Fe^{2+} reduction is facilitated by the oxidation of OH^- ions to OH free radicals in the M1 and M3 sites of the amphibole structure.

Chapter V.

Abstract

Samples of calcic plagioclase (labradorite, An63, from Chihuahua, Mexico) have been shock-loaded to pressures up to 496 kilobars. Optical and electron microscopic studies of the recovered samples show the effects of increasing shock pressures on this mineral. At pressures up to 287 kilobars, the recovered specimens are still essentially completely crystalline, with just an optically non-resolvable amount of glass present at 287 kilobars. At pressures above 300 kilobars, the recovered specimens are almost 100% shock glasses. Diaplectic glasses are produced up to 400 kilobars and shock-fused glasses at higher pressures. No fine scale shock deformation structures were produced in any of the specimens. The most prominent physical feature is the pervasive irregular fracturing caused by the shock crushing.

Introduction

Shock-loading experiments under closely controlled conditions were performed on labradorite (An63) to determine the effects produced by high pressure shock waves on this common rock-forming mineral. Since calcic plagioclase is a major constituent of gabbroic and basaltic rocks, the significance of those experiments in the interpretation and understanding of shock metamorphic histories of such rocks is obvious. It becomes even more important when one considers the range of shock effects observed in plagioclase and other tectosilicates compared to the effects of shock-loading on denser and less compressible materials, especially ferromagnesian minerals, the other major constituents of mafic rocks. The behavior of tectosilicates during shock-loading, whether experimental or in a meteorite impact, is the primary key to interpreting the metamorphic history of such shocked rocks. Accordingly, this study is particularly applicable to the petrography of naturally shocked lunar and terrestrial rocks and meteorites.

In the past decade there has been increased research on naturally shocked plagioclase from all three of those sources. This includes extensive studies of plagioclase shock glasses and other shock features in meteorites (for example, in shergottite class meteorites

by Duke, 1968 and Bunch et al., 1967 and in chondritic meteorites by Levi-Donati, 1971), in lunar rocks (for example, Engelhardt et al., 1970; Chao et al., 1970; and numerous others), and in rocks from terrestrial impact craters (for example, Bunch et al., 1968; Chao, 1968; and Engelhardt and Stöffler, 1968). There has also been research on artificially shocked plagioclase. Primarily, this has been on plagioclase from artificially-produced explosion craters (for example, Bunch, 1968) and random shock-loading experiments (for example, Milton and DeCarli, 1963). Only recently have systematic shock-loading experiments been started (Gibbons, 1973 and Stöffler and Hornemann, 1972) to fully characterize the effects of shock compression on this important mineral and to clear up some of the confusion about terminology and interpretation which has arisen as a result of recent increased interest in shocked rocks.

The nomenclature applied to shock-produced deformation features appears to be generally accepted by researchers in the field (for example, Stöffler, 1972). However, the terminology for shock glasses is not. In particular, glasses shock-produced in the solid state are defined as 'diaplectic' or 'thetomorphic'. The term 'diaplectic' was introduced by Engelhardt et al. (1967; quoted in French, 1966) to describe glasses of

quartz and feldspar shock-produced in the solid state. 'Thetomorphic' was introduced by Chao (1967), who recommended that it be used to describe the glass phase shock-produced in the solid state from any crystalline mineral. Since 1967 both terms have been used ('diaplectic' by Engelhardt and co-workers; 'thetomorphic' by Chao and co-workers) with each group claiming priority for its term, both terms getting scattered throughout the literature on shock studies, and no agreement being reached to avoid more confusion. With the interest of many new workers in shock metamorphism, both terms are also sometimes used rather loosely to describe any shock glass, without sufficient regard to its mode of formation.

In this work I will use the term 'diaplectic' to describe shock-produced solid state glass and 'shock-fused' to describe glass produced by shock melting. In toto, both types will be referred to as 'shock' glasses. I propose that this terminology be used by others describing shock glasses in shock metamorphosed rocks. I will use 'diaplectic' rather than 'thetomorphic' to be consistent with the bulk of the recent literature on experimental shock studies. In particular, Stöffler and co-workers (for example, Stöffler, 1971, 1972 and Stöffler and Hornemann, 1972) have used 'diaplectic' extensively in discussions of experimentally shocked materials and in

applications of petrographic data on naturally and experimentally shocked materials to Hugoniot equation of state data (for example, those of Ahrens et al., 1969 and Ahrens and Rosenberg, 1968). On the other hand, 'thetomorphic' has not been used extensively in experimental studies and has mainly been used in petrographic accounts of naturally or artificially shocked rocks (for example, Chao, 1968 and James, 1969a). The term 'maskelynite', a varietal name that has been used to describe terrestrial, meteoritic, and experimentally-produced diaplectic plagioclase glass (for example, Dworak, 1969; Binns, 1967; and Milton and DeCarli, 1963, respectively), will not be used either, in favor of the generic term, diaplectic.

Experimental Procedures

Controlled laboratory shock experiments on calcic plagioclase (labradorite, An63) were performed to peak pressures as great as 496 kb. Thirteen discs of the single crystal feldspar were shocked to appropriate Hugoniot states between 58 and 496 kb. Most of those specimens were completely recovered intact after the shock-loading. Details of the experimental conditions of the shock-loading are given in Table 8. All the sample discs were shocked in stainless steel 304 containers; both the 1-inch and 3/4-inch diameter designs were used. Tungsten flyer plates were used on all except the 58 kb and 106 kb shots, when aluminum 2024 and stainless steel 304 plates were used, respectively. The peak shock pressures were determined graphically (see Figure 8) using the given measured projectile impact velocities, as described earlier. Those pressures are accurate to approximately $\pm$ 3%.

The original sample material was small, sub-rounded fragments of translucent, essentially colorless semi-precious gemstone quality plagioclase. It was obtained from Burminco, Monrovia, California where it was described as bytownite from Chihuahua, Mexico. Electron microprobe analysis revealed its composition as labradorite, An63. The probe analysis and some measured physical properties are given in Table 9.

TABLE 8

Experimental Conditions For Labradorite Recovery Shots

Shot Number	Flyer[c] Plate (on Lexan)	Sample Thickness, mm	Impact Velocity, m s^{-1}	Peak Shock Pressure, kb
175[a]	Al 2024	0.5	500	58
174[a]	S.S.304	0.5	550	106
173[a]	W	0.5	531	143
172[a]	W	0.5	702	195
163[a]	W	0.5	987	287
143[b]	W	0.5	1092	322
145[b]	W	0.5	1142	340
144[b]	W	0.5	1170	350
133[b]	W	0.875	1200	363 $\pm$ 17
148[b]	W	0.5	1337	410
171[a]	W	0.5	1466	458
147[b]	W	0.5	1535	484
113[b]	W	0.875	1572	496

[a] Stainless steel 304 sample container, 1-inch diameter

[b] Stainless steel 304 sample container, 3/4-inch diameter

[c] 2.5 mm thick tungsten (W), stainless steel 304, and aluminum 2024 flyer plates

TABLE 9

Analysis of Labradorite From Chihuahua, Mexico[a]

Oxide	Weight %
SiO_2	53.38
Al_2O_3	31.23
CaO	11.85
Na_2O	3.59
K_2O	0.37
FeO[b]	0.35
	100.77

Mole %	
Albite (Ab)	34.6
Anorthite (An)	63.1
Orthoclase (Or)	2.3

Refractive Indices

n_α	1.560 ± 0.001
n_β	1.565 ± 0.001
n_γ	1.570 ± 0.001

Density

D	2.70 ± 0.02	g/cm^3

[a] Chemical analysis by A. Chodos using the California Institute of Technology electron microprobe, May 26, 1972.

[b] Total Fe as FeO.

TABLE 9

Analysis of Labradorite From Chihuahua, Mexico[a]

Oxide	Weight %
SiO_2	53.38
Al_2O_3	31.23
CaO	11.85
Na_2O	3.59
K_2O	0.37
FeO[b]	0.35
	100.77

Mole %	
Albite (Ab)	34.6
Anorthite (An)	63.1
Orthoclase (Or)	2.3

Refractive Indices

n_α	1.560 ± 0.001
n_β	1.565 ± 0.001
n_γ	1.570 ± 0.001

Density

D	2.70 ± 0.02	g/cm^3

[a] Chemical analysis by A. Chodos using the California Institute of Technology electron microprobe, May 26, 1972.

[b] Total Fe as FeO.

For shock-loading the samples were sawn into small slabs which were cored into 4.75 mm diameter discs. The discs were then hand-ground to suitable thicknesses; two samples (113, 133) were ground to 0.875 mm and all the others to 0.5 mm. The samples were of such excellent quality that the disc grinding was quite routine. With careful handling and wax mounting on the grinding tools, the discs were very resistant to fracturing and spalling; they had the grinding characteristics of a hard glass. However, crystallographic orientation was a problem. The original fragments were of such small and irregular sizes that they had to be sawn to give the largest sized slabs in order to core drill into the 4.75 mm discs. Accordingly, the crystallographic orientation of the shock-loaded discs was random relative to the impact direction of the flyer plates and the propagation direction of the shock wave. Since most of the discs were shocked to pressures above the Hugoniot elastic limit to shock states along the plastic Hugoniot, this may not be a problem. Pre-shock observations on the discs revealed that the closest any came to the crystallographic axes was approximately 10° from (010).

After recovery, the sample containers were machined open on a lathe to expose the shocked discs. These exposed discs were then carefully examined using a binocular

microscope before any material was removed for further studies. Those further studies included refractive index measurements on fragments from various parts of the recovered discs. Standard immersion techniques and interference microscopy were used. The interference microscopy was done at the laboratory of Dr. E. C. T. Chao, United States Geological Survey, Washington, D.C.

In addition several grain mounts of fragments from each disc were thoroughly examined using a polarizing microscope in a study of shock-produced physical features. Attempts were made to prepare thin sections from parts of the discs from shots 163 and 173 but the fragments were too fragile because of the pervasive fracturing and got destroyed. For observation of some of the physical features of the still crystalline shock-loaded samples, the universal stage technique was employed (for example, Turner, 1947). Specially prepared grain mounts were used.

In a further search for vitrification and fine planar features in the crystalline samples, fragments from shot 163 (287 kb, the highest pressure plagioclase not transformed to shock glass) were examined with a transmission electron microscope (see Phakey et al., 1972). This was done with the cooperation of Dr. John

Christie who helped prepare the specimens and operated the JEM-7A 120 kv electron microscope at the University of California at Los Angeles.

Shock Vitrification

The data on the refractive index measurements of the shocked plagioclase are given in Table 10. These data are graphically presented in Figure 23 with some similar data for quartz, orthoclase, and microcline (Kleeman and Ahrens, 1973; Kleeman, 1971; and Robertson, 1972). Refractive indices of the crystalline and amorphous phases are correlated with the peak shock pressure to which the specimen was shock-loaded.

For shock-loading to peak pressures of 287 kb and less, the amount of shock-produced vitrification of the plagioclase was insignificant on the basis of refractive index change. No change in refractive index was observed within the error of measurement ($\pm$ 0.001) of the immersion technique used. However, for peak shock pressures of 340 kb and higher, the recovered samples were essentially completely amorphous. This was directly reflected in the changes in refractive indices observed. For the 340 kb sample, index changes were measured of 0.0086 to 0.0180 from the mean index, $\underline{n}$ = 1.565, of the crystalline plagioclase. Similar changes were observed for the sample shocked to 363 kb; changes of 0.0180 to 0.0261 were observed for the 350 kb sample. For the discs shock-loaded to 484 and 496 kb, a mean refractive index change of 0.025 was measured.

TABLE 10

Refractive Index Measurements Of Glass Shock-Produced From Plagioclase, An63[a]

Shot Number	Shock Pressure kb ± 3%	Refractive Index (n)
145	340	1.5470 to 1.5564
144	350	1.5389 to 1.5468
133	363 ± 17	1.5472 to 1.5534
147	484	1.540 ± 0.002
113	496	1.540 ± 0.001

[a] The refractive indices of the crystalline plagioclase were $n_\alpha = 1.560$, $n_\gamma = 1.570 \pm 0.001$.

FIGURE 23

Refractive index versus peak pressure for experimentally shocked labradorite, orthoclase, microcline, and quartz. Vertical bars indicate variations of refractive indices.

⊙ Labradorite, this work

○ Labradorite glass, this work

◇ Orthoclase, Kleeman (1971)

× Orthoclase glass, Kleeman (1971)

△ Quartz, Kleeman and Ahrens (1973)

▽ Quartz glass, Kleeman and Ahrens (1973)

⊡ Microcline, Robertson (1972)

⬡ Labradorite, An67, (Bell and Chao, 1969)
Shock glass
Annealed shock glass

The refractive index of normal orthoclase or microcline glass is 1.486 (Barth, 1969). Synthetic silica glass has a refractive index of 1.458.

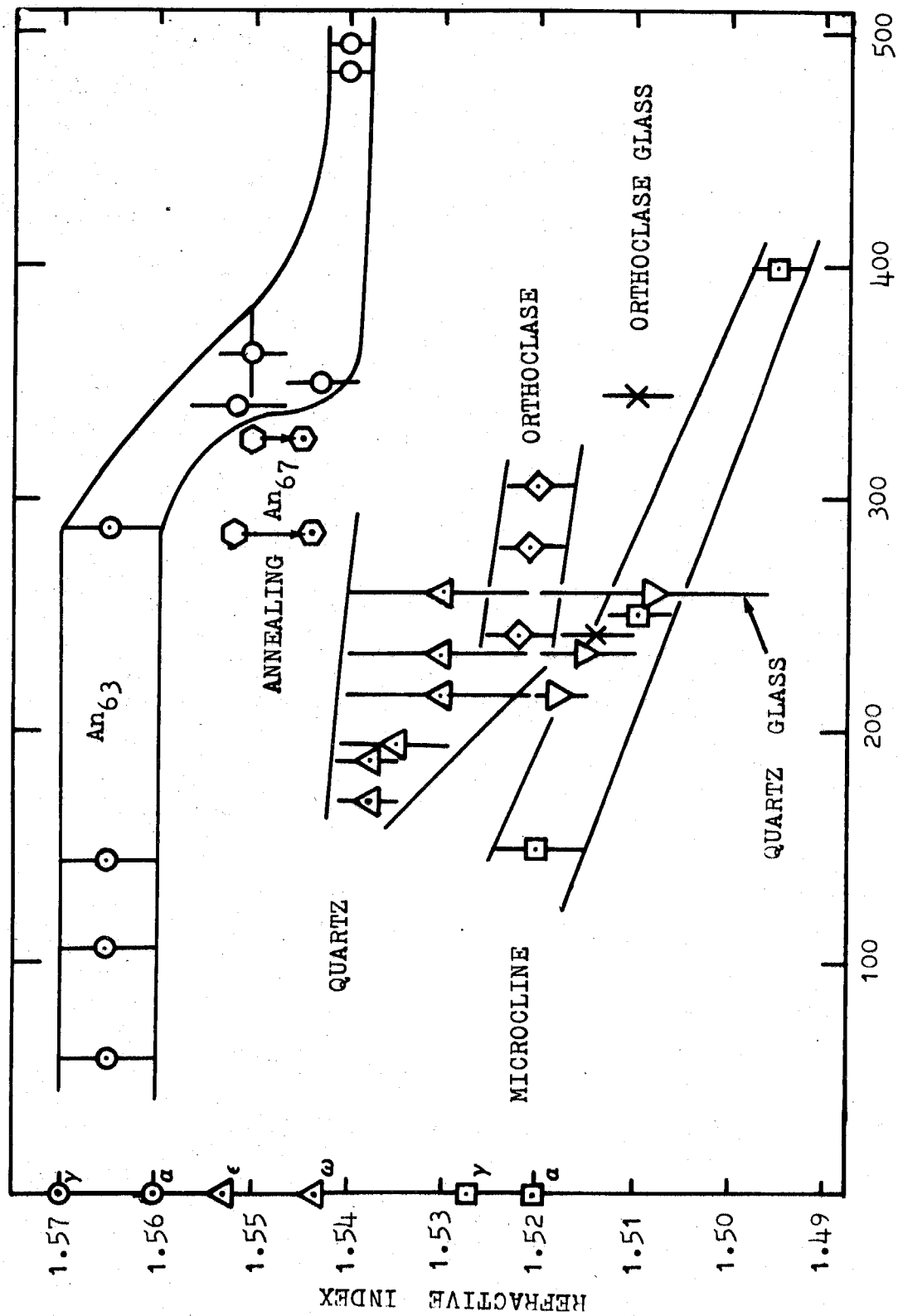
REFRACTIVE INDEX
1.57
1.56
1.55
1.54
1.53
1.52
1.51
1.50
1.49
γ
α
ε
ω
γ
α
100
200
300
400
500
PRESSURE, KB
An63
An67
ANNEALING
QUARTZ
MICROCLINE
ORTHOCLASE
ORTHOCLASE GLASS
QUARTZ GLASS

It is uncertain why shot 133 does not fit the downward trend of refractive index exhibited by shots 145 and 144. It may be that such a steep trend is not genuine and that the total trend of all three samples together is the more realistic. On the other hand, the pressure determination for shot 133 was based on powder load (12 g H110, Figure 4), since the projectile velocity measurement device failed; its error of $\pm$ 17 kb may actually place it between shots 145 and 144, in which case it does fit their trend. On the basis of the refractive index studies of fused silica and soda-lime glasses presented earlier, in particular, the observations on the rapid index decreases probably caused by annealing at high pressures, I believe the steep index decrease exhibited by the glass recovered in shots 144 and 145 is a real effect. Also supporting this conclusion are the annealing experiments done by Bell and Chao (1969) on two glasses shock-produced from labradorite, An67 at pressures of 285 and 325 kb. They found that refractive index changes of 0.0065 occurred as a result of annealing those shock glasses at 850°C for times of seven to fourteen seconds. According to calculated post-shock temperatures for silica (Figure 17), the shock-loading temperatures were probably in the correct range. The index decrease is possibly predominantly an annealing effect. The pre- and post-annealing refractive indices measured by Bell and Chao on their

two shocked glasses are given in Figure 23 for comparison with those measured in this work. The refractive indices measured for the shock glasses produced at 484 and 496 kb are so consistent around 1.540 that those glasses probably are fully annealed shock-melted plagioclase, that is, shock-fused glasses.

On the basis of the refractive index measurements on shocked samples, it appears that the glass produced at pressures up to 350 kb is produced in the solid state at temperatures below the glass transition temperature; that is, they are diaplectic glasses. The glasses formed at higher shock-loading pressures appear to be shock-produced at temperatures above the glass transition temperature and are essentially shock-fused glasses. This is corroborated by the fact that in Figure 24 the refractive indices of the shock glasses produced in this work completely intersect the field of diaplectic glasses defined by Stöffler and Hornemann (1972). The indices of the glasses produced around 350 kb fall mainly within the diaplectic field; those of the glasses formed at higher pressures fall just below the line of indices for normal plagioclase glasses.

Of course, it is not an absolute rule that diaplectic glasses must fall within this defined field, as Stöffler and Hornemann point out. There are examples of calcic

FIGURE 24

Refractive index versus anorthite-content of plagioclase glasses. Solid lines represent mean refractive indices of plagioclase crystals and synthetic plagioclase glasses (Barth, 1969). Vertical bars indicate measured variations of refractive indices.

⊙, Ries crater (Stöffler, 1967 and Stöffler and Hornemann, 1972)

◇, Ries crater (Engelhardt et al., 1967)

△, Ries crater (An_{37}), Sedan nuclear crater (An_{36}), Manicouagan crater (An_{54}), Clearwater Lake West (An_{58}) (Bunch et al., 1968)

▨, Shergotty meteorite (Bunch et al., 1967)

X, *, Manicouagan crater (Dworak, 1969)

▽, Shergotty meteorite (Duke, 1968)

▲, Chateau Renard (An_9) and Padvarninkai meteorites (Binns, 1967)

+, Mare Tranquillitatis (An_{83}-An_{96}), Apollo 11, 10084,106; 10085,25 and 10085,26 (Engelhardt et al., 1970)

●, Ries crater (Bell and Chao, 1969)

⊠, Shock experiments (Bell and Chao, 1969)

■, (An_{80}), shock experiments (Milton and DeCarli, 1963)

■, shock experiments, (An_{24} = No. 12; An_{51} = No. 13, Stöffler and Hornemann, 1972)

■, (An_{54}), shock experiment (Muller and Hornemann, 1967)

▯, Data from this work for An63 (otherwise this figure is the data compiled by Stöffler and Hornemann (1972) for their figure 5)

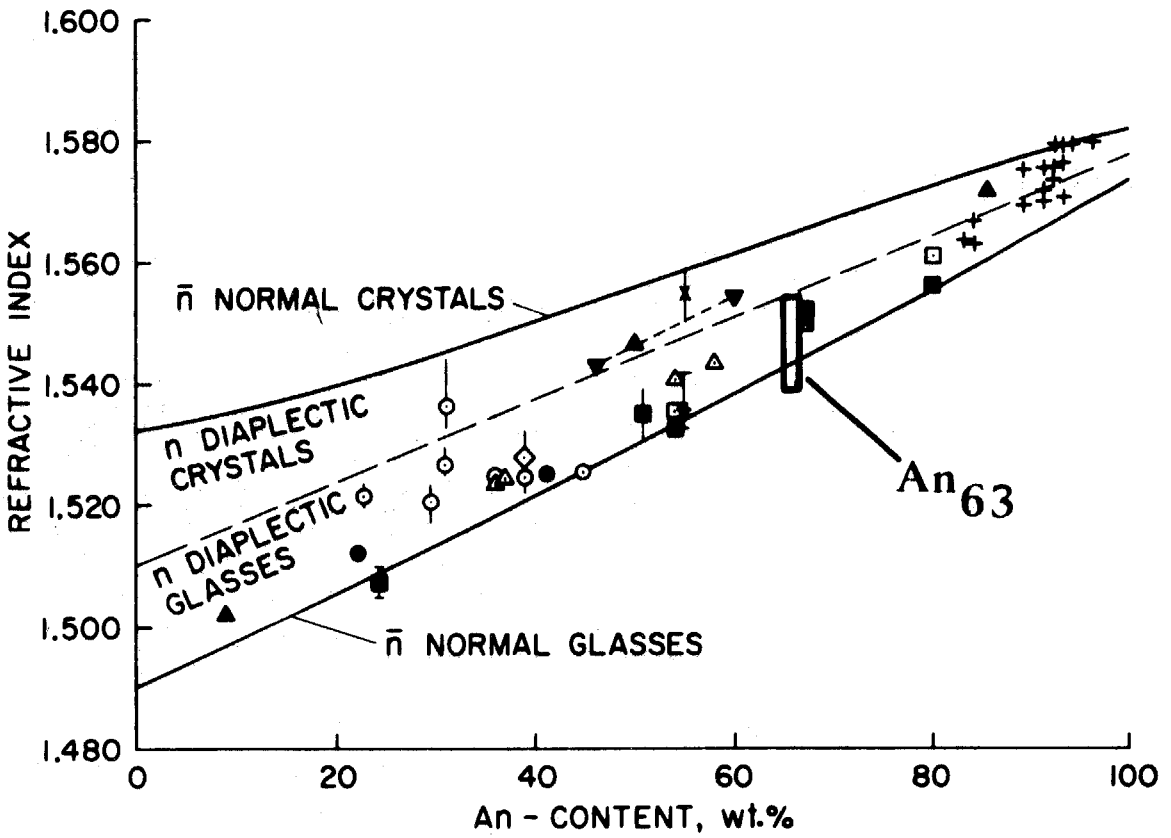
1.600
1.580
1.560
1.540
1.520
1.500
1.480
REFRACTIVE INDEX
n̄ NORMAL CRYSTALS
n DIAPLECTIC CRYSTALS
n DIAPLECTIC GLASSES
n̄ NORMAL GLASSES
An63
0
20
40
60
80
100
An - CONTENT, wt.%

plagioclase shock glasses from shergottite class meteorites (Shergotty: Duke, 1968 and Bunch et al., 1967; Padvarninkai: Binns, 1967) and anorthitic lunar glasses (for example, Apollo 11, Engelhardt et al., 1970) which have refractive indices much higher than the diaplectic field shown in Figure 24 but which are believed by their investigators to be diaplectic glasses. Some of these glasses have indices near the mean indices of crystalline plagioclase. The reason for their high indices may be that those glasses were subjected to high pressures subsequent to shock formation. Such pressures could be produced by multiple shock impacts in the case of both lunar rocks and meteorites and could result in permanent densification (for example, Gibbons and Ahrens, 1971) sufficient to move them out of the diaplectic glass field of Figure 24, though they were originally formed in the solid state. On the other hand, there is no evidence to date that shock glasses which have indices within the diaplectic field are not produced by shock in the solid state. Accordingly, henceforth, those plagioclase glasses shock-produced in this work at pressures up to 350 kb and having refractive indices in the diaplectic field will be referred to as diaplectic glasses. Those having indices of and below the indices of normal synthetic plagioclase glasses will be referred to as shock-fused glasses.

On the basis of my refractive index and optical microscopic results alone, I have demonstrated that, in multiple-shock reflection-type shock recovery experiments, minimal to negligible vitrification is caused by shock pressures lower than 287 kb, solid state vitrification to diaplectic glass is caused by shock-loading to pressures between 287 and 350 kb, and the formation of shock-fused glass is caused by peak shock pressures greater than 350 kb. Other experimental data on plagioclases agree with these results. Diaplectic and shock-fused glasses were produced from plagioclase, An80, by Milton and DeCarli (1963) in two gabbro specimens shock-loaded to estimated pressures of 250 to 350 kb and 600 to 800 kb, respectively. Diaplectic glass was formed from two fragments of labradorite, An67, single crystal shock-loaded to pressures of approximately 285 and 325 kb by DeCarli and Ahrens (in Bell and Chao, 1969). Stöffler and Hornemann (1972) also produced diaplectic and shock-fused glasses by shock-loading plagioclase, but their peak pressure regimes for the different glass phases do not quite match mine. They concluded from their data that diaplectic glasses were formed from feldspars at shock pressures between about 300 and 450 kb but pressures exceeding about 430 kb were necessary to produce shock-fused glasses. I accept their lower bound of 300 kb as

compatible with my data for the formation of diaplectic glass. However, I prefer a lower figure for the beginning of shock-fusion. My data suggest 350 kb. Maybe an intermediate pressure of 400 kb is more reasonable than either of the two extremes.

Differences between experimental conditions in the two techniques of shock-loading may explain those differences in pressures. Stöffler and Hornemann used a shock wave generating technique consisting of an explosive plane wave generator and 'momentum traps' (for example, Stöffler, 1972). I used a shock-loading propellant gun (for example, Gibbons and Ahrens, 1971). Stöffler and Hornemann used a single-shock technique for pressures up to 300 kb and a multiple-shock reflection technique for higher pressures. I used the multiple-shock reflection technique for all experiments. There may be enough differences between the experimental techniques to explain the different observations. Lower temperatures are reached in the multiple-shock reflection-type experiments than in single-shock type experiments at pressures above about 200 kb (see the data for fused silica in Figure 17). Thus, Stöffler and Hornemann actually had slightly higher temperatures in their samples shocked to 300 kb. However, above 300 kb they also used the multiple-shock reflection-type technique, making the experiments

essentially temperature consistent in the range of interest, 300 to 500 kb. Some other effect must be causing the inconsistency of our data.

The post-shock states of the recovered glass must be considered. Stöffler and Hornemann distinguished between only diaplectic glass and vesicular glass (their shock-fused glass). I do not equate shock-fused with vesicular glass. In my experiments on non-porous single crystal plagioclase, no vesiculation occurred in the shock-fused glass. However, I have shock-loaded porous, powdered rhodonite in which extensive vesiculation and melting occurred at pressures within the regime of diaplectic non-porous rhodonite. Maybe Stöffler and Hornemann have a range of shock-fused glass between their diaplectic and vesiculated shock-fused glass that would bring their pressure of initial shock fusion of plagioclase down to about 400 kb.

Other data, on orthoclase, quartz, and microcline (Kleeman, 1971; Kleeman and Ahrens, 1973; and Robertson, 1972), are presented in Figure 23 for comparison with my labradorite data. The overall behavior is duplicated in all three cases. At lower pressures, no change in refractive index is observed. At higher pressures shock glasses begin to appear; finally the crystalline mineral is completely transformed to shock glass. A difference

from the labradorite is that there is a large range over which diaplectic glass and crystal coexist (both as separate phases and as diaplectic crystals). This was observed by Kleeman in both quartz and orthoclase and by Robertson in microcline. Kleeman (1971) observed the first vestiges of diaplectic glass at 242 kb in orthoclase and complete transformation to diaplectic glass at just above 300 kb. In quartz, Kleeman and Ahrens (1973) observed the first traces of diaplectic glass at 216 kb and 40% glass and diaplectic crystals at 260 kb, their peak pressure.

It is not clear why similar behavior was not observed in my labradorite below 287 kb. It may be that its density and compressibility characteristics are such that 287 kb is the threshold for diaplectic glass formation. This is the lowest pressure sample in which any shock glass is observed; the amount was too small to be detected optically. However, it was observable using transmission electron microscopy. In grain mounts examined on a JEM-7A 120 kv electron microscope, vestiges of glass were observed in an otherwise totally crystalline specimen.

Summarizing the vitrification data on my labradorite and the plagioclase, potassium feldspars, and quartz of the other workers, we may estimate where the recovered materials fit on a typical tectosilicate Hugoniot, the

composite feldspar Hugoniot in Figure 25 (Ahrens et al., 1969b). Considering Kleeman's data on quartz and orthoclase, we may take 225 kb as a boundary for the first appearance of diaplectic glass in tectosilicates. This pressure falls in the middle of the Hugoniot mixed phase regime. On the basis of my data and those of Stöffler and Hornemann (1972) on plagioclase, we can take 400 kb as an appropriate boundary for the shock-fusion of tectosilicates. This pressure is approximately the boundary between the mixed and high pressure phase regimes on the Hugoniot. One conclusion from these results is that no vitrification is caused by shock-loading within Regime I and at lower pressures within Regime II, diaplectic vitrification is caused at pressures of 225 to 400 kb within Regime II, and shock-fused glasses are formed by shock-loading to pressures greater than 400 kb to Hugoniot states within Regime III. On this basis, shock metamorphism of rocks containing tectosilicates can be discussed in terms of Hugoniot data and mineral vitrification for pressures up to 500 kb or so.

FIGURE 25

Composite Hugoniot of the feldspars (Ahrens et al., 1969b). 1 = oligoclase, 2, 3, 4 = anorthosite (polycrystalline andesine), 5 = albitite, 6 = albite, 7 = labradorite, 8 = microcline. The three distinct phase regimes (I, low pressure; II, mixed; and III, high pressure) are indicated as well as a range of Hugoniot elastic limits. Three release adiabats are shown for oligoclase. Note their positions relative to the Hugoniot. The density of zero pressure hollandite structure feldspar is also noted.

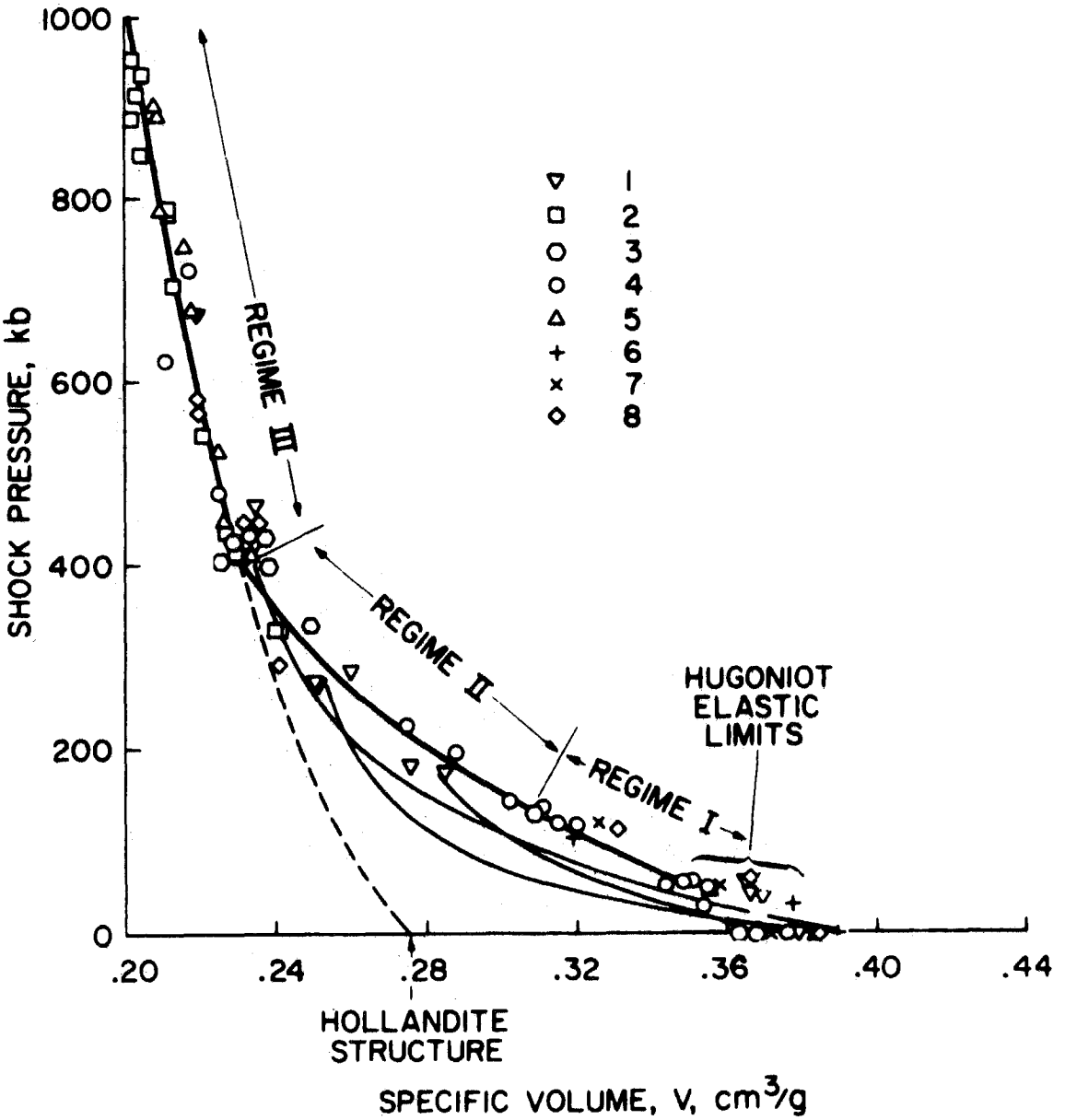
1000
800
600
400
200
0
SHOCK PRESSURE, kb
.20
.24
.28
.32
.36
.40
.44
SPECIFIC VOLUME, V, cm³/g
REGIME III
REGIME II
REGIME I
HUGONIOT
ELASTIC
LIMITS
HOLLANDITE
STRUCTURE
1
2
3
4
5
6
7
8

Shock-Produced Deformation Features

To complement the vitrification data, one must look at shock-induced planar features. Considerable study has been done on planar features observed in rocks from terrestrial impact craters (for example, Chao, 1967a, b, 1968; Robertson et al., 1968; Dworak, 1969; and Stöffler, 1972). Most of this has been on tectosilicates, mainly because they have been more abundant than any other mineral classes but also because tectosilicates yield the greatest variety of distinguishable shock effects in the most critical pressure range, 0 to about 500 kb. This behavior is directly related to their physical properties and the character of their Hugoniots. They are much less dense and more compressible than other common rock-forming silicates. Their Hugoniots exhibit broader mixed phase regimes (in terms of both pressure and volume changes) as well as distinct high pressure phase characteristics above 300 - 400 kb. This contrasts with pyroxenes, for example, which are much less compressible and exhibit a much narrower mixed phase regime (especially in volume change), though they do have similar high pressure phase behavior. Consequently, tectosilicates have been studied much more exhaustively in natural occurrences and as a result they have also received much more attention experimentally, although only very recently. Planar features have been

studied most extensively by static deformation techniques (for example, Carter, 1971; Borg and Heard, 1970). Only very recently have we started experimental studies on shock-produced planar features in feldspars (for example, Robertson, 1972; Gibbons, 1973).

Previous studies of possibly shock-induced planar features in plagioclase have mainly been made on materials recovered from terrestrial impact craters (for example, from craters in Canada, Robertson et al., 1968 and Dworak, 1969). Some studies have also been made on plagioclase shocked in nuclear and chemical explosions (for example, James, 1969a). Most planar features identified in labradorite have been parallel to crystallographic planes of low Miller indices, many of which are also the common cleavage and twin composition planes. Other planar features include fractures not assignable to any rational crystallographic planes. Some of the measured features include (001), (010), (100), (101), (111), (120), (012), and (203) (Robertson et al., 1968 and Dworak, 1969). On the basis of the correspondence of most of these features to cleavage and twin composition planes, Chao (1967a) has concluded that the interaction of plagioclase with a shock wave is closely controlled by its crystal structure and, therefore, the directions of planar features in a plagioclase crystal cannot and do not reflect the direction of

shock compression. Planar features of some of these orientations have also been produced by static deformations at pressures as low as 2 kb (for example, (010) slip and albite and pericline twins, Carter, 1971). Accordingly, there are those who say that the presence of any such planar features, regardless of orientations, is not sufficient as evidence of shock-loading and must only be considered in conjunction with other shock features, for example, diaplectic vitrification. Those structurally controlled planar features are also generally assigned to a pressure range of 150 to 300 kb (for example, Stöffler, 1972). Since plagioclase is completely shock-vitrified at 300 kb, this is an upper limit. A lower limit is more difficult to define but it may be as low as the static deformation yield strength of about 2 kb.

The labradorite discs shock-loaded in this work were almost gem quality material with no cleavages and no twinning. Of the discs shock-loaded, four were essentially completely crystalline and satisfactory for post-shock study of shock deformation features. Those discs were recovered from shots 175 (58 kb), 174 (106 kb), 173 (143 kb), and 163 (287 kb). In their original condition in the sample containers, these discs were no longer colorless gray, translucent discs but finely crushed, opaque white powder. There was no significant difference in

appearance from 58 kb to 287 kb. The material was very fragile and flaked very readily from a needle point. Grain mounts of some of the fine fragments were used for optical microscopic examinations. Grain mounts of shot 163 (287 kb) and a thin section of shot 174 (106 kb) were also examined by transmission electron microscopy.

Upon examination with an optical polarizing microscope, the most prominent feature of the sample shocked to 58 kb was the abundant irregular fracturing and lack of any cleavage. No fine deformation lamellae or mechanical twinning was detected at magnification up to 1000X. No anomalous interference was observed.

Likewise, the specimen shocked to 106 kb is characterized by pervasive irregular fracturing which gives the sample a completely shock-crushed appearance. No fine shock-produced planar elements were observed. However, occasional fragments contain coarse cleavage or parting features; one feature is parallel to (001) and a less pronounced feature, (010), as shown in Figure 26 for a typical-sized fragment. Figure 27 is a photomicrograph of a thin section made of this sample disc. It shows the mosaicism created by the irregular crushing described above. This thin section was ion thinned and examined using a 800 kv transmission electron microscope at U.S. Steel Research Center, Pennsylvania. At a mag-

FIGURE 26

Shot 174, 106 kilobars, plagioclase. No fine planar features; mostly just irregular fractures with occasional development of coarse cleavage or parting in two sets approximately perpendicular. No change in refractive index observed. Scale: long side of photomicrograph equals 0.3 mm.

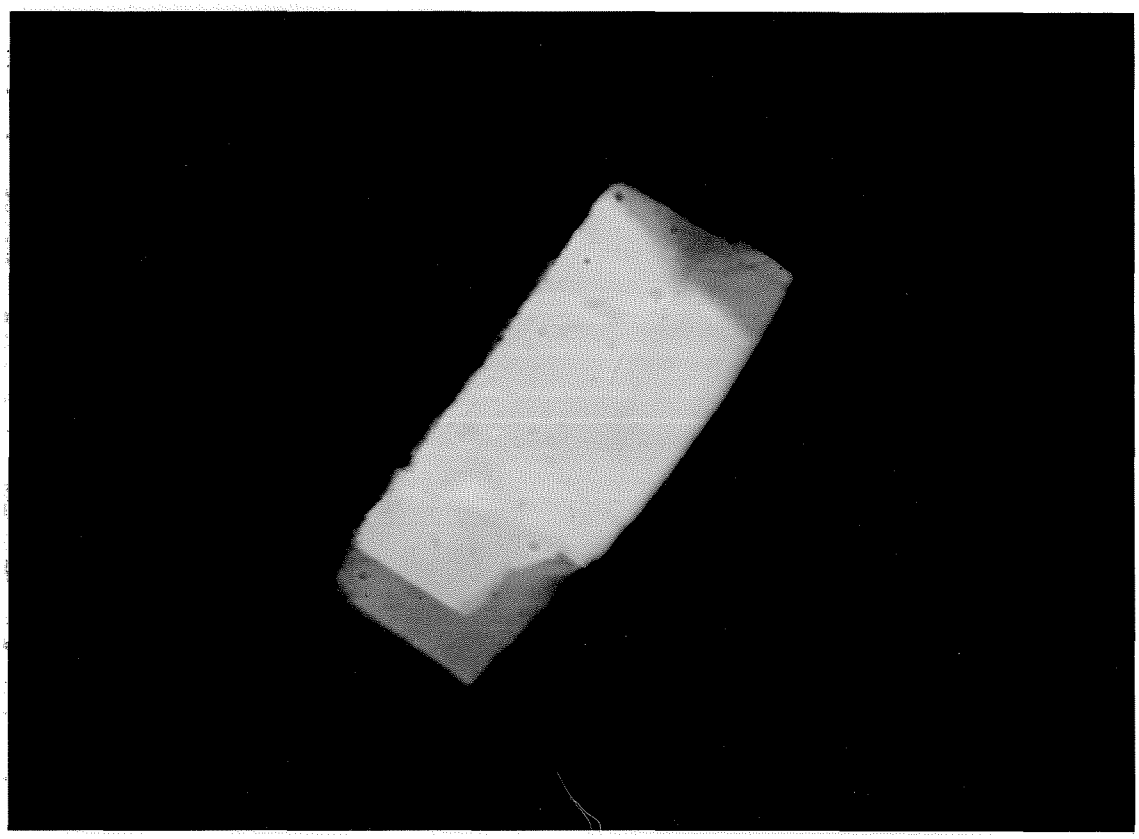

FIGURE 27

Shot 174, 106 kilobars, plagioclase. Note the mosaic-like appearance of the irregular fracturing caused by the shock-loading. Disc diameter equals 4.75 mm.

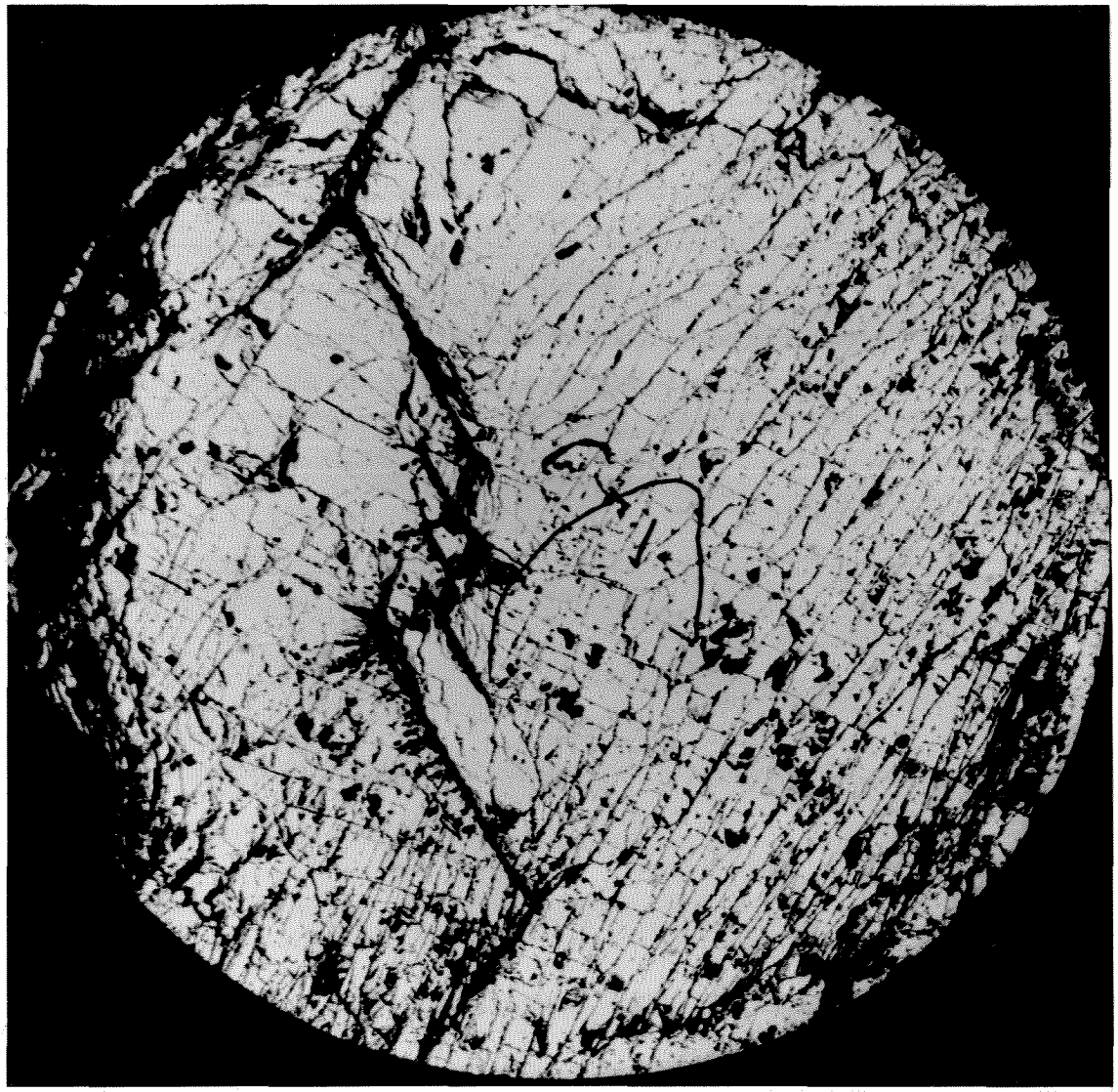

nification of 22,700X, no vitrification or fine planar elements were observed. Figure 28 shows the typical fracturing that is present on this fine scale.

Plagioclase shocked to 143 kb is optically similar to that shocked to 106 kb. Irregular fractures are the most prominent feature. Occasional fragments show coarse cleavage or parting as described for shot 174 (106 kb). No fine planar elements were detected. However, some small fragments show undulatory extinction between crossed nicols; none was observed at 106 kb. This may be because 143 kb is within the mixed phase regime along the Hugoniot, whereas 106 kb is still approximately within the low pressure phase regime (Figure 25).

Figures 29 and 30 are photomicrographs of fragments of the labradorite shocked to 287 kb. The observed shock features include the predominant irregular fractures and two sets of approximately perpendicular coarse cleavages, as described for the lower pressure shots. The (001) cleavage is better developed than at lower pressures; the other is still rather imperfect. A small amount of undulatory extinction is also observed. No fine planar features were observed optically. This sample was also examined with a 120 kv transmission electron microscope at the University of California, Los Angeles. No fine planar features were detected using specially prepared

FIGURE 28

Shot 174, 106 kilobars, plagioclase. This is a photomicrograph of the very small scale fracturing caused by shock-loading, as resolved by transmission electron microscopy at a magnification of 22,700X.

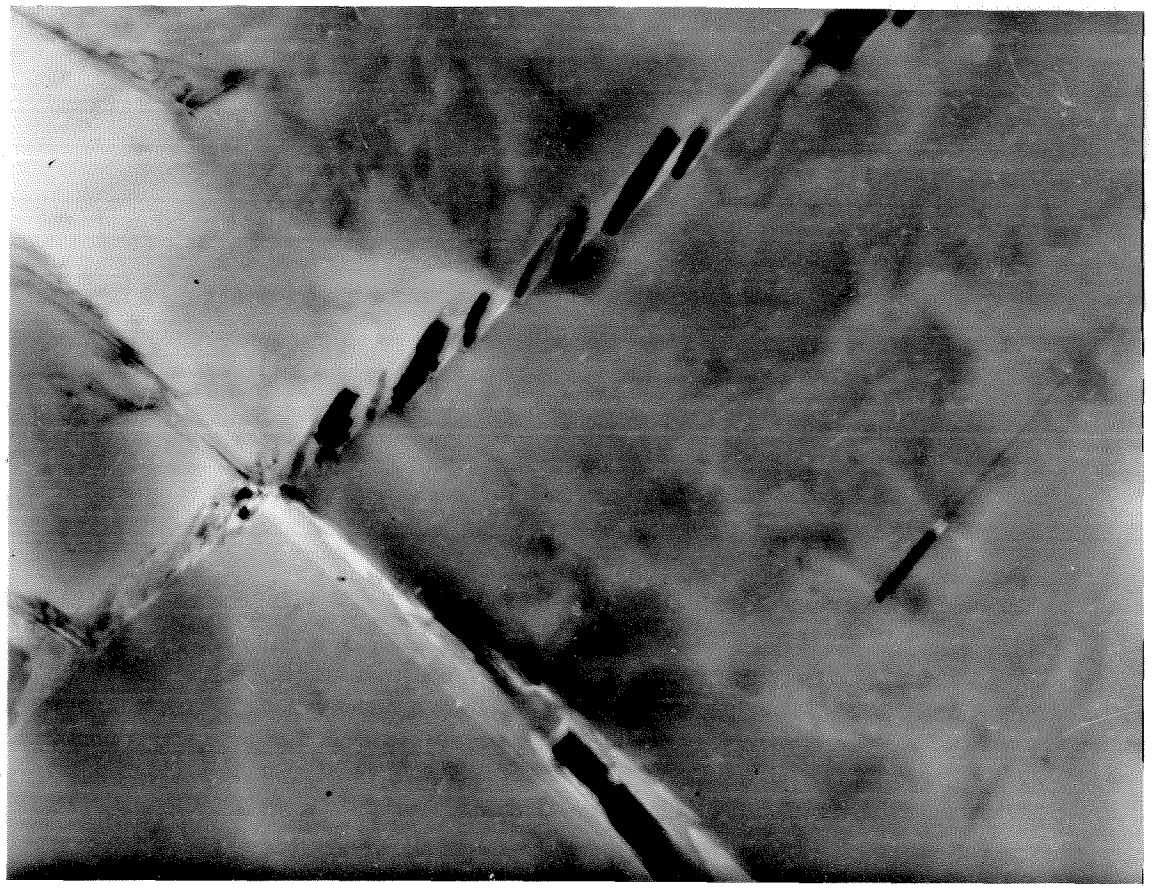

FIGURE 29

Shot 163, 287 kilobars, plagioclase. Two approximately perpendicular sets of coarse cleavage or parting are present in some fragments, like that shown. No fine planar features were resolved optically or with a 120 kv transmission electron microscope. Less than 1% glass was observed with the electron microscope; none was detected optically. Scale: long side of photograph equals 0.3 mm.

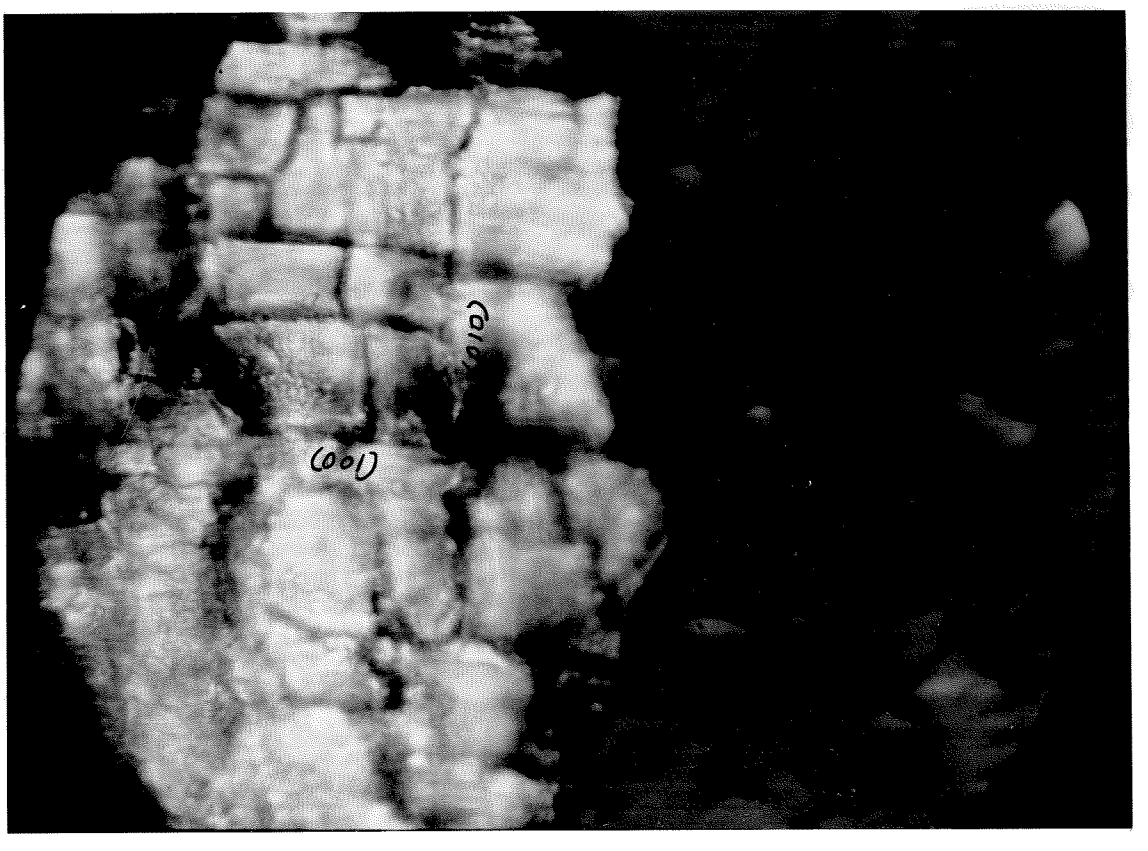
(010)
(001)

FIGURE 30

Shot 163, 287 kilobars, plagioclase. A photomicrograph showing typical fracturing of a crystal fragment. Scale: long side of photograph equals 0.3 mm.

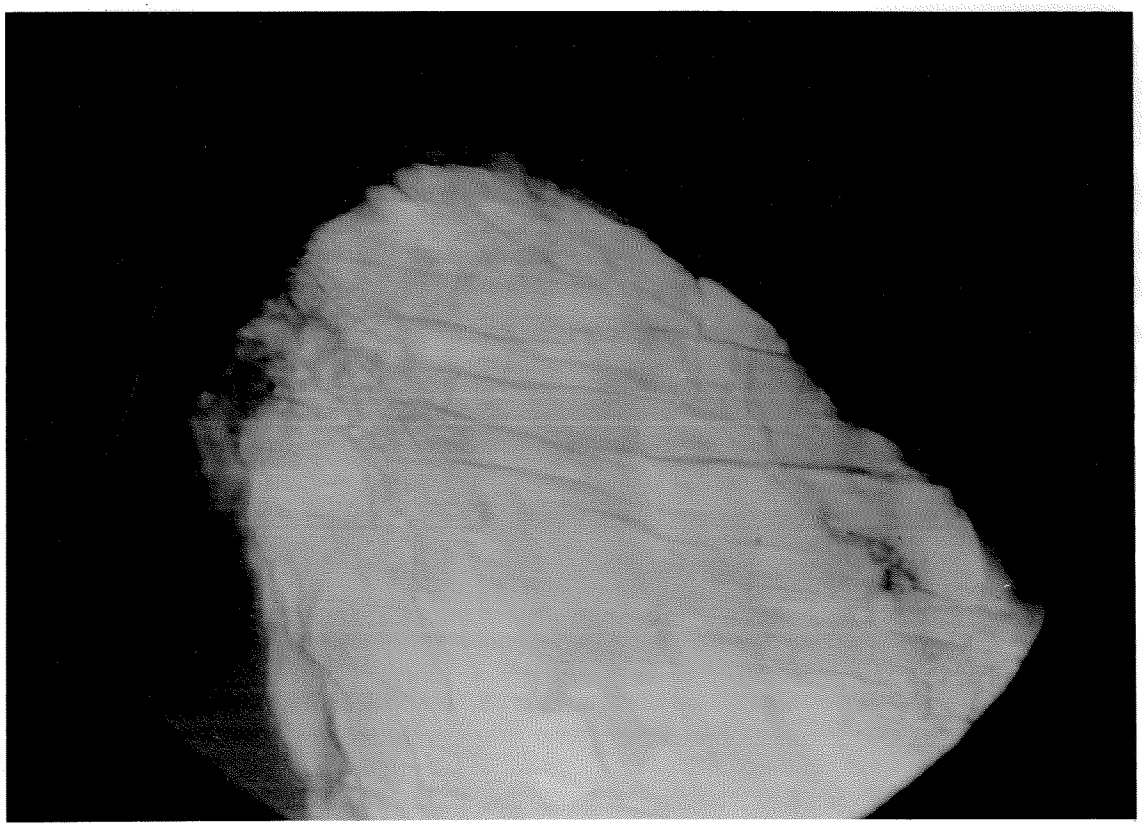

grain mounts.

The diaplectic and shock-fused glasses were also examined for deformation features. None were observed. In shot 143 (340 kb), the plagioclase is diaplectic glass with refractive indices ranging from 1.5468 to 1.5564. Approximately 1% exhibited anomalous extinction between crossed nicols; the remainder was optically isotropic glass. The specimen from shot 113 (496 kb) is completely shock-produced glass with refractive index 1.540 ± 0.001. The only physical features observed were pseudo-conchoidal fractures produced in removing the sample material from the stainless steel containers.

It is not clear why none of the very fine planar features so often observed in naturally shocked plagioclase are present in the labradorite experimentally shocked in this work. None were resolved in optical microscopic examinations; none were detected in transmission electron microscopy of specimens shocked to 106 and 287 kb. I suggest that this may be related to the original state of the specimen. In this work, the material used was of semi-precious gemstone quality with no pre-shock planar elements. Maybe the presence of cleavage and twinning in most natural materials has some control over the shock production of fine deformation features.

Conclusion

Labradorite shock-loaded to Hugoniot states within the low pressure phase regime and to 287 kb across the mixed phase regime remain in the crystalline state upon adiabatic release to zero pressure. Excessive shock-induced fracturing results and some coarse cleavage develops but no fine shock deformation features are produced. These physical features are due to a combination of shock compression and relaxation following pressure release.

Labradorite shock-loaded to Hugoniot states within the mixed phase regime between pressures of 287 and 400 kb is shock-vitrified in the solid state to diaplectic plagioclase glass of characteristic refractive index and density.

Labradorite shock-loaded to pressures greater than 400 kb to Hugoniot states in the high pressure phase regime is transformed to a shock-fused glass upon reversion from the high pressure polymorph to a short range order phase at post-shock temperatures exceeding the transition temperature of the glass.

Chapter VI.

THE EFFECTS OF SHOCK PRESSURES AS HIGH AS 528 kb ON BAMLE ORTHOPYROXENE, En86

Abstract

Samples of orthopyroxene (bronzite, En86, from Bamle, Norway) have been shock-loaded to pressures up to 528 kilobars. Optical and electron microscopic studies of the recovered samples show the effects of increasing shock pressures on this variety of pyroxene. Optically, no vitrification occurs to the peak pressure of 528 kb but increasing anomalous extinction is present at pressures above 143 kilobars. No measurable change in refractive index is detected at any pressure. Using transmission electron microscopy, a very small amount of shock glass was observed at 226 kilobars. At all pressures from 58 to 528 kilobars, the most significant optical feature is the presence of shock-produced deformation twin lamellae in a number of fragments from each specimen.

Introduction

This chapter describes some shock-loading experiments on Bamle bronzite. The experiments were performed to determine the shock effects produced in orthopyroxene under closely controlled experimental conditions at shock pressures up to about 500 kb. The significance of those experiments lies in the application of such information on shock-produced effects in pyroxenes to understanding and interpreting the shock metamorphic histories of shocked pyroxene-bearing rocks, for example, lunar and terrestrial rocks and meteorites. This information is especially important as complementary data to the experimental results of shock studies on tectosilicates, particularly plagioclase.

In pyroxenes from terrestrial and lunar shock metamorphosed rocks the main type of shock deformation structure observed has been polysynthetic mechanical twin lamellae (for example, Chao et al., 1970; Engelhardt et al., 1971; Christie et al., 1973; and Stöffler, 1972). Similar twin lamellae have also been observed in hypersthene from some meteorites (for example, Levi-Donati, 1971) and in augite from basaltic rocks shocked in a nuclear explosion (James, 1969a). They have also been produced in laboratory shock experiments on clinopyroxene (diopside: Hornemann and Müller, 1971). The orientation

of the apparently shock-produced twin lamellae in all these cases was (001).

However, similar mechanical twin lamellae on both (001) and (100) occur in pyroxene in tectonically deformed rocks and have also been produced in static deformation experiments (Raleigh and Talbot, 1967). Accordingly, their presence is not unequivocal evidence or proof of shock-loading. Thus, information on experimentally induced shock deformation structures in bronzite can only be used to complement other shock wave effects in a rock.

Some of these effects come under shock-induced structural disorder. Dundon and Hafner (1971) looked at the cation disorder produced in the Fe,Mg distribution in the M1 and M2 structural sites in Bamle bronzite by shock-loading a number of samples to pressures of 1 mb and 150-450 kb. They found that bronzite shocked to 1 mb gets highly disordered but that shocked at 450 kb or less remains structurally undisturbed. Thus, there is a pressure between 450 and 1000 kb at which the barrier to cation distribution is overcome. On the other hand, Pollack and Decarli (1969) looked at stacking disorder caused by shock-loading Bamle bronzite to pressures of 150-200 kb, 400-450 kb, and 1000 kb. Likewise, they

detected no disorder caused by the two low pressure shocks but some disorder for the 1000 kb shock, caused by a combination of the high shock pressure and high post-shock temperatures. Significant results of both those pieces of research on Bamle bronzite are (1) that it was still crystalline after shock-loading to 1000 kb and (2) that the high pressure phase indicated by the Hugoniot (Figure 31) was not detected by their x-ray powder diffraction studies. Another form of disorder is the mosaicism and loss of long range order described by Hörz and Quaide (1973). These features were also noted by the other workers. Hörz and Quaide x-rayed four specimens of Bamle bronzite shock-loaded to pressures of 63, 91, 117, and 141 kb. They noted a loss of reflections in the back reflection area as well as streakiness and line broadening in Debye-Scherrer x-ray patterns. Several observers have reported on some of these disorder features in meteoritic pyroxenes which have apparently had a shock history (for example, Pollack, 1966, 1968; and Reid and Cohen, 1967).

On the Hugoniot in Figure 31, the bronzite high pressure phase regime starts at approximately 350 kb. Maybe this phase will occur in some shock metamorphosed rocks. A garnet structure phase which could be this high pressure phase has been discovered in the Coorara

FIGURE 31

Hugoniot curve for bronzite. Note the low pressure phase, mixed phase, and high pressure phase regimes and the Hugoniot elastic limit (HEL). To 483 kb the Hugoniot is that of Bamle bronzite determined by Ahrens and Gaffney (1971). Above 483 kb the curve follows data for Stillwater bronzitite from McQueen et al. (1967).

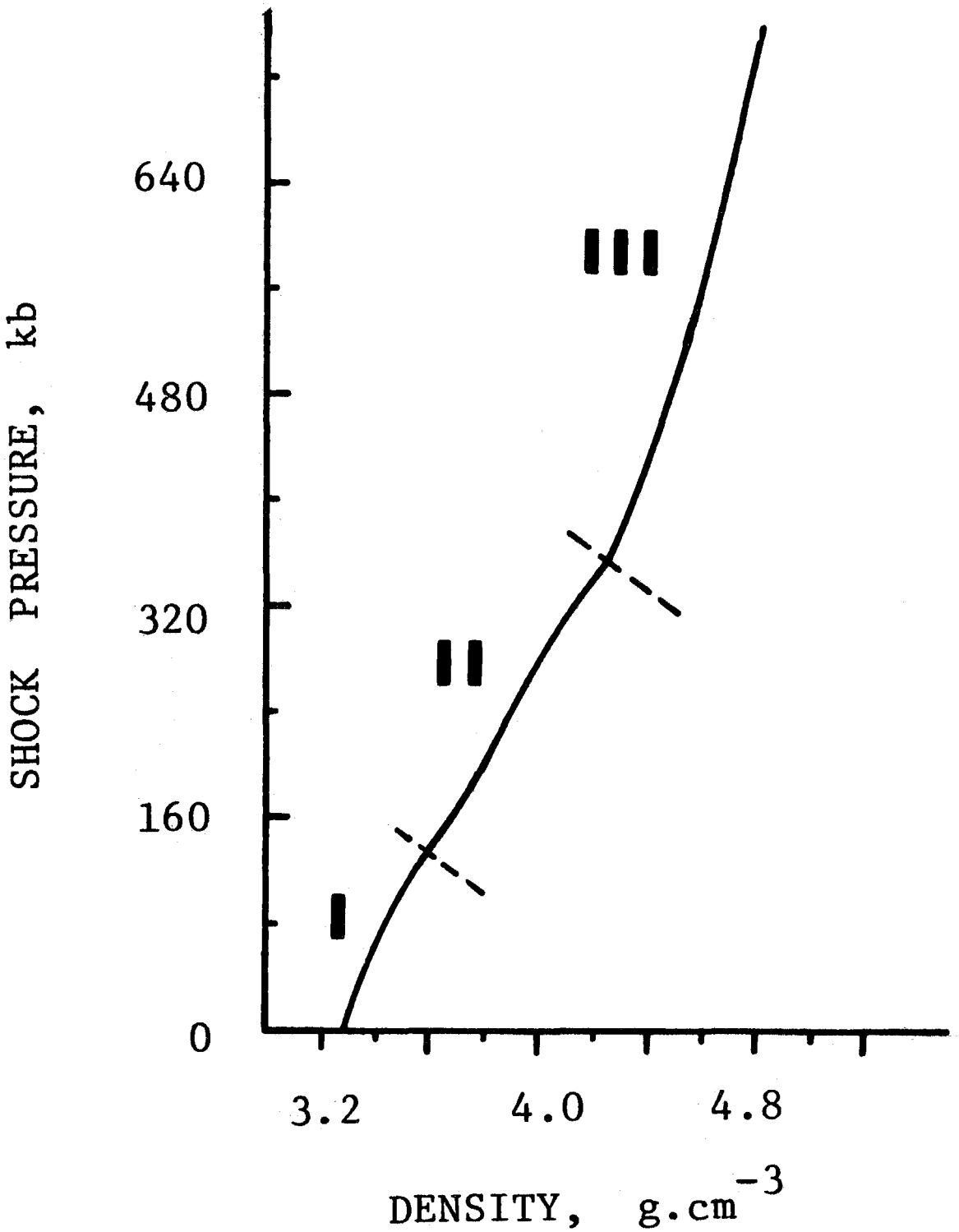
640
480
320
160
0
SHOCK PRESSURE, kb
I
II
III
3.2
4.0
4.8
DENSITY, g.cm^{-3}

meteorite (Smith and Mason, 1970). However, it has not been detected in any experimental shock recovery experiments.

Experimental Procedures

Shock-loading experiments to pressures as great as 528 kb were performed on Bamle orthopyroxene (bronzite, En86). Ten discs of single crystal material were shocked to Hugoniot states between 58 and 528 kb. Details of the experimental conditions are given in Table 11. All the sample discs were shocked in stainless steel 304 containers; the 1-inch diameter design was used in all but shot 126, in which the 3/4-inch design was used. Tungsten flyer plates were used on all except the 58 and 106 kb shots, on which aluminum 2024 and stainless steel 304 were used, respectively. The peak shock pressures were determined graphically from Figure 8 using the measured projectile velocities, as described earlier. The pressures are accurate to approximately $\pm$ 3%.

The original sample material was the large single crystal variety of bronzite from Bamle, Norway. This is typical of the Bamle bronzite that has been used for many other shock-wave experiments (for example, the Hugoniot equation of state studies by Ahrens and Gaffney, 1971). It has generally been referred to as Bamle enstatite in previous work despite numerous analyses that have shown its composition to be bronzite, En86. Details of an averaged electron microprobe chemical analysis and some measured physical properties are given

in Table 12. One microprobe analysis made by A. Chodos was recalculated into the molecular formula $(Mg_{0.86}, Fe_{0.14}, Ca_{0.005}, Al_{0.003})\ Si_{0.99}O_3$. Another analysis by the author gave similar proportions for the major elements plus the small amount of manganese indicated in the analysis in Table 12 (recalculated to molecular percent, $Mn_{0.01}$). In terms of the Mg,Fe endmembers of the orthopyroxene solid solution series, the specimen can be adequately described as bronzite, En86,Fs14 or $(Mg_{0.86}, Fe_{0.14})\ SiO_3$.

This result is corroborated by microscopic observations, particularly refractive index measurements and the optic sign. The refractive index measurements were made using standard immersion techniques with both white and monochromatic Na light. The measurements of $n_\alpha = 1.6695$ and $n_\gamma = 1.6820$ indicate a composition of En86 $\pm$ 0.015 according to the determinative curves for orthopyroxene of Hess (1952). In addition, the optic sign of the material is negative, indicating that the composition is more Fe-rich than En88. Accordingly, this material is rightly called Bamle bronzite, not Bamle enstatite.

Other physical properties of this material include density and lattice constants. The sample was x-rayed using both Debye-Scherrer (114.6 mm) and Guinier cameras

TABLE 11

Experimental Conditions For Bamle Bronzite Recovery Shots

Shot Number	Flyer[a] Plate (on Lexan)	Sample Thickness, mm	Impact Velocity, m s^{-1}	Peak Shock Pressure, kb
177	Al 2024	0.55	520	58
176	S.S.304	0.55	560	106
169	W	0.55	530	143
168	W	0.55	632	173
167	W	0.55	802	226
164	W	0.55	1018	297
165	W	0.55	1191	358
166	W	0.55	1276	386
170	W	0.55	1337	410
126[b]	W	1.1	1650	528

[a] 2.5 mm thick, of tungsten (W), stainless steel 304 (S.S.304), and aluminum 2024 (Al 2024)

[b] 1-inch diameter, stainless steel 304 sample containers were used in all shots except 126, in which a 3/4-inch diameter S.S.304 container was used.

and Fe Kα and Cu Kα radiation, respectively. The data given in Table 13 are the Guinier data; a least squares fit to these data using a computer program (Fortran IV) gave the d_{calc} tabulated in Table 13 and the lattice constants in Table 12. On the basis of these data and a molecular weight of 104.824 (determined using the probe analyses), an x-ray density of 3.325 $g.cm^{-3}$ was calculated. The density was not measured otherwise; however Ahrens and Gaffney (1971) give density measurements for fifteen fragments cut from the same stock of Bamle single crystals. Their average density is 3.287 ± 0.011 $g.cm^{-3}$. The difference between the measured and x-ray densities may represent the porosity of the samples, caused by the pervasive cleavages, of approximately 1%.

For sample disc preparation for shock-loading, slabs approximately 70 mm square and 5 mm thick were sawn from the (010) face of a large crystal. More than two dozen discs 4.75 mm in diameter were cored from those slabs. Before shock-loading the discs had to be hand-ground to a suitable thickness, usually accepted as 1 mm or less. Using standard grinding procedures it proved impossible to grind the discs even as thin as 1 mm without excessive fracturing and spalling; only one disc of 1.1 mm thickness stayed intact out of the first batch ground. It was shock-loaded in shot 126. Some changes were made in

TABLE 12

Analysis[a] of Orthopyroxene From Bamle, Norway

Oxide	Weight %
SiO_2	56.7
MgO	33.9
FeO[b]	9.7
MnO	0.2
CaO	0.2
Al_2O_3	0.1
	100.8

Refractive Indices

n_α	1.6695 ± 0.0010
n_β	1.676 ± 0.001
n_γ	1.682 ± 0.001

Density, $g.cm^{-3}$

D (calc. from x-ray data)	3.325
D (measured)	3.287 ± 0.011[c]

Lattice Constants

a_o	$18.216 \pm .039$ Å
b_o	$8.826 \pm .019$ Å
c_o	$5.210 \pm .011$ Å

[a] Variety, bronzite, En86, analysis on the California Institute of Technology electron microprobe

[b] Total Fe as FeO

[c] Average of 15 measurements in Table 1, Ahrens and Gaffney (1971)

TABLE 13

X-ray Powder Data For Bamle Bronzite

[a] d(Å)	I/I$_1$	d_{obs}(Å)[b]	d_{calc}(Å)[c]	hkl
4.43	3	4.42771	4.41279	020
4.028	1	4.01664		211
3.314	6	3.30220	3.31119	121
3.175	100	3.17823	3.16909	420
		3.16242	3.15836	221
2.946	16	2.94339	2.94480	321
2.878	54	2.87073	2.87094	610
2.832	9	2.82640	2.82824	511
2.710	10	2.70725	2.70754	421
2.540	25	2.53696	2.53673	131
2.497	18	2.49303		202
2.477	18	2.46931	2.47285	521
2.364	1	2.37901		302
2.257	3	2.24819	2.25108	711
2.239	3	2.23291	2.23270	431
2.116	12	2.10806	2.11273	630
2.100	12	2.09806	2.09553	531
2.060	5	2.05267	2.05909	721
2.025	7	2.01848	2.02353	820
		2.01848	2.01239	422
1.988	9	1.98255		421
1.961	11	1.95366	1.95787	631
1.888	4	1.88267	1.88626	821
1.681	1	1.69594	1.70189	831
1.610	11	1.60797		023
		1.60247	1.60221	10.2.1
1.591	6	1.58623	1.58814	931
1.591	6	1.58623	1.58455	840
1.529	5	1.52330	1.51945	551
1.522	7	1.52330	1.51803	12.0.0
1.488	23	1.48397	1.48456	10.3.1
1.473	17	1.47038	1.47093	060
		1.39081	1.39074	11.3.1

[a] Data from Pollack and Ruble (1964)

[b] Guinier powder data, Cu Kα radiation

[c] Least squares fit to Guinier data

the mounting medium and preparation techniques for the second batch; nine discs were still intact after grinding to 0.55 mm thickness. Those comprise the other shock-loaded samples.

The recovered sample containers were machined open on a lathe to expose the shocked discs. The exposed discs were then carefully examined using a binocular microscope before any material was removed for further studies. Those further studies were predominantly an optical microscopic characterization of the physical changes caused by the shock-loading.

Several grain mounts of fragments from each disc were examined using a polarizing microscope to observe shock-produced physical changes. Refractive indices were checked concomitantly using standard immersion techniques with white and monochromatic Na light. The universal stage technique (for example, Turner, 1947) was employed on some thin sections and specially prepared grain mounts to confirm the microscopic observations on shock-produced planar features and their orientations. Polished thin sections were made of the unshocked and of a number of the shocked samples. The pervasive fracturing and crushing of the discs made it impossible to make thin sections of all. Some samples were actually recovered as totally crushed and powdered specimens

rather than as coherent discs; this was probably due to a combination of the pre-shock cleavages and fractures and the post-shock additional planar features.

In a further search for indications of shock vitrification and for fine planar features, a number of selected specimens were prepared for examination with a transmission electron microscope (see Phakey et al., 1972). This was done with the cooperation of Dr. John Christie who helped prepare the specimens and operated the JEM-7A 120 kv electron microscope at the University of California at Los Angeles. Dr. Christie also arranged for the examination of an ion-thinned section of the specimen from shot 167 (226 kb) on an 800 kv transmission electron microscope at U.S. Steel Research Center, Pennsylvania.

Experimental Results and Discussion

Those experiments deal primarily with the study of crystalline bronzite shock-loaded to pressures between 58 and 528 kb. As described in Table 11, ten specimens of Bamle bronzite were shocked within this pressure range and essentially completely crystalline bronzite discs were recovered.

Grain mounts and thin sections of fragments from the shocked specimens were examined using a polarizing microscope. Refractive indices and crystallinity were monitored concomitant with the petrographic examination. However, in the absence of any optically resolvable vitrification, the prime purpose of the examination was to study the shock-induced planar deformation features, which had not previously been observed in experimentally shock-loaded orthopyroxene.

In the recovered samples, no change in refractive index was observed from the indices of the unshocked material (Table 12).

One feature characteristic of all the samples is the crushing and fracturing caused by the shock-loading. This increases in intensity with the shock pressure. The other feature present in all samples is the fine (001) deformation features; it is observed at all pressures from 58 to 526 kb. However, it is most

outstanding in the lower pressure samples. This appears to be because of the additional crushing of the samples at higher pressures. Figures 32 and 33 are photomicrographs of fragments from shot 177 (58 kb) which contain excellent examples of those planar features. No such features are present in the unshocked samples. Optically, these features appear to be very fine, micron-sized, polysynthetic twin lamellae. This agrees with previous observations on pyroxenes from naturally shocked terrestrial and lunar rocks (for example, Chao et al., 1970; Engelhardt et al., 1971; Stöffler, 1972), meteorites (for example, Levi-Donati, 1971), basaltic rocks from nuclear explosion craters (for example, James, 1969a), and laboratory experiments (diopside: Hornemann and Müller, 1971). In their shock experiments on diopside, Hornemann and Müller found that the (001) twin lamellae occurred at all pressures from 50 to 390 kb. My observations on orthopyroxene show that they occur at the lowest pressure and persist throughout the whole shock-loading range, 58 to 528 kb.

At pressures below 173 kb, no optically anomalous interference was observed in the shocked bronzite. However, at 173 kb, some indications of undulatory extinction were apparent on a number of fragments. At 226 kb, there were more fragments exhibiting the anomalous

FIGURE 32

Photomicrograph of Bamle bronzite shock-loaded to 58 kb (shot 177). Crossed nicols, transmitted light, 50X magnification. Note the very fine (001) deformation features. Scale: long side of photograph equals 0.3 mm.

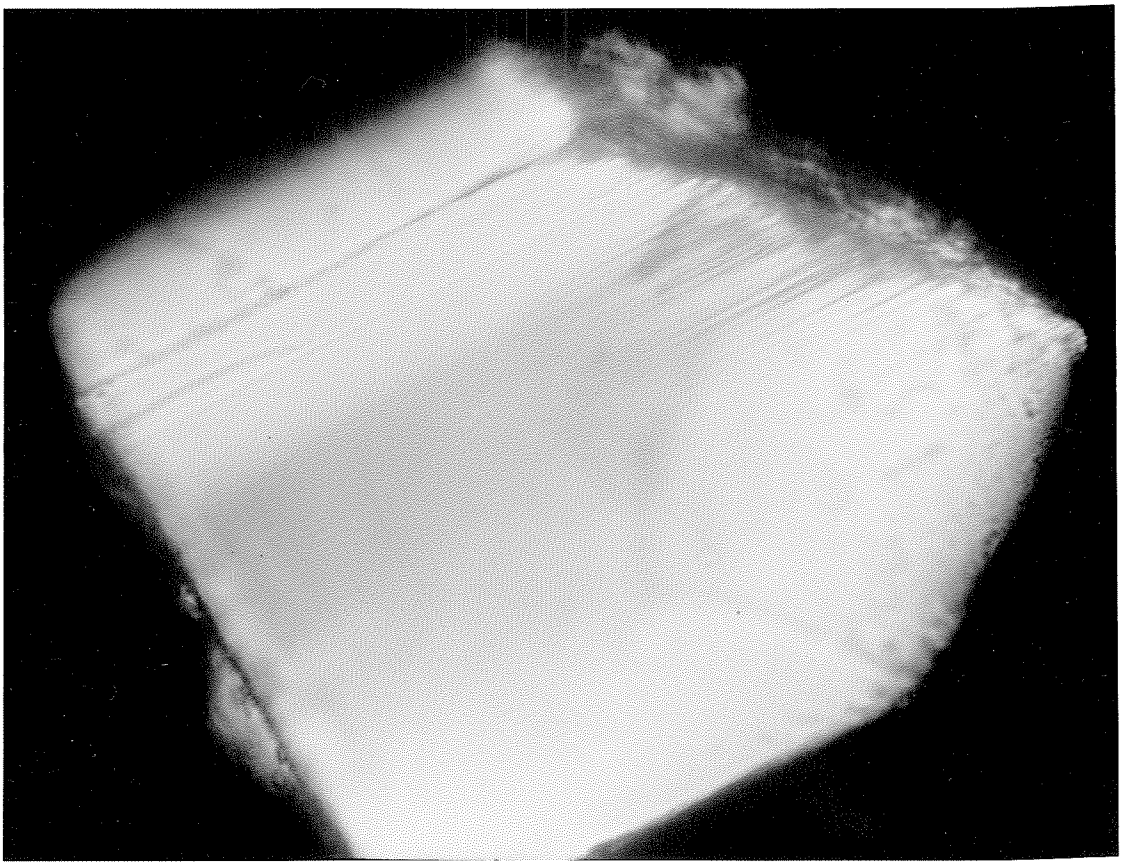

FIGURE 33

Photomicrograph of Bamle bronzite shock-loaded to 58 kb (shot 177). Crossed nicols, transmitted light, 100X magnification. A different fragment from that in Figure 33 containing similar fine deformation structures on (001). Scale: long side of photograph equals 0.15 mm.

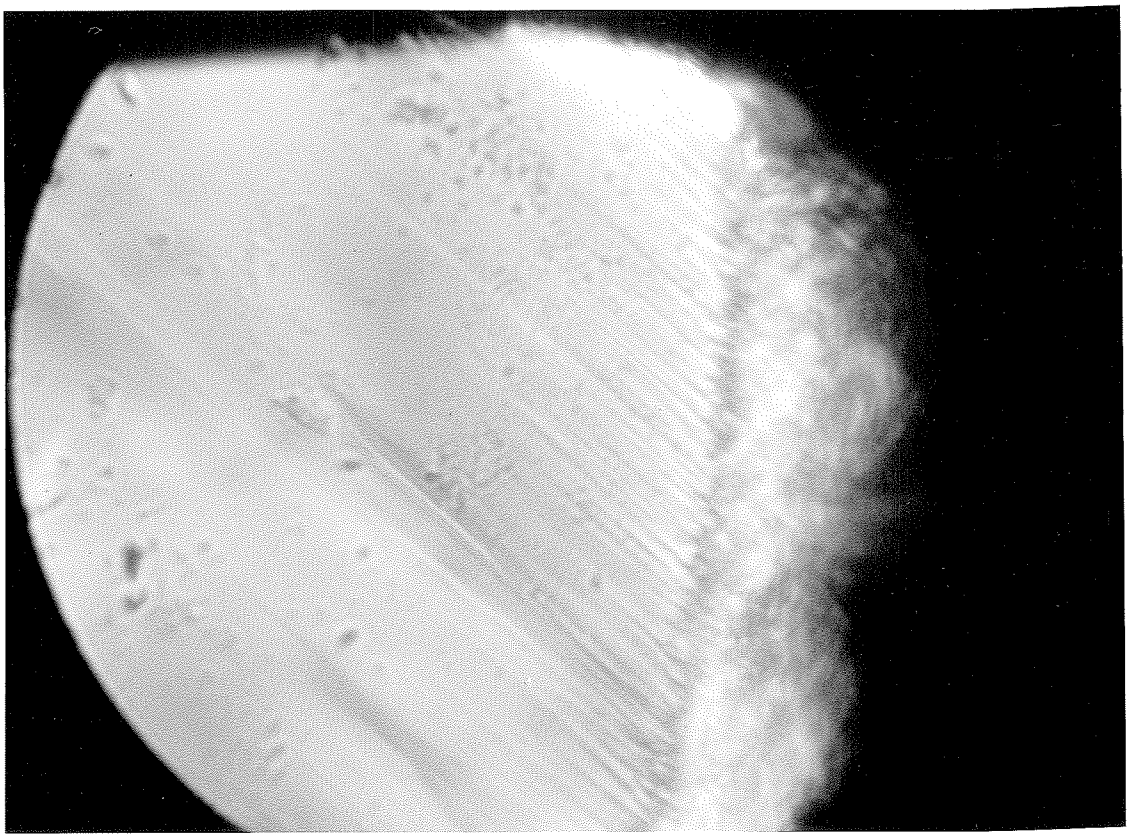

extinction. This remained so at all pressures to 528 kb. Those anomalous optical properties were caused by shock-produced mosaicism (Hörz and Quaide, 1973).

No shock vitrification was detected optically at any pressure. However, in an ion-thinned section of shot 167 (226 kb), a very small amount of glass was detected on fractures using a 800 kv transmission electron microscope. Figure 34 is a photomicrograph of a part of that thin section showing shock-produced dislocation features at 11,500X magnification. The glass is not resolved in this photograph. The significance of the discovery of this glass is that it had not previously been observed in shock-loaded single crystal pyroxene, even at pressures of 1000 kb. However, it must be emphasized that the amount produced was very small and is still optically non-resolvable at 526 kb. More studies are required on pyroxene to determine whether the glass might be forming in a region of the specimen being subjected to anomalous shock pressures and temperatures.

FIGURE 34

Shot 167, 226 kilobars, Bamle bronzite. Transmission electron microscope photograph at 11,500X magnification showing increased dislocation population caused by shock-loading. A very small amount of shock glass has been observed in this thin-section; it is not resolved in the photograph.

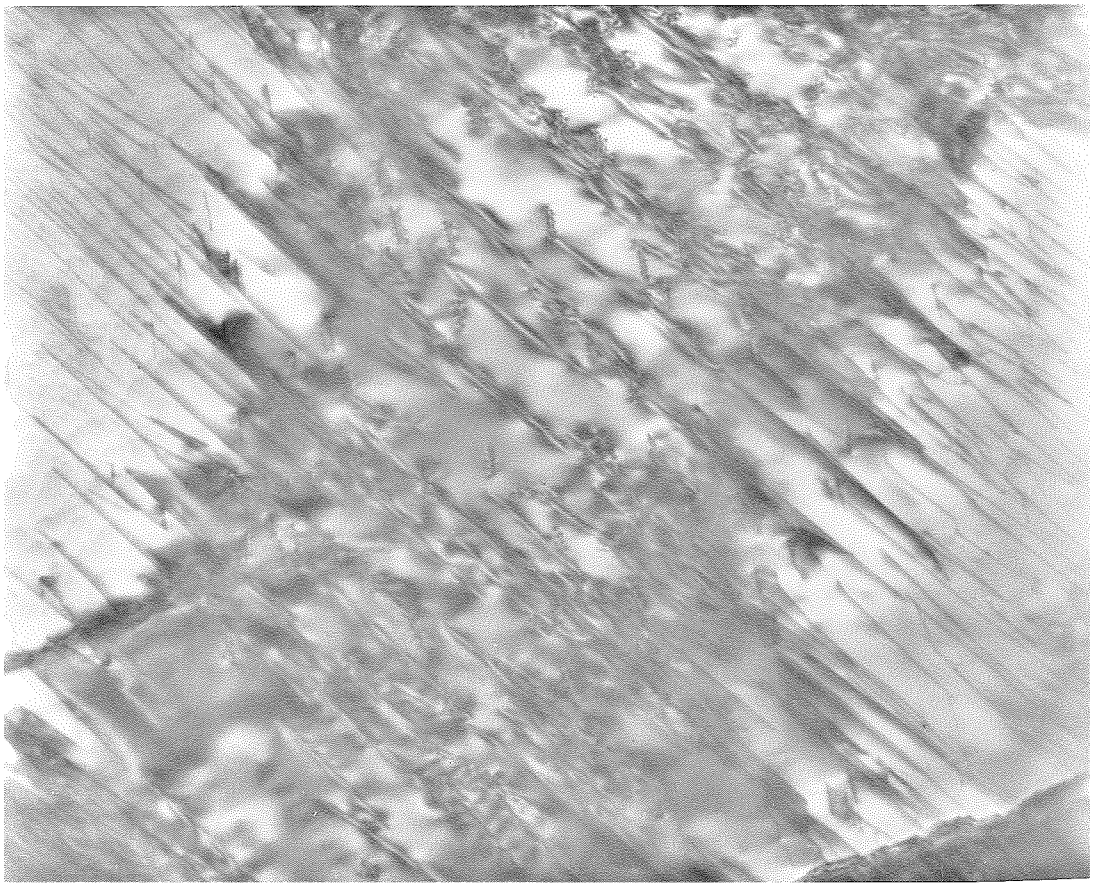

Conclusion

Bamle bronzite shock-loaded to Hugoniot states throughout the shock-loading range of 58 to 528 kb remains almost entirely in the crystalline state upon adiabatic release to zero pressure. Throughout this whole range, excessive shock-induced fracturing and crushing results. Fine micro-sized deformation twins are also produced at all pressures from 58 to 528 kb. These physical features are due to a combination of shock compression and relaxation following pressure release.

No shock vitrification is resolved optically. However, a very small amount of glass was detected at 226 kb using a 800 kv transmission electron microscope. This glass needs to be studied more carefully before its significance can be fully determined.

Chapter VII.

SHOCK METAMORPHISM:

A VIEW BASED ON EXPERIMENTAL RESULTS..... 186

In 1966 French suggested that a working definition of shock metamorphism might be 'the totality of observed effects in natural rocks resulting from the passage of transient high-pressure shock waves'. In view of (1) the implication that these are only natural phenomena and (2) the increasing abundance of data on experimentally-produced shock metamorphic phenomena, I propose that his definition be slightly changed to read 'the totality of the permanent effects caused in any material by the passage of transient high pressure shock waves'.

The phenomena and processes of shock metamorphism are totally different from those of normal terrestrial metamorphism. However, shock metamorphism can be studied in terms of facies or zones or grades of metamorphism just like normal load metamorphism. In essence, the variations in shock phenomena that have been observed in experimentally and naturally shocked rocks are really a particular metamorphic facies series characterized by high shock pressures and their accompanying shock and post-shock temperatures.

Recently, a number of workers have proposed schemes of progressive shock metamorphism (that is, shock metamorphic facies series) based primarily on observations on naturally shocked rocks but tied to the minimal available

experimental data. The major proposals have been those based (1) on studies of the Ries crater, Germany, especially Chao (1967a, 1967b, 1968), Stöffler (1966, 1967) and Engelhardt (1968), and (2) on studies of Canadian craters (Dence, 1968), with a word of caution from DeCarli (1968) that the anomalous features observed in meteorites and 'shocked' terrestrial rocks must still be viewed with some skepticism in view of the limitations of our present knowledge on the experimentally-induced effects of shock waves on rocks and minerals.

More recently, Stöffler (1971, 1972) reviewed these classifications and emphasized a derivation of progressive stages of shock metamorphism from Hugoniot equation of state data on framework silicates, using the latest available experimental data in the assigning of boundaries to his metamorphic facies. A serious limitation has been imposed on his classification by (1) the lack of any actual measurements on post-shock temperatures, (2) the lack of experimental data on minerals and rocks shock-loaded to pressures greater than 500-600 kb and (3) the emphasis on tectosilicates, although he does consider the observations made by James (1969a) and Short (1969) on basalt shock metamorphosed by a nuclear explosion. I will correlate Stöffler's classification to one that I propose on the basis of the present work on

labradorite and bronzite and other recent experimental studies.

In proposing any scheme of progressive shock metamorphism, I believe that experimental shock wave data on the common rock-forming minerals warrant primary consideration, for correlation with the permanent 'shock' effects observed in naturally shocked rocks. Before any consideration of experimentally-induced 'permanent' shock features, it is worthwhile to look at Hugoniot data for some common minerals. Within the last decade, Hugoniot curves have been measured for most of the common rock-forming silicates and oxides, by Ahrens and coworkers, McQueen and coworkers, and others (for example, Ahrens et al., 1969b; McQueen et al., 1970; Wackerle, 1962). The Hugoniots of four silicates are given in Figure 35, namely, two framework silicates, quartz and oligoclase, a chain silicate, orthopyroxene, and an orthosilicate, forsterite. Note the relative shapes of those Hugoniots and their positions in P-V space. The tectosilicates exhibit one type of behavior, with large volume changes in their mixed phase regimes, while the mafic pyroxene and olivine behave quite differently. These differences are quite dependent on the mineral compressibilities and densities, as shown in Figure 36. The change in the compressibility-density relations from tectosilicates to garnets correlates with

FIGURE 35

Relative Hugoniots of quartz (Wackerle, 1962), oligoclase (Ahrens et al., 1969b), bronzitic orthopyroxene (Ahrens and Gaffney, 1971; McQueen and Marsh, 1966), and forsterite (Ahrens et al., 1971; McQueen and Marsh, 1966). Note the behavior of the framework silicates contrasted to the more dense and less compressible ortho- and chain-silicates. In particular, note the relative difference in volume change in their mixed phase regimes.

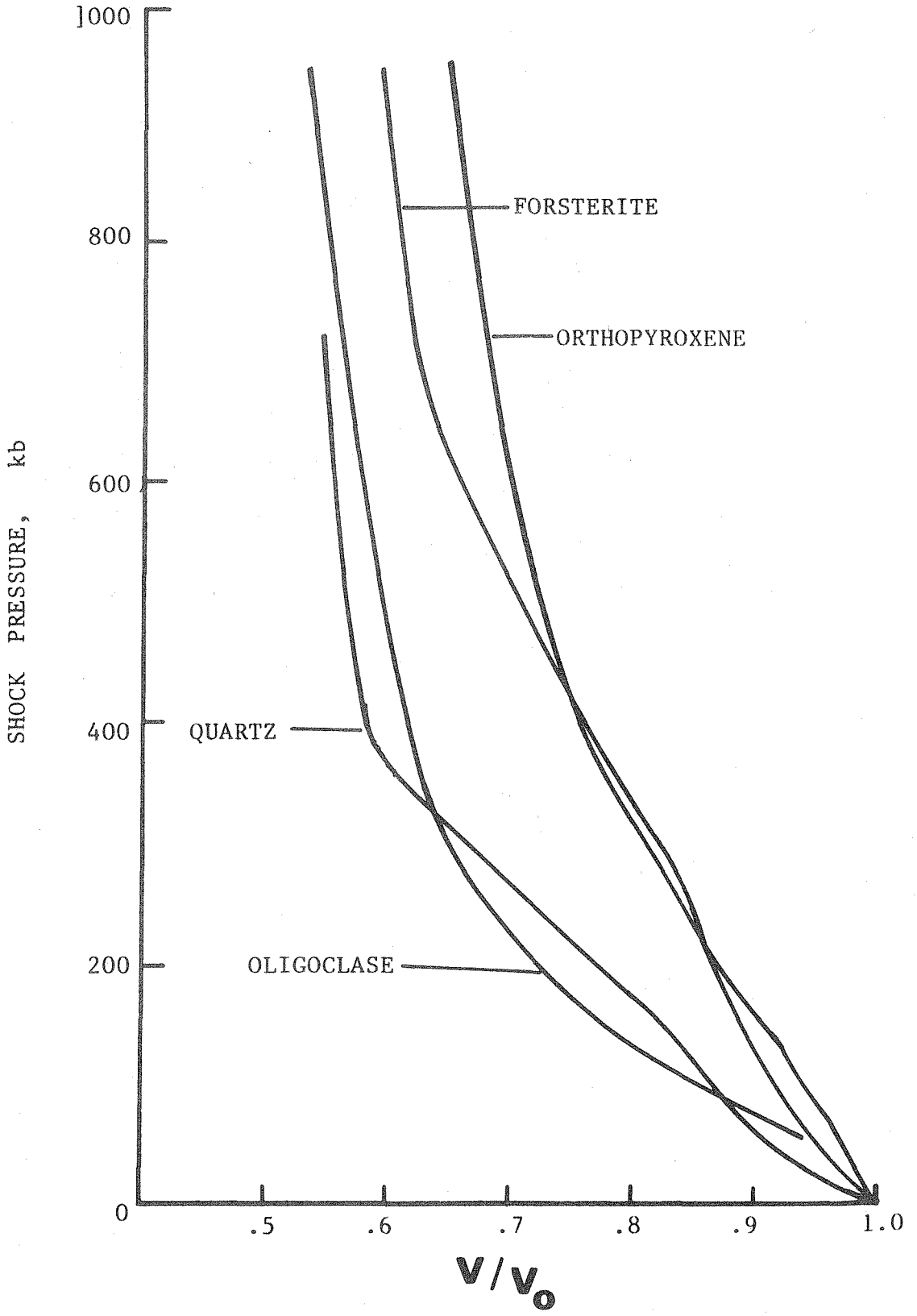
1000
800
600
400
200
0
SHOCK PRESSURE, kb
FORSTERITE
ORTHOPYROXENE
QUARTZ
OLIGOCLASE
.5
.6
.7
.8
.9
1.0
V/Vo

FIGURE 36

Compressibility versus density relationships of common rock-forming minerals (Data from Birch, 1966).

Feldspars

Mica

Amphiboles

Pyroxenes

Olivines

Garnets

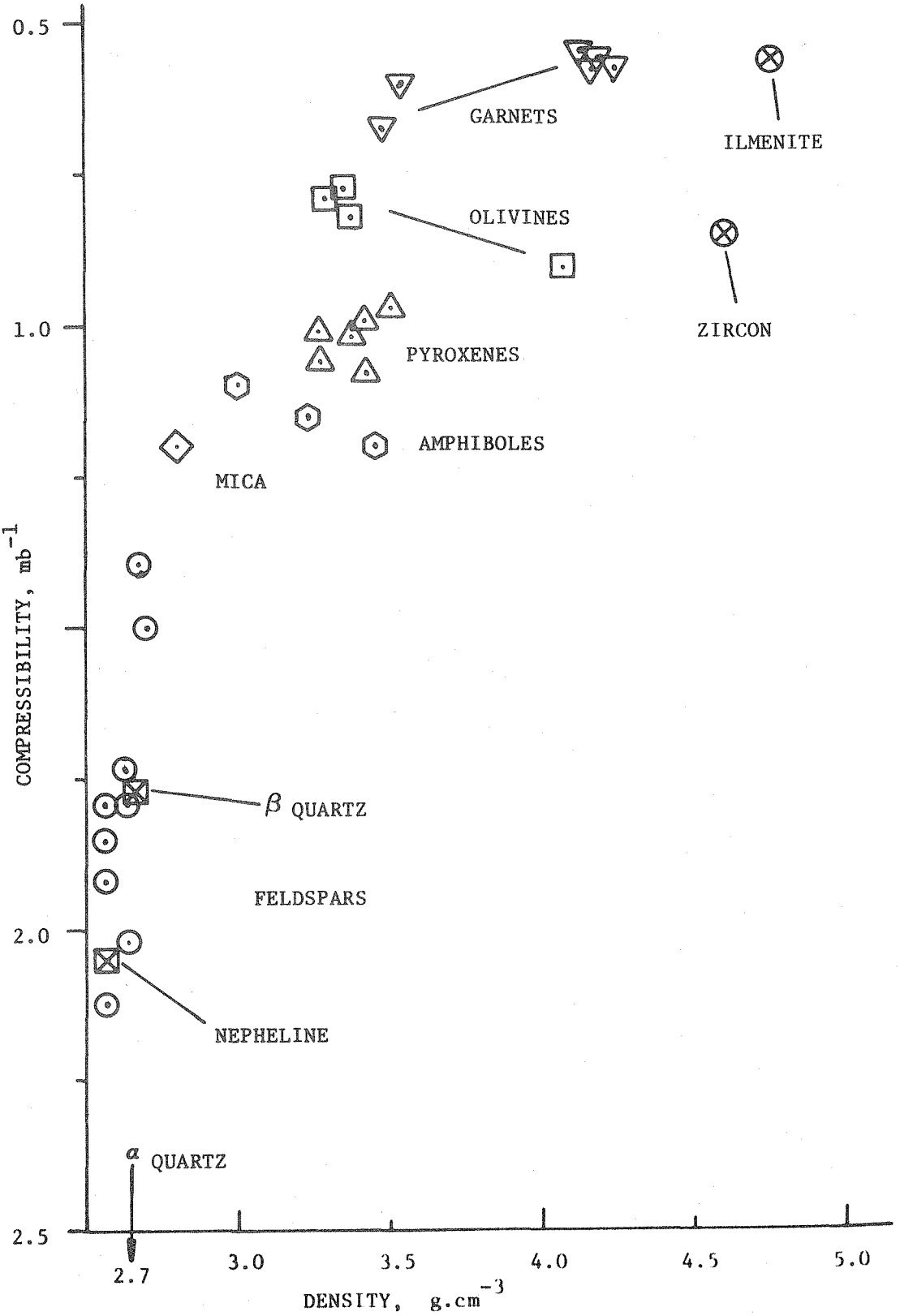
0.5
1.0
2.0
2.5
COMPRESSIBILITY, mb^{-1}
GARNETS
ILMENITE
OLIVINES
ZIRCON
PYROXENES
AMPHIBOLES
MICA
β QUARTZ
FELDSPARS
NEPHELINE
α QUARTZ
2.7
3.0
3.5
4.0
4.5
5.0
DENSITY, g.cm^{-3}

the change in Hugoniot behavior.

This behavior can also be correlated with shock and post-shock temperatures. In tectosilicates these temperatures are higher at lower pressures and increase faster with pressure than they do in chain silicates. The temperatures presently available have been calculated, rather than measured, based mainly on data of Ahrens and coworkers (for example, Ahrens et al., 1969b). Although calculated using the latest experimental data, there is reason to use these temperatures with some skepticism since they tend to be lower than one would like to believe. However, until actual measurements of shock and post-shock temperatures are made, they are the best estimates available.

In my proposed classification of shock metamorphism, I emphasize the shock pressure since it can be measured very accurately in a shock-loading experiment. Shock pressure is correlated with common silicate Hugoniots and the permanent effects induced by shock-loading in those common silicate minerals (Figure 37). The boundary between shock zone I and shock zone II is placed at 225 kb, the pressure of the first appearance of diaplectic glass in tectosilicates. At pressures below 225 kb, the recovered material is essentially the initial low pressure phases with shock-induced deformation features but no

FIGURE 37

Correlation of progressive stages of shock metamorphism with shock pressure and some common silicate Hugoniots (same as those in Figure 35). Zone I: predominantly low pressure phases with shock-induced deformation features; in quartz-bearing rocks, stishovite may be present at pressures above 90 kb (Kleeman and Ahrens, 1973). Zone II: diaplectic tectosilicates + their possible high pressure phases + low pressure phases. Zone III: shock-fused tectosilicates + crystalline ortho- and chain- silicates (including their possible high pressure phases). An upper limit of Zone III could be the formation of diaplectic or shock-fused glasses from pyroxenes or olivines. This has not yet been achieved in laboratory-scale experiments on single crystal material but appears to be above 1000 kb (Dundon and Hafner, 1971). The shock pressures required for total shock melting and vaporization of mafic rocks have also not yet been determined in the laboratory.

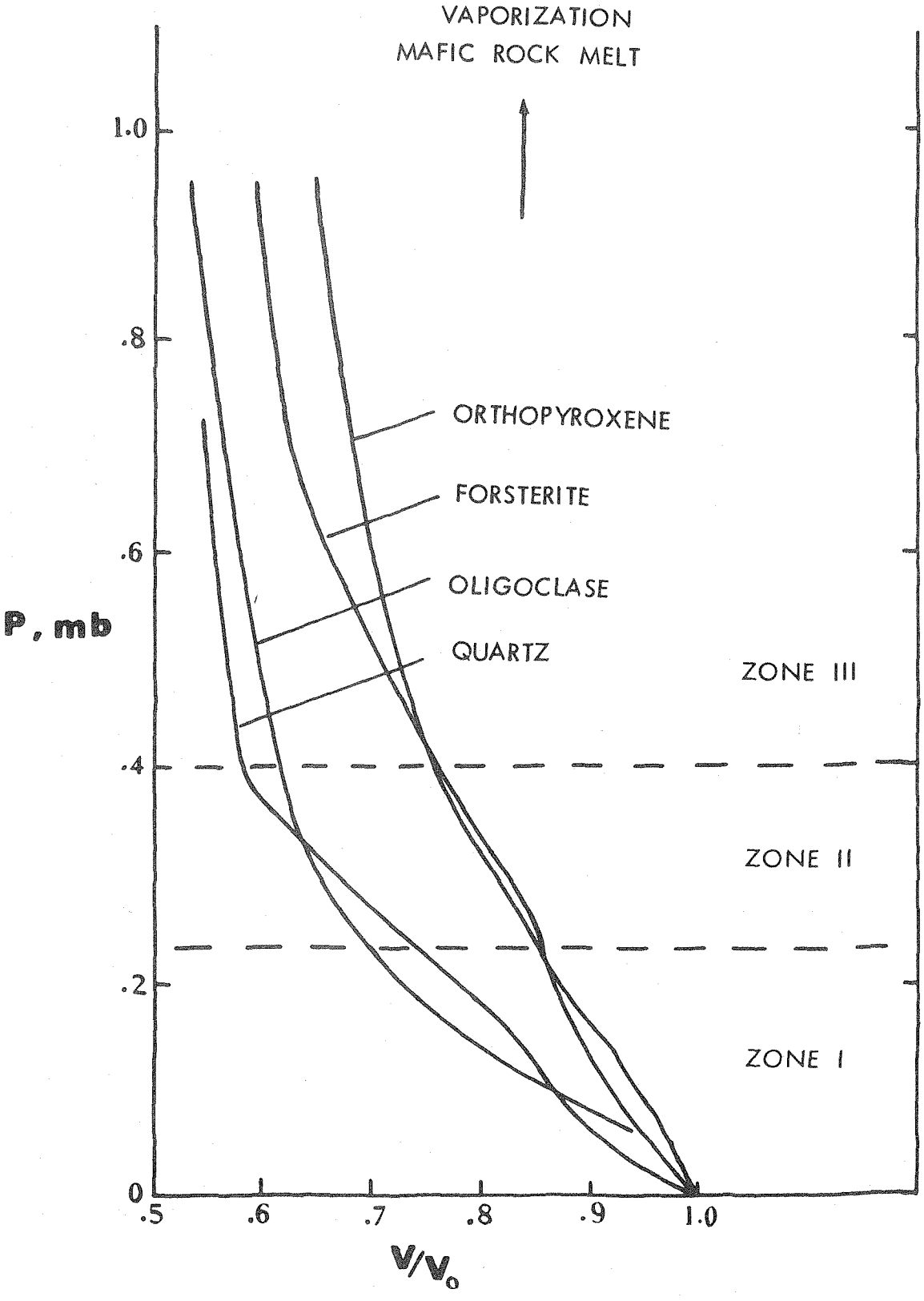
VAPORIZATION
MAFIC ROCK MELT
1.0
.8
.6
.4
.2
0
P, mb
ORTHOPYROXENE
FORSTERITE
OLIGOCLASE
QUARTZ
ZONE III
ZONE II
ZONE I
.5
.6
.7
.8
.9
1.0
V/V₀

other physical changes. In quartz specimens stishovite is present in minute amounts at pressures above 90 kb (Kleeman and Ahrens, 1973). It decreases in abundance above 230 kb in the range in which diaplectic glass is increasing rapidly. In quartz-rich rocks it may be useful to denote a sub-zone between 90 and 225 kb, characterized by the first appearance of stishovite. This pressure range also correlates with the lower part of the mixed phase regime of the quartz Hugoniot. It also correlates with part of the mixed phase regime of the plagioclase Hugoniot. However, neither the hollandite structure feldspar (Ringwood et al., 1968; Kinomura et al., 1971) nor jadeite (James, 1969b) has yet been observed in experimental shock recovery experiments so these phases cannot be used as index minerals in expanding the classification further.

Zone II extends from 225 kb to 400 kb. The upper boundary of zone II is marked by shock-fusion of tectosilicates. Throughout zone II, the phases present include diaplectic tectosilicate glasses, diaplectic tectosilicate crystals, initial low pressure phases, and possible high pressure phases. Deformation features are still present in all materials. A smaller amount of stishovite is present than in zone I (Kleeman and Ahrens, 1973). No other high pressure phases have been

recovered from shock experiments. On the basis of observations on natural materials, coesite may also be present in this zone (Chao et al., 1960). Since this is also within the mixed phase regimes of olivine and pyroxene, one might expect to find high pressure phases of those minerals appearing also. The high pressure phase of pyroxene (Ringwood and Major, 1966, 1968) has not been recovered from shock-loading experiments; however, Smith and Mason (1970) have observed majorite (a garnet-structure mineral of pyroxene stoichiometry) in the Coorara meteorite, so it may be a candidate index mineral for somewhere in this zone in naturally shocked rocks. Likewise, ringwoodite, a high pressure phase of olivine, has been observed in a meteorite (Binns, 1970; Binns et al; 1969) so it may also occur in naturally shocked rocks. It has not yet been identified in experimentally shocked rocks.

Zone III is marked by the shock-fusion of tectosilicates. It is also the beginning of the high pressure phase regime of the plagioclase Hugoniot (see Figure 26). The mafic minerals are still essentially initial low pressure phase materials although this zone is mainly in the high pressure phases of their Hugoniots as well. If high pressure phases of pyroxene and olivine can be produced by experimental shock-loading, they should be present in this zone. However, the absence of those

phases, on the basis of the experimental results, does not indicate a lower pressure than 400 kb. On the contrary, pyroxene is apparently still crystalline and stable at pressures as high as 1000 kb (Dundon and Hafner, 1971) in single crystal shock-loading experiments. Thus, pyroxene is not shock-melted at pressures up to a megabar. I would put the shock vitrification of pyroxene or olivine as the boundary of zone IV. Since this has not been experimentally achieved on single crystals, I have not defined any new zones between 400 and 1000 kb. Zone III consists essentially of tectosilicate melt including crystalline mafic minerals. The shock pressure at which the post-shock temperature of this melt will be sufficient to melt those mafic minerals has not yet been determined experimentally. Experimental shock-loading studies of basaltic rocks will resolve this question and delineate the P,T conditions at which rock melting will be achieved (for example, Dence, 1971). At still higher pressures extensive shock vaporization will occur. Both these problems require a great deal of study and experimental shock-loading research.

REFERENCES

Ahrens, T. J., D. L. Anderson and A. E. Ringwood, Equations of state and crystal structures of high pressure phases of shocked silicates and oxides, Rev. Geophys. 7, 667-707, 1969a.

Ahrens, T. J., R. L. Fleischer, P. B. Price and R. T. Woods, Erasure of fission tracks in glasses and silicates by shock waves, Earth Planet. Sci. Lett. 8, 420, 1970.

Ahrens, T. J. and E. S. Gaffney, Dynamic compression of enstatite, J. Geophys. Res. 76, 5504-5514, 1971.

Ahrens, T. J. and V. G. Gregson, Jr., Shock compression of crustal rocks: data for quartz, calcite, and plagioclase, J. Geophys. Res. 69, 4839-4874, 1964.

Ahrens, T. J., J. H. Lower and P. L. Lagus, Equation of state of forsterite, J. Geophys. Res. 76, 518-528, 1971.

Ahrens, T. J. and J. D. O'Keefe, Shock-melting and vaporization of lunar rocks and minerals, The Moon 4, 214-249, 1972.

Ahrens, T. J., C. F. Petersen and J. T. Rosenberg, Shock compression of feldspars, J. Geophys. Res. 74, 2727-2746, 1969b.

Ahrens, T. J. and J. T. Rosenberg, Shock metamorphism: experiments on quartz and plagioclase, in Shock

Metamorphism of Natural Materials, edited by B. M. French and N. M. Short, Mono Book Corporation, Baltimore, 59-81, 1968.

Anderson, O. L. and E. Schreiber, The relation between refractive index and density of minerals related to the earth's mantle, J. Geophys. Res. 70, 1463, 1965.

Arndt, J., U. Hornemann and W. F. Müller, Shock-wave densification of silica glass, Phys. Chem. Glasses 12, 1-7, 1971.

Bancroft, G. M. and R. G. Burns, Interpretation of the electronic spectra of iron in pyroxenes, Amer. Mineral. 52, 1278-1287, 1967.

Barth, T. F. W., Feldspars, Wiley-Interscience, New York, 1969.

Bell, P. and E. C. T. Chao, Annealing experiments with naturally and experimentally shocked feldspar glasses, Carnegie Inst. Wash. Yearbk. 68, 336-339, 1969.

Binns, R. A., Stony meteorites bearing maskelynite, Nature 213, 1111-1112, 1967.

Binns, R. A., $(Mg,Fe)_2SiO_4$ - spinel in a meteorite, Phys. Earth Planet. Interiors 3, 156-160, 1970.

Binns, R. A., R. J. Davis and S. J. B. Reed, Ringwoodite, natural $(Mg,Fe)_2SiO_4$ - spinel, in the Tenham meteorite, Nature 221, 943-944, 1969.

Birch, F., Compressibility, in Handbook of Physical Constants, edited by S. P. Clark, Jr., Geol. Soc. Amer.

Memoir 97, 97-173, 1966.

Bless, S. J., The effects of magnetic pinch pressure on boron nitride, cadmium sulfide, graphite, silica glass, and some other materials, Ph.D. thesis, Massachusetts Institute of Technology, Boston, 1970.

Borg, I. Y., Some shock effects in granodiorite to 270 kilobars at the Piledriver site, Geophysical Monograph Series Vol. 16, 1972.

Borg, I. Y. and H. C. Heard, Experimental deformation of plagioclase, in Experimental and Natural Rock Deformation, edited by P. Paulitsch, Springer, New York, 375-403, 1970.

Bridgman, P. W. and I. Simon, Effects of very high pressure on glass, J. Appl. Phys. 24, 405, 1953.

Bunch, T. E., Some characteristics of selected minerals from craters, in Shock Metamorphism of Natural Materials, edited by B. M. French and N. M. Short, Mono Book Corporation, Baltimore, 413-432, 1968.

Bunch, T. E., A. J. Cohen and M. R. Dence, Shock-induced structural disorder in plagioclase and quartz, in Shock Metamorphism of Natural Materials, edited by B. M. French and N. M. Short, Mono Book Corporation, Baltimore, 509-518, 1968.

Bunch, T. E., M. R. Dence and A. J. Cohen, Natural terrestrial maskelynite, Amer. Mineralogist 52, 244-253, 1967.

Burdick, L. J. and R. V. Gibbons, Post-impact temperatures in Al 2024, Bull. Amer. Phys. Soc., Series II, 17, 1088, 1972. (Abstract)

Burns, R. G., Mineralogical Applications of Crystal Field Theory, Cambridge University Press, 1970.

Burns, R. G. and R. G. J. Strens, Structural interpretation of polarized absorption spectra of the Al-Mn-Fe-Cr epidotes, Min. Mag. 36, 204-226, 1967.

Burns, R. G., J. A. Tossell and D. J. Vaughan, Pressure-induced reduction of a ferric amphibole, Nature 240, (5375), 33-35, 1972.

Carter, N. L., Static deformation of silica and silicates, J. Geophys. Res. 76, 5514-5540, 1971.

Chao, E. C. T., Shock effects in certain rock-forming minerals, Science 156, 192-202, 1967a.

Chao, E. C. T., Impact metamorphism, in Researches in Geochemistry 2, edited by P. H. Abelson, John Wiley and Sons, New York, 204-233, 1967b.

Chao, E. C. T., Pressure and temperature histories of impact metamorphic rocks --- based on petrographic observations, in Shock Metamorphism of Natural Materials, edited by B. M. French and N. M. Short, Mono Book Corporation, Baltimore, 135-158, 1968.

Chao, E. C. T. and P. M. Bell, Annealing characteristics of dense feldspar glass, Carnegie Inst. Wash. Yearbk. 67, 126, 1968.

Chao, E. C. T., O. B. James, J. A. Minkin, J. A. Boreman, E. D. Jackson and C. B. Raleigh, Petrology of unshocked crystalline rocks and evidence of impact metamorphism in Apollo 11 returned lunar sample, Geochim. Cosmochim. Acta, Suppl. 1, 1, 287-314, 1970.

Chao, E. C. T., E. M. Shoemaker and B. M. Madsen, First natural occurrence of coesite, Science 132, 220-222, 1960.

Christie, J. M., A. H. Heuer, J. S. Lally, G. L. Nord, Jr., S. V. Radcliffe, R. M. Fisher and D. T. Griggs, Electron petrography of Apollo 14 and 15 breccias and shock-produced analogs, Geochim. Cosmochim. Acta, Suppl. 4, 1, 365-382, 1973.

Craig, H., Density and refractive index hysteresis in compressed silicate glasses, J. Geophys. Res. 74, 4910, 1969.

Davis, T. S., J. P. Fackler and J. M. Weeks, Spectra of manganese(III) complexes. The origin of the low energy band, Inorg. Chem. 7, 1994-2002, 1968.

DeCarli, P. S., Observations of the effects of explosive shock on crystalline solids, in Shock Metamorphism of Natural Materials, edited by B. M. French and N. M. Short, Mono Book Corporation, Baltimore, 129-134, 1968.

DeCarli, P. S. and D. J. Milton, Stishovite: Synthesis by shock wave, Science 147, 144, 1965.

Dence, M. R., Shock zoning at Canadian craters: Petrography and structural implications, in Shock Metamorphism of Natural Materials, edited by B. M. French and N. M. Short, Mono Book Corporation, Baltimore, 169-184, 1968.

Dence, M. R., Impact melts, J. Geophys. Res. 76, 5552-5565, 1971.

Dingle, R., The visible and near-infrared spectrum of manganese(III) complexes, Acta Chem. Scand. 20, 33-44, 1966.

Dremin, A. N. and G. A. Adadurov, The behavior of glass under dynamic loading, Soviet Phys. Solid State, 1379, 1964.

Drickamer, H. G., V. C. Bastron, D. C. Fisher and D. C. Grenoble, The high-pressure chemistry of iron, J. Solid State Chem. 2, 94-104, 1970.

Drickamer, H. G. and C. W. Frank, Electronic Transitions and High Pressure Chemistry and Physics of Solids, Chapman and Hall, London, Ch. 9, 10, 1972.

Duke, M. B., The Shergotty meteorite: magmatic and shock metamorphic features, in Shock Metamorphism of Natural Materials, edited by B. M. French and N. M. Short, Mono Book Corporation, Baltimore, 613-622, 1968.

Dundon, R. W. and S. S. Hafner, Cation disorder in shocked orthopyroxene, Science 174, 581-593, 1971.

Duvall, G., Concepts of shock wave propagation, Bull. Seismol. Soc. Amer. 52, 869-893, 1962.

Duvall, G. E., Shock waves in solids, in Shock Metamorphism of Natural Materials, edited by B. M. French and N. M. Short, Mono Book Corporation, Baltimore, 19-29, 1968.

Duvall, G. E. and G. R. Fowles, Shock waves, in High Pressure Physics and Chemistry, edited by R. S. Bradley, McGraw-Hill, New York, 2, 209-291, 1963.

Dworak, U., Stosswellenmetamorphose des Anorthosits von Manicouagan-Krater, Quebec, Canada, Contr. Mineral. and Petrol. 24, 306-347, 1969.

Engelhardt, W. von, J. Arndt, W. F. Müller and D. Stöffler, Shock metamorphism of lunar rocks and origin of the regolith at the Apollo 11 landing site, Geochim. Cosmochim. Acta, Suppl. 1, 1, 363-394, 1970.

Engelhardt, W. von, J. Arndt, W. F. Müller and D. Stöffler, Shock metamorphism and origin of the regolith and breccias at the Apollo 11 and 12 landing sites, Geochim. Cosmochim. Acta, Suppl. 2, 1, 833-854, 1971.

Engelhardt. W. von, J. Arndt, D. Stöffler, W. F. Müller, H. JeziorKowski and R. A. Gubser, Diaplektische Glaser in den Breccien des Ries von Nördlinger als Anzeichen fur stosswellenmetamorphose, Contr. Miner. and Petrol. 15, 91-100, 1967.

Engelhardt, W. von and D. Stöffler, Stages of shock metamorphism in crystalline rocks of the Ries Basin, Germany, in Shock Metamorphism of Natural Materials, edited by B. M. French and N. M. Short, Mono Book Corporation, Baltimore, 159-169, 1968.

French, B. M., Shock metamorphism of natural materials, Science 153, 903-906, 1966.

French, B. M. and N. M. Short (editors), Shock Metamorphism of Natural Materials, Mono Book Corporation, Baltimore, 1968.

Gibbons, R. V., Shock reduction of Mn^{3+} to Mn^{2+} in rhodonite, Bull. Amer. Phys. Soc., Series II, 17, 1106, 1972. (Abstract)

Gibbons, R. V., Experimentally induced shock effects in plagioclase and pyroxene, EOS, Transactions of the American Geophysical Union 54, 351, 1973. (Abstract)

Gibbons, R. V. and T. J. Ahrens, Shock metamorphism of silicate glasses, J. Geophys. Res. 76, 5489-5498, 1971.

Gibbons, R. V., T. J. Ahrens and G. R. Rossman, A spectrographic interpretation of the shock-produced color change in rhodonite ($MnSiO_3$): The shock-induced reduction of Mn(III) to Mn(II), Amer. Miner. 59, 177-182, 1974.

Gibbons, R. V. and J. D. Kleeman, Refractive index measurements of artifically shocked glasses and of glasses formed by shock-loading crystalline phases, EOS, Trans. Amer. Geophys. Union, 51, 770, 1970. (Abstract)

Hess, H. H., Orthopyroxenes of the Bushveld type, ion substitutions and changes in unit cell dimensions, Amer. J. Sci., Bowen Volume, 173-187, 1952.

Hornemann, U. and W. F. Müller, Shock-induced deformation twins in clinopyroxene, N. Jahrb. Miner. Mh.6, 247-256, 1971.

Hörz, F. (editor), Meteorite Impact and Volcanism, J. Geophys. Res. 76, 5381-5798, 1971.

Hörz, F. and T. J. Ahrens, Deformation of experimentally shocked biotite, Amer. J. Sci. 267, 1213-1229, 1969.

Hörz, F. and W. L. Quaide, Debye-Scherrer investigations of experimentally shocked silicates, The Moon 6, 45-82, 1973.

Jahn, H. A. and E. Teller, Stability of polyatomic molecules in degenerate electronic states. I. Orbital degeneracy, Proc. Royal Soc. (London), A 161, 220-235, 1937.

James, O. B., Shock and thermal metamorphism of basalt by nuclear explosion, Nevada Test Site, Science 166, 1615-1620, 1969a.

James, O. B., Jadeite: shock-induced formation from oligoclase, Ries Crater, Germany Science 165, 1005-1008, 1969b.

Keester, K. L. and W. B. White, Crystal-field and chemical bonding in manganese minerals, Proc. 5th Int. Min. Assoc., Cambridge, 22-35, 1966.

Kelley, K. K., Contributions to the data on theoretical metallurgy, XIII, High-temperature heat-content, heat-capacity, and entropy data for the elements and inorganic compounds, U. S. Bur. Mines Bull. 584, 160, 1960.

Kennedy, G. C., G. J. Wasserburg, H. C. Heard and R. C. Newton, The upper three-phase region in the system SiO_2-H_2O, Amer. J. Sci. 260, 501, 1962.

Kinomura, N., M. Koizumi and S. Kume, Germanate alkali feldspars under pressure, J. Geophys. Res. 76, 2035-2037, 1971.

Kleeman, J. D., Formation of diaplectic glass by experimental shock-loading of orthoclase, J. Geophys. Res. 76, 5499-5503, 1971.

Kleeman, J. D. and T. J. Ahrens, Shock-induced transition of quartz to stishovite, J. Geophys. Res. 78, 5954-5960, 1973.

Levi-Donati, G. R., Petrological features of shock metamorphism in chondrites: Alfianello, Meteoritics 6, 225-236, 1971.

Low, W. and S. Zeira, ESR spectra of Mn^{2+} in heat-treated aragonite, Amer. Mineral. 57, 1115-1124, 1972.

Manning, P. G., Absorption spectra of the manganese-bearing chain silicates pyroxmangite, rhodonite, bustamite, and serandite, Canad. Mineral. 9, 348-357, 1968.

Manning, P. G., Effect of second-nearest-neighbor interaction on Mn^{3+} absorption in pink and black tourmalines, Canad. Mineral. 11, 971-977, 1973.

McQueen, R. G., J. N. Fritz and S. P. Marsh, On the equation of state of stishovite, J. Geophys. Res. 68, 2319-2322, 1963.

McQueen, R. G. and S. P. Marsh, Hugoniot data in Birch (1966).

McQueen, R. G., S. P. Marsh and J. N. Fritz, Hugoniot equation of state of twelve rocks, J. Geophys. Res. 72, 4999-5036, 1967.

McQueen, R. G., S. P. Marsh, J. W. Taylor, J. N. Fritz and W. J. Carter, The equations of state of solids from shock wave studies, in High Velocity Impact Phenomena, edited by R. Kinslow, Academic Press, 294-419, 1970.

Milton, D. J. and P. S. DeCarli, Maskelynite: formation by explosive shock, Science 140, 670-671, 1963.

O'Connell, E., A Catalog of Meteorite Craters and Related Features with a Guide to the Literature, The Rand Corporation, Santa Monica, California, 1965.

Peacor, D. R. and N. Niizeki, The redetermination and refinement of the crystal structure of rhodonite $(Mn,Ca)SiO_3$, Zeitschrift fur Kristallographie 119, 98-116, 1963.

Petersen, C. F., W. J. Murri and M. Cowperthwaite, Hugoniot and release adiabat measurements for selected geologic materials, J. Geophys. Res. 75, 2063-2072, 1970.

Phakey, P., G. Dollinger and J. Christie, Transmission electron microscopy of experimentally deformed olivine crystals, Geophysical Monograph Series Vol. 16, 117-138, 1972.

Pollack, S. S., Disordered orthopyroxene in meteorites, Amer. Mineral. 51, 1722-1726, 1966.

Pollack, S. S., Disordered pyroxenes in chondrites, Geochim. Cosmochim. Acta 32, 1209-1217, 1968.

Pollack, S. S. and P. S. DeCarli, Enstatite: Disorder produced by a megabar shock event, Science 165, 591-592, 1969.

Pollack, S. S. and W. D. Ruble, X-ray identification of ordered and disordered ortho-enstatite, Amer. Mineral. 49, 983-992, 1964.

Radcliffe, S. V., J. M. Christie, G. L. Nord, Jr., J. S. Lally, A. H. Heuer, D. T. Griggs and R. M. Fisher, Electron petrographic evidence concerning the origin and lithification of the lunar breccias, Lunar Science V, part II, 613-615, 1974.

Raleigh, C. B. and J. L. Talbot, Mechanical twinning in naturally and experimentally deformed diopside, Am. J. Sci. 265, 151-165, 1967.

Reid, A. M. and A. J. Cohen, Some characteristics of enstatite from enstatite chondrites, Geochim. Cosmochim. Acta 31, 661-672, 1967.

Rice, M. H., R. G. McQueen and J. M. Walsh, Solid State Physics, Academic Press, New York, 6, 1-63, 1958.

Ringwood, A. E. and A. Major, High pressure transformation in pyroxenes, Earth Planet. Sci. Lett. 1, 351-357, 1966.

Ringwood, A. E. and A. Major, High-pressure transformations in pyroxenes II, Earth Planet. Sci. Lett. 5, 76-78, 1968.

Ringwood, A. E., A. F. Reid and A. B. Wadsley, High pressure $KAlSi_3O_8$, an aluminosilicate with six-fold coordination, Acta Cryst. 23, 1093-1095, 1968.

Robertson, P. B., Experimental deformation of microcline, E@S, Trans. Amer. Geophys. Union, 53, 427, 1972. (Abstract)

Robertson, P. B., M. R. Dence and M. A. Vos, Deformation in rock-forming minerals from Canadian craters, in Shock Metamorphism of Natural Materials, edited by B. M. French and N. M. Short, Mono Book Corporation, Baltimore, 433-452, 1968.

Rosenberg, J. T., T. J. Ahrens and C. F. Petersen, Dynamic properties of rocks, report prepared for Headquarters, Defense Atomic Support Agency, Washington, D. C., at Shock and High Pressure Department, Stanford Research Institute, Menlo Park, California, July, 1968.

Roy, R. and H. M. Cohen, Effects of high pressure on glass: A possible piezometer for the 100 kb region, Nature 190, 798, 1961.

Shoemaker, E. M., Impact mechanics at Meteor Crater, Arizona, in The Solar System, 4, The Moon, Meteorites, and Comets, edited by B. M. Middlehurst and G. P. Kuiper, Univ. of Chicage Press, 301-336, 1963.

Short, N. M., Experimental microdeformation of rock materials by shock pressures from laboratory-scale impacts and explosions, in Shock Metamorphism of Natural Materials, edited by B. M. French and N. M. Short, Mono Book Corporation, Baltimore, 219-241, 1968a.

Short, N. M., Nuclear-explosion-induced microdeformation of rocks: an aid to the recognition of meteorite impact structures, in Shock Metamorphism of Natural Materials, edited by B. M. French and N. M. Short, Mono Book Corporation, Baltimore, 185-210, 1968b.

Short, N. M., Shock metamorphism of basalt, Mod. Geol. 1, 81-95, 1969.

Short, N. M., Evidence and implications of shock metamorphism in lunar samples, Geochim. Cosmochim. Acta, Suppl. 1, 1, 865-871, 1970.

Smith, J. V., Crystal structure and stability of the $MgSiO_3$ polymorphs: Physical properties and phase relations of Mg,Fe pyroxenes, Mineral. Soc. Amer. Spec. Pap. 2, 1969.

Smith, J. V. and B. Mason, Pyroxene-garnet transformation in Coorara meteorite, Science 168, 832-833, 1970.

Stöffler, D., Zones of impact metamorphism in the crystalline rocks of the Nördlinger Ries crater, Contr. Miner. Petrol. 12, 15-24, 1966.

Stöffler, D., Deformation and umwandlung von plagioklas durch stosswellen in den gesteinen des Nordlinger Ries, Contr. Miner. Petrol. 16, 51-83, 1967.

Stöffler, D., Progressive metamorphism and classification of shocked and brecciated crystalline rocks at impact craters, J. Geophys. Res. 76, 5541-5551, 1971.

Stöffler, D., Deformation and transformation of rock-forming minerals by natural and experimental shock processes. I. Behavior of minerals under shock compression, Fortschr. Miner. 49, 50-113, 1972.

Stöffler, D. and U. Hornemann, Quartz and feldspar glasses produced by natural and experimental shock, Meteoritics 7, 371-394, 1972.

Turner, F. J., Determination of plagioclase with the four-axis universal stage, Amer. Mineral. 32, 389-410, 1947.

Wackerle, J., Shock-wave compression of quartz, J. Appl. Phys. 33, 922-937, 1962.

Walsh, J. M. and R. H. Christian, Equation of state of metals from shock wave measurement, Phys. Rev. 97, 1544-1556, 1955.